AD NUMBER

ADB271344

NEW LIMITATION CHANGE

TO

Approved for public release, distribution unlimited

FROM

Distribution: Further dissemination only as directed by George C. Marshall Space Flight Ctr., NASA, Huntsville, AL 35812, Jun 63; or higher DoD authority.

AUTHORITY

NASA, per DTIC Form 55, dtd 20 Aug 2002

GENERAL MOTORS CORPORATION

SUMMARY REPORT

STUDY OF THE PHENOMENA OF HYPERVELOCITY IMPACT

Request No. TP 2—84081

Contract No. NAS8—5067

PREPARED FOR

GEORGE C. MARSHALL SPACE FLIGHT CENTER

NASA, HUNTSVILLE, ALABAMA

GM DEFENSE RESEARCH LABORATORIES

SANTA BARBARA, CALIFORNIA

AEROSPACE OPERATIONS DEPARTMENT

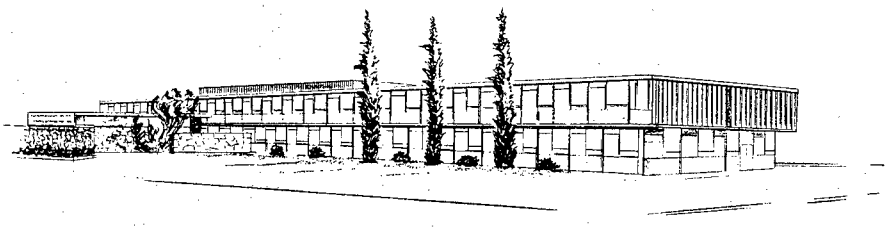

TR63—216

JUNE 1963

Copy No 00119

GENERAL MOTORS CORPORATION

SUMMARY REPORT

STUDY OF THE PHENOMENA OF HYPERVELOCITY IMPACT

53159

Prepared by

D.R. Christman

J.W. Gehring

C.J. Maiden

A.B. Wenzel

Request No. TP 2—84081

Contract No. NAS8—5067

PREPARED FOR

GEORGE C. MARSHALL SPACE FLIGHT CENTER

NASA, HUNTSVILLE, ALABAMA 35812

GM DEFENSE RESEARCH LABORATORIES

SANTA BARBARA, CALIFORNIA

AEROSPACE OPERATIONS DEPARTMENT

Jun 63

DISTRIBUTION STATEMENT F:

Further dissemination only as directed by

_____

or higher DoD authority.

TR63—216

JUNE 1963

ABSTRACT

This report is a critical investigation of the meteoroid hazard and of theoretical, empirical, and experimental investigations of hypervelocity impact. Simple and complex models of cratering and perforation are considered, as are the limitations and requirements imposed by practical engineering considerations. Results presented in this report are based on a detailed review of the published works of the many investigators in the field of hypervelocity impact and on a number of independent experimental and theoretical research programs being conducted at GM Defense Research Laboratories. The conclusions are summarized, and specific recommendations are made concerning future experimental and theoretical studies of hypervelocity impact.

APPROACH

This study was conducted at GM Defense Research Laboratories by the Flight Physics Laboratory of Aerospace Operations. The work was carried out under National Aeronautics and Space Administration Contract NAS 8-5067, with technical direction of the program by the Physics and Astrophysics Branch, Research Projects Division, George C. Marshall Space Flight Center.

To introduce the subject of hypervelocity impact and the need for both a theoretical and an experimental definition of the phenomena, a brief review has been made of the expected meteoroid hazard to space vehicles. This hazard, as it now exists, has been defined from the available references. The damage mechanisms that might operate as a result of hypervelocity impact are described, and the requirements for simulating the impact hazard in the laboratory are discussed.

Published empirical and semi-empirical relationships for describing the craters formed by hypervelocity impact have been reviewed, and six relationships were selected for discussion and comparison. Also, these relationships are compared with recent experimental data obtained at GM Defense Research Laboratories for velocities up to 8.6 km/sec. In addition, these relationships have been applied to the practical problem of spacecraft design.

Previous theoretical treatments of hypervelocity impact have been reviewed with a brief history of the development of impact theory. Emphasis has been placed on the assumptions underlying these earlier theories. Cratering in semi-infinite targets is analyzed, and several approaches to establishing a model of hypervelocity impact have been discussed. The physical observations of crater formation are presented and developed into a model intended to represent physical reality.

Included are the problems that face the design engineer in the practical application of hypervelocity impact theories, such as the behavior and effects of thin targets, stressed structures, spalling, oblique impact, target strength, and projectile configurations.

The final section of the report has been devoted to a summary of pertinent results and conclusions. Specific recommendations and suggestions are made concerning future studies on both the experimental and theoretical treatment of hypervelocity impact. The objective of these future studies would be to provide a more complete and definitive description of the phenomena of hypervelocity impact.

In using this document, note that each of the first four sections has a separate list of references; and Section 4 has a reference list after each subsection. This mode of referral is intended to make particular references more readily available, and to make each section of the report complete in itself.

Typist: Do not put up page numbers.

TABLE OF CONTENTS

End

LIST OF ILLUSTRATIONS

SECTION I

INTRODUCTION

The problems of hypervelocity impact, especially those concerned with meteoroid hazard and AICBM or satellite-defeat mechanisms, are the source of much interest and concern. This report is directed at the meteoroid hazard, although some consideration is made of the lethality of fragments and the vulnerability of structures to these fragments. A review and analysis have been made of experimental and theoretical data on hypervelocity impact phenomena for the purpose of establishing theories which will correlate with the data on particle sizes, particle velocities, and the physical characteristics of particles and targets.

This review is not a novel approach. Other summaries have been done by Van Valkenburg, Clay, and Huth (Ref. 1), Rodriquez (Ref. 2), Bjork (Ref. 3), Herrmann and Jones (Ref. 4), Jaffe and Rittenhouse (Ref. 5), Bruce (Ref. 6), Eichelberger and Gehring (Ref. 7), and others. Recent developments in both the theoretical and experimental treatment of hypervelocity impact and the increasing demand for a satisfactory definition of the mechanisms involved have established the need for this analysis. Following is a brief review of the expected meteoroid hazard to space vehicles (Refs. 8-14) and a definition of the meteoroid hazard as it now exists.

1.1 METEOROID HAZARD

Proper assessment of potential damage to space vehicles from impact by meteoroids requires knowledge of meteroid size, shape, mass, material, and velocity, and of the frequency of their occurrence at a given location in space. To acquire this knowledge, investigators have extracted data from numerous sources, among them astronomical observations (Ref. 15), studies of the Zodiacal light and the Solar corona (Refs. 16-19), luminous intensity measurements of meteors (Refs. 20, 21), satellite and space vehicle data (Refs. 18, 22-25), radar measurements (Refs. 26, 27), studies of meteoroids and

meteoroid craters found on the earth (Refs. 28-34), and visual observations (Ref. 35).* From thorough evaluation of these data, some quantitative estimates can be made.

Estimates of particle diameter range from less than 1 micron (10^{-6}m) for dust particles up to nearly 1,000 km for bodies found in the asteroid belt. From the standpoint of potential damage, the large meteoroids and asteroids are an improbable hazard because of their rarity; and micron-sized meteoroids, though abundant, do not cause extensive damage because of their relatively low impact energy. The meteoroids of intermediate size (10^{-3} to 1 cm) are the ones that present the greatest hazard.

Meteoroid shapes vary from highly irregular to nearly spherical. However, at the velocities involved in meteoroid encounters, the shape of the meteoroid should not be a significant factor in the resulting damage.

Meteoritic particles that have been collected and analyzed are divided into two general classes: metallic and stony. The metallics are primarily iron and nickel, but include manganese, chromium and the precious metals. Stony particles are found to include such minerals as ferropigeonite, anorthite, and ferrougite (Ref. 36). When applied to the size range given above, estimates of meteoroid density (0.05 gm/cm^3 up to 8.0 gm/cm^3) give a possible range in mass of about 10^{-14} gm to 10^{24} gm. Since most meteoroids are thought to be of cometary origin and of composition similar to stone, the densities of meteoroids of intermediate size should range from 0.5 to 3.0 gm/cm^3, giving a range in mass of about 10^{-7} gm to 3.0 gm.

Velocity and distribution of meteoroids in space is another area in which some quantitative estimates can be made. Figure 1.1 is a summary of mass frequency distribution data. Unfortunately, the bulk of this data is not applicable to space in general, for observations and measurements have shown that the meteoroid flux distribution in space is not uniform (Ref. 9), varying with solar latitude (Refs. 37, 38, and Fig. 1.2) and with distance from the plane of the ecliptic (Ref. 15 and Fig. 1.3), the plane of revolution of the earth about the sun. (The

*For additional references on meteoroids, see Astron. J., Vol. 67, No. 5, Jun 1962, papers and abstracts from "Symposium on Small Meteoric Particles in the Earth's Neighborhood," Cambridge, Mass., Apr 2, 1962

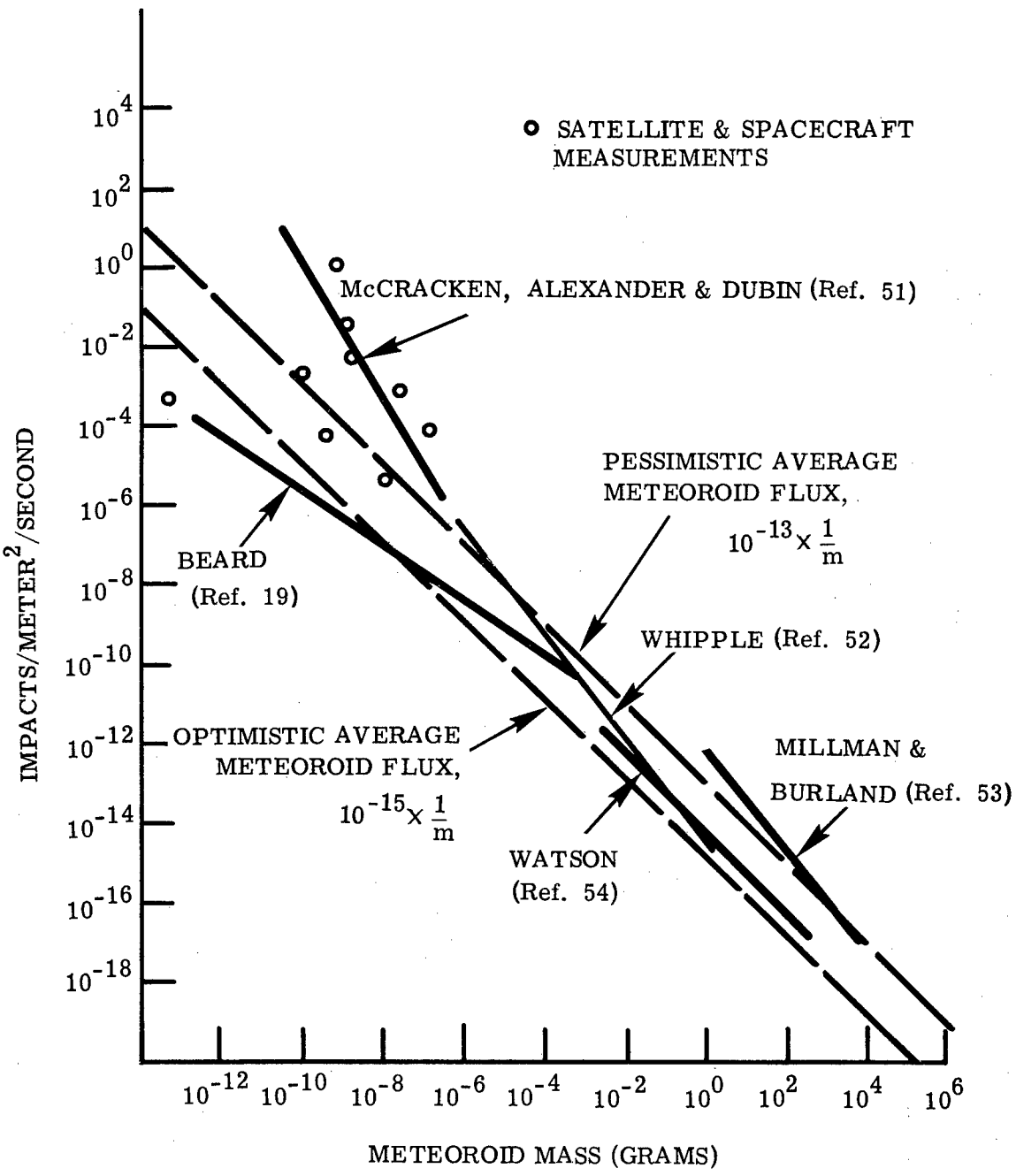

Fig. 1.1 Meteoroid Frequency vs. Meteoroid Mass

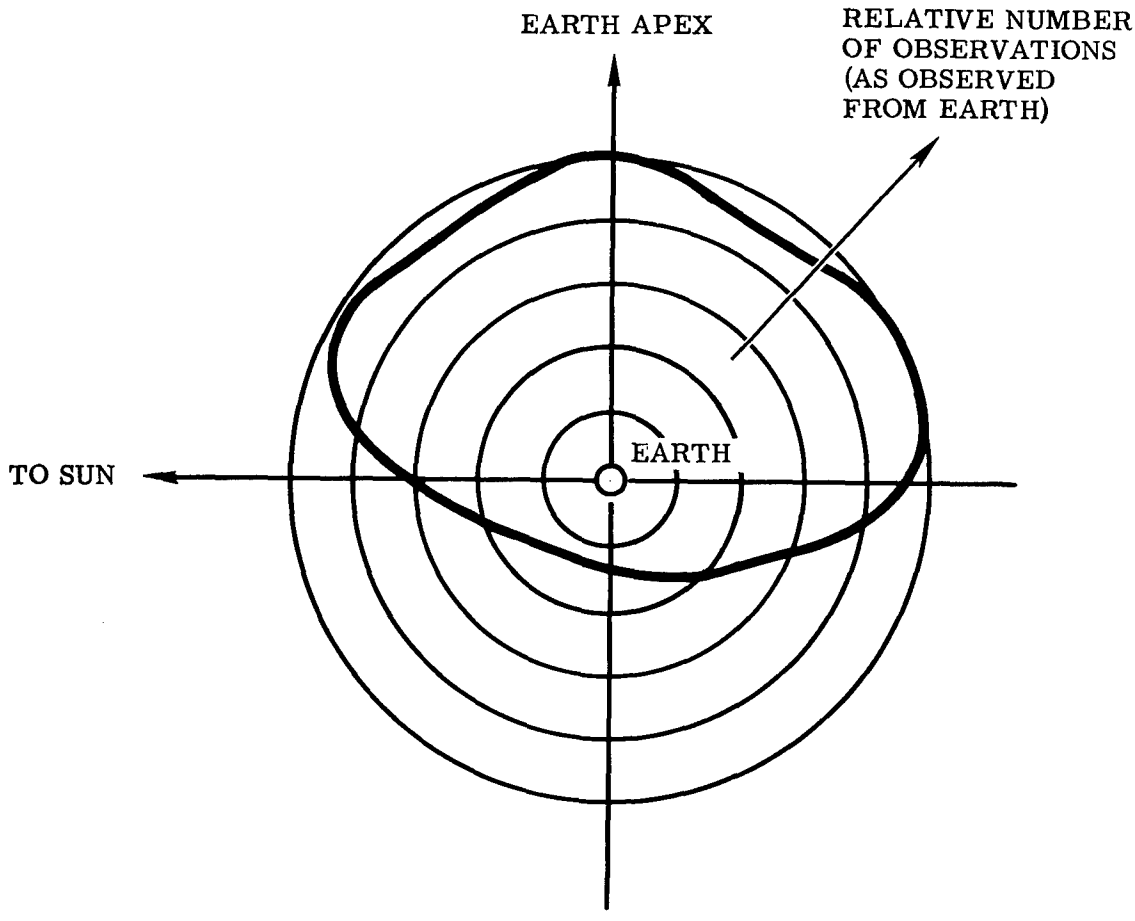

Fig. 1.2 Meteoroid Distribution With Respect To Solar Longitude (from Ref. 15)

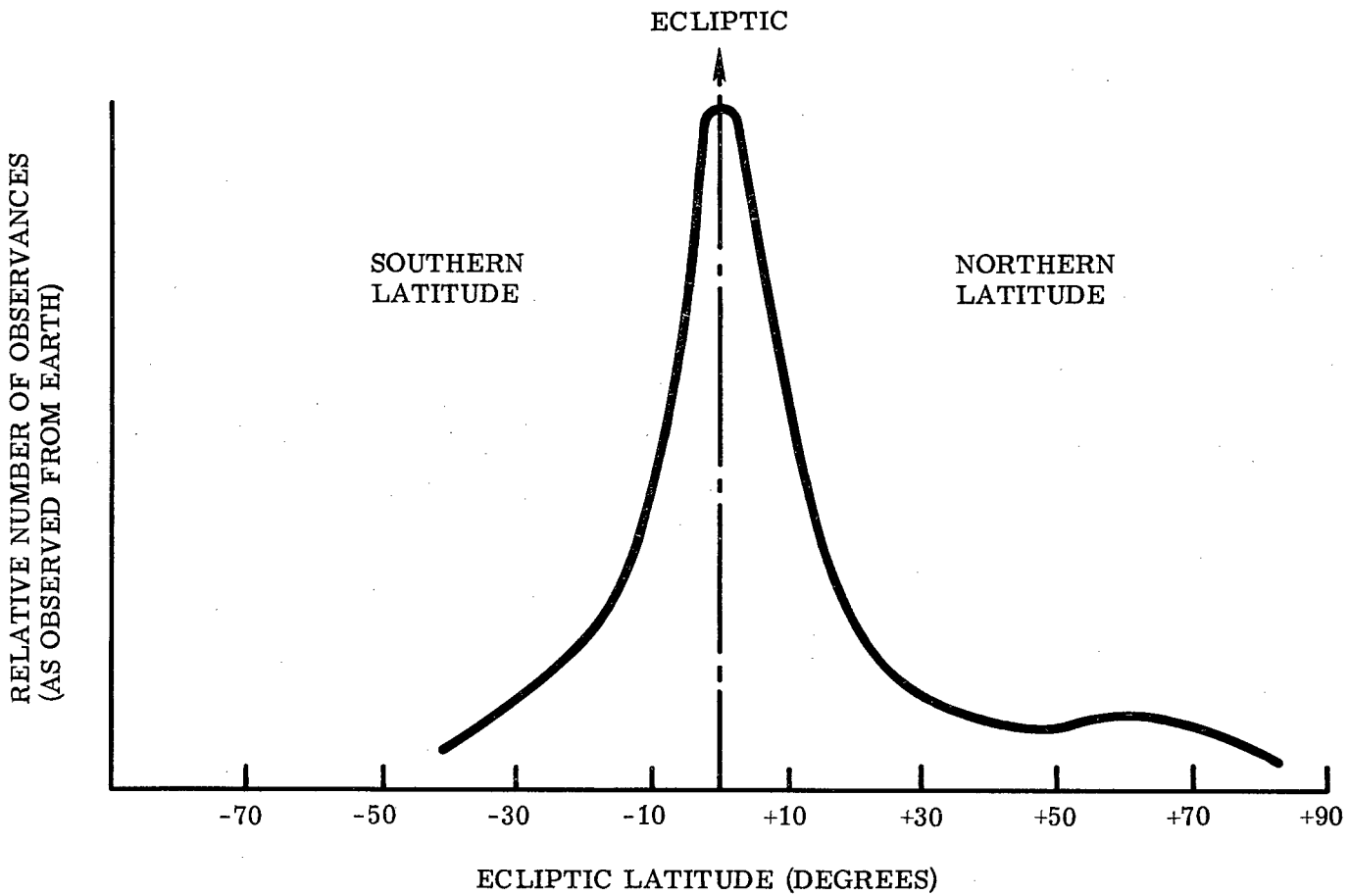

Fig. 1.3 Meteoroid Distribution with Respect to Ecliptic Latitude (from Ref. 15)

data shown in Figs. 1.2 and 1.3 represent the results of visual and radio-echo observations of sporadic meteors over a period of several years. Diurnal and seasonal variations in meteoric activity as well as the contributions of meteor showers are not reflected on these graphs.) In general, the meteoroid flux density, at least of dust-like particles less than 10^{-4} gm, decreases the greater the distance from the earth and the ecliptic plane, although it increases in the vicinity of the sun and the planets (Refs. 10, 19).

Also shown in Fig. 1.1 are the "optimistic average meteoroid flux" and the "pessimistic average meteoroid flux". These two average flux curves are intended to bracket the actual meteoroid distribution in space. This actual or true distribution is really a nebulous factor, since it is time-and-space dependent; that is, it does not necessarily remain constant with time and, as noted, there will be some variation with location in the solar system. Both fluxes are represented by equations of the form $\phi = k/m$, where k is a constant and m is meteoroid mass. As more information on meteoroid flux is made available through the use of satellites and spacecraft, a change in the form of this equation may be justified. A more accurate relationship may be $\phi = k/m^a$, where a is greater than one, thereby reducing the frequency of the larger meteoroids.

The expected range of velocities for meteoroids is generally agreed to be from 11 to 72 km/sec, relative to the earth. Meteoroid impact velocity, relative to interplanetary spacecraft, could be in the range of 0–83 km/sec. *

1.2 DAMAGE MECHANISMS

The damage mechanisms that will operate on a space vehicle during impact with a meteoroid can be divided into six classes. These six classes are not independent, so some overlap exists.

1.2.1 Erosion.

Also called sputtering. The relatively slow (less than 100 A/year) etching away of surface material due to the impact of small (diameter of less than 10 microns) meteoritic particles. Structural damage from erosion would be negligible, but

*For a more detailed discussion of the meteoroid hazard see "Meteoroid Impact," by C. J. Maiden, GM Defense Research Laboratories Report TM 63-203, Apr 1963.

degradation of protective coatings or optical surfaces could be significant. (See, for example, Refs. 5, 39, and 40).

1.2.2 Evaporation.

Vaporization of surface atoms and molecules as a result of thermal energy generated by impact of small meteoritic particles. Same damage conditions as with erosion. (See Ref. 41.)

1.2.3 Cratering.

Also called penetration. The formation of large craters (of greater volume, in general, than the volume of the impacting meteoroid) caused by the ejection of material from the target surface. Structure strength can be considerably decreased and operation of moving parts can be seriously impaired. (See Ref. 42.)

1.2.4 Spalling.

Also called scabbing. Fracturing of a material and, usually, the ejection of debris near a free surface by the action of a stress wave generated at another location in the material. Structure strength can be considerably decreased and damage inflicted inside the space vehicle by the ejecta. (See, for example, Refs. 43, 44.)

1.2.5 Perforation.

Also called puncture. Complete penetration. Structure strength can be greatly decreased, and pressure vessels and liquid- or vapor-filled tubes can be made inoperative. (See Refs. 9, 45.)

1.2.6 Deformation.

The physical displacement of structural components. Tubes can be constricted, operation of moving parts impaired, and vehicle reference axes distorted.

1.3 LABORATORY SIMULATION

Once the meteoroid hazard has been defined, the problem of simulating this hazard in the laboratory arises. Figure 1.4 is a plot of average frequency distribution (taken from Fig. 1.1) and kinetic energy versus meteoroid mass. This plot shows the potential range of meteoroid impact energies that must be simulated, but it should be noted that impact energy is not necessarily the only parameter that might be considered.

For example, meteoroid momentum could also be simulated. The current laboratory capabilities in meteoroid impact energy simulation, using a variety of techniques, are given in Fig. 1.5. This plot shows the range of kinetic energy and particle mass possible for microparticles, simple shapes, and short jets. In particular, Fig. 1.5 demonstrates that, although laboratory velocity capabilities extend only into the lower part of the expected meteoroid impact velocity range, laboratory energy capabilities adequately cover the expected meteoroid impact energy range. An indication of the ranges of velocity and projectile mass that are of interest to the investigator of impact phenomena in general and not of just the meteoroid hazard is given in Fig. 1.6. Here the potential range in velocity is from 0.3 km/sec to 72 km/sec, while projectile masses may range from 10^{-14} grams to 10^{6} grams.

Laboratory tests are important in developing and evaluating theoretical models of impact phenomena and in generating empirical data for use by the design engineer who is working on military systems and space vehicles. The efforts of the laboratory scientist in the study of all hypervelocity impact phenomena can be divided into four areas as follows:

1.3.1 Environment.

Every experimental program in hypervelocity impact imposes some conditions on the test environment; however, recent advances in high-vacuum technology, cryogenic systems, heat and radiation simulation devices, and other fields, have greatly lessened the difficulty of simulating a given environment. In fact, the scientist's main problem is not in devising experimental techniques to simulate a particular environment, but in deciding exactly how close he must come to simulating an operating environment in order to obtain results that will be truly representative.

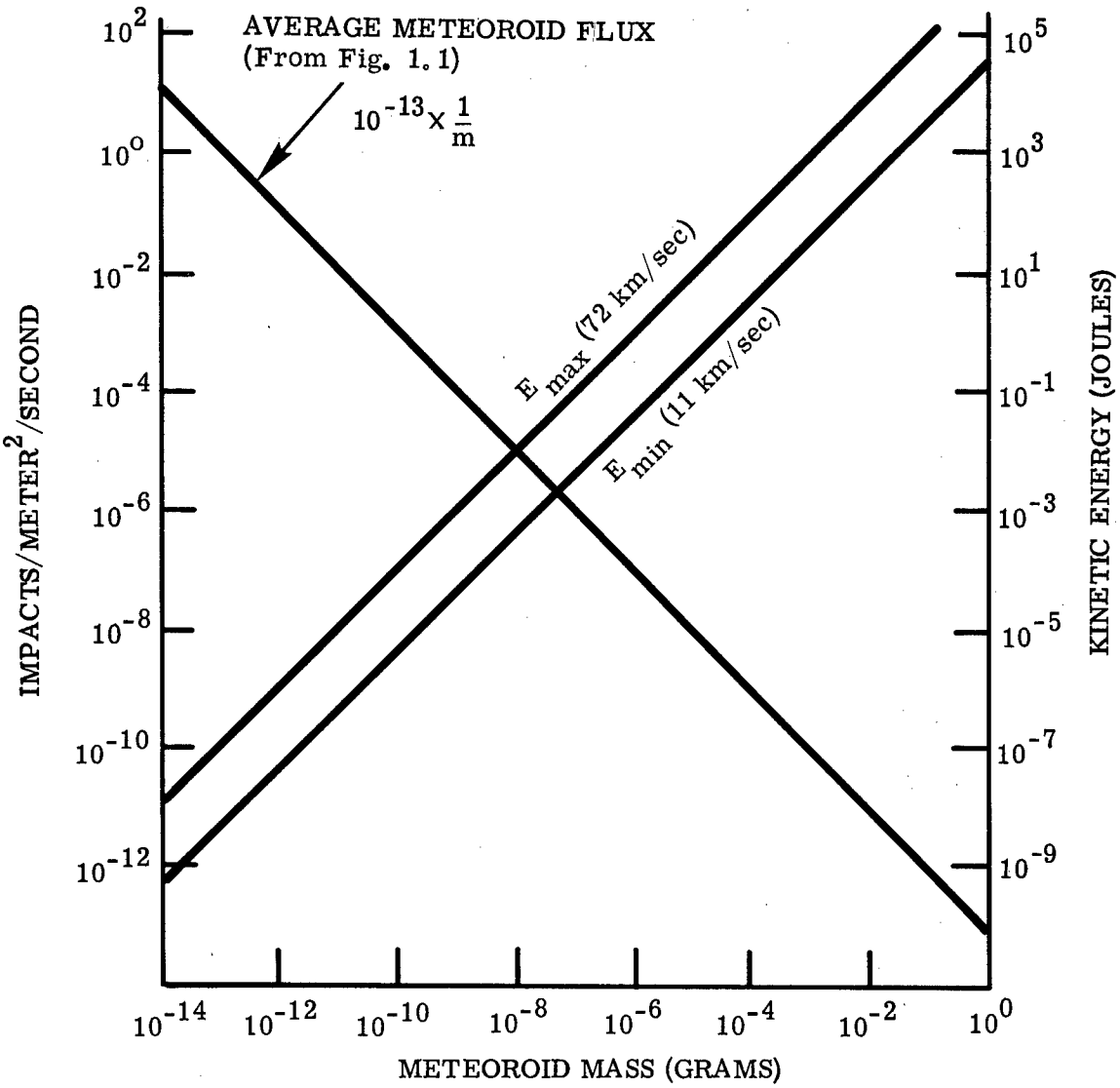

Fig. 1.4 Average Meteoroid Frequency and Kinetic Energy vs. Meteoroid Mass

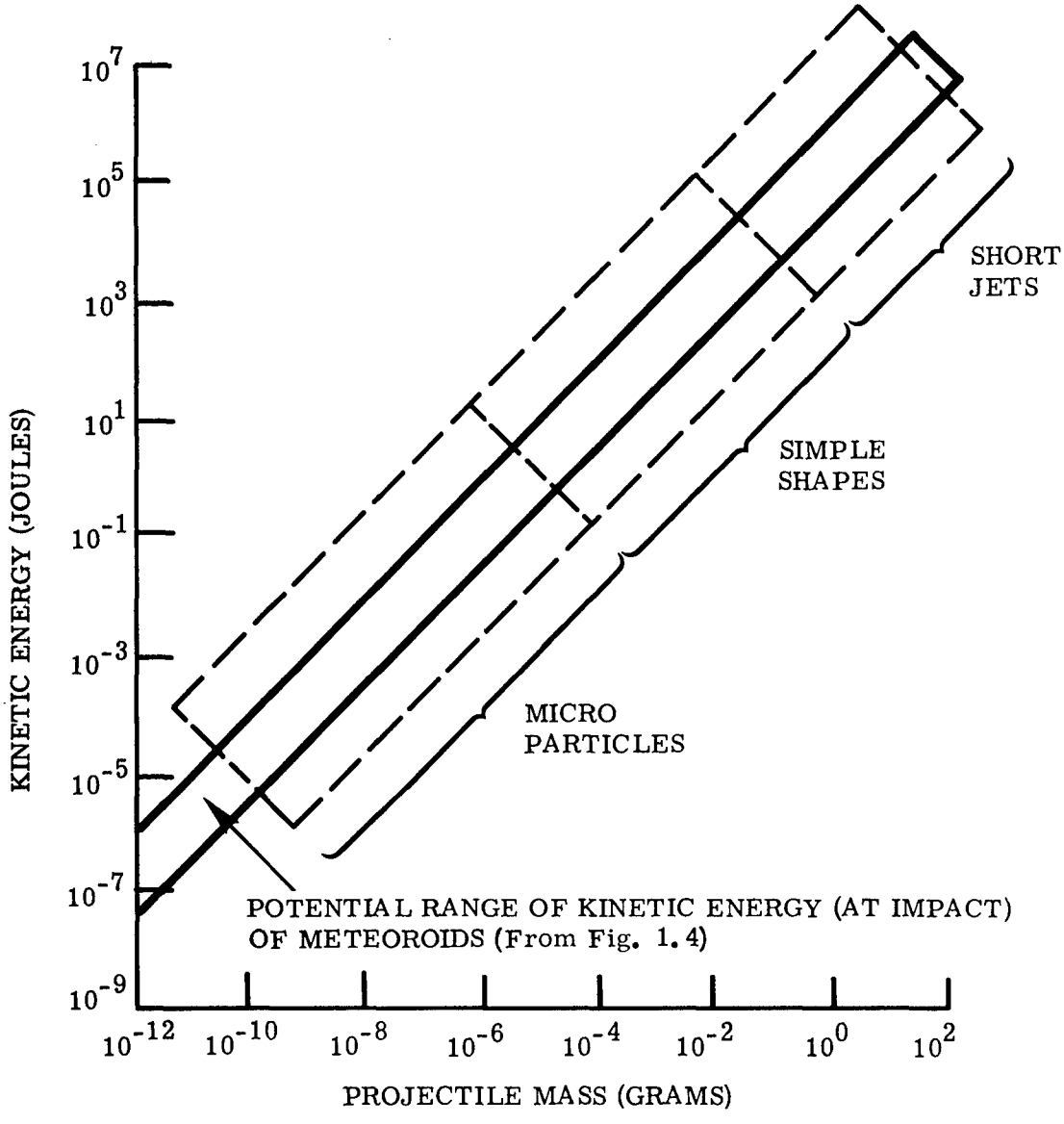

Fig. 1.5 Laboratory Simulation of Meteoroid Impact Energies

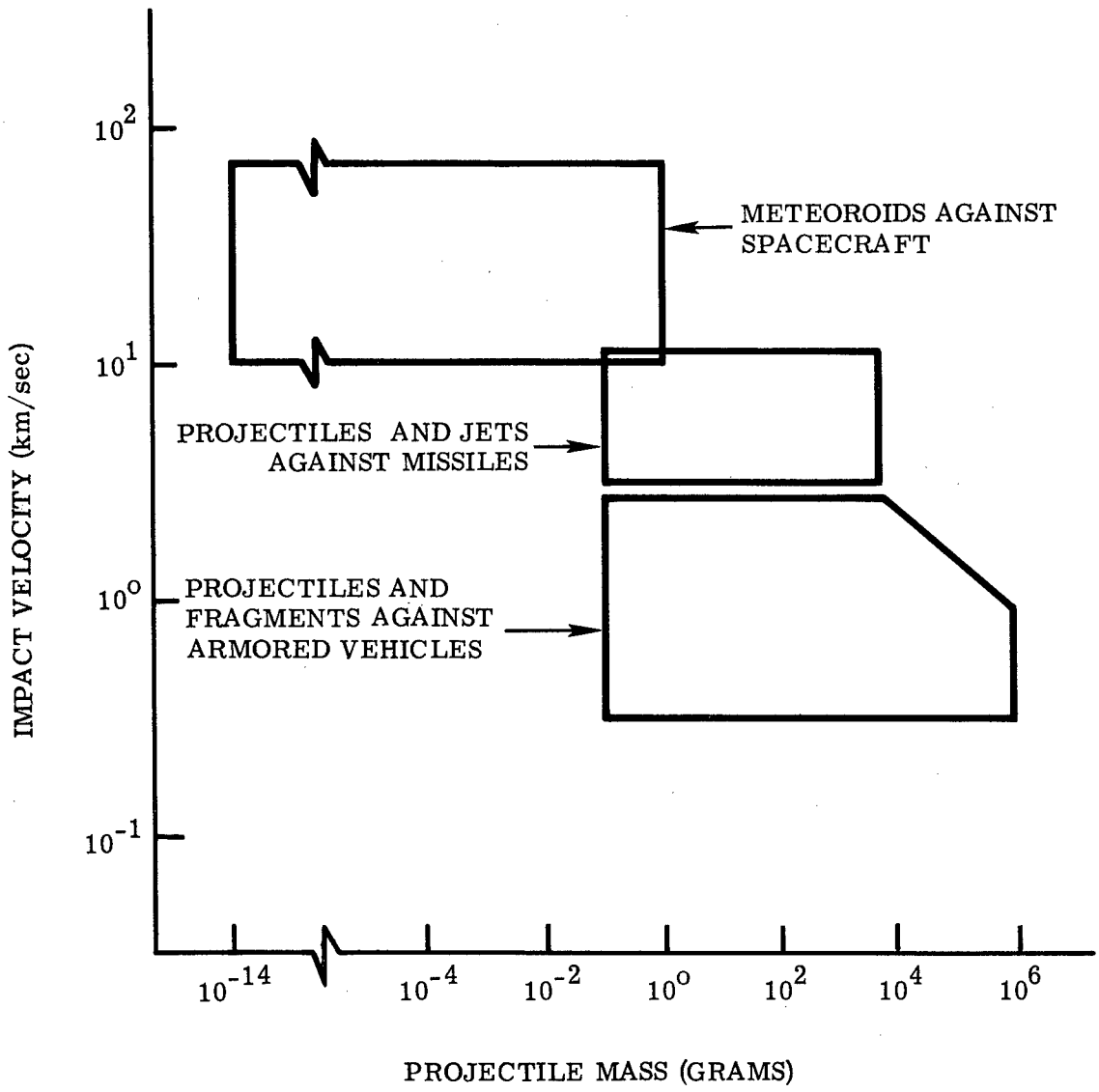

Fig. 1.6 Impact Velocity vs. Projectile Mass for Military and Space Missions

1.3.2 Projectile.

In selecting a projectile for a particular impact experiment, the scientist must establish requirements for mass, density, size, shape, and material. These requirements usually fall into two categories: (1) when projectile parameters are the prime factors in the experiment; and (2) when projectile parameters are of secondary importance and need be capable only of measurement and reproducibility. Although obviously not a "property" of the projectile, the impact velocity can be considered a projectile requirement because of the limitations imposed on the projectile by the velocity being considered. In general, the simpler the projectile shape, the higher the velocity obtainable. For example, a 1/8-in.-diam aluminum sphere (0.046 gm) has been accelerated to greater than 28,000 ft/sec, and 0.07-gram polyethylene cylinders have been accelerated to greater than 32,000 ft/sec with accelerated-reservoir, light-gas guns (Ref. 46). Explosive techniques have been used in accelerating short, rod-like projectiles to velocities in excess of 50,000 ft/sec. Numerous other projection techniques available for impact studies below 30,000 ft/sec include exploding wire devices, electric discharge accelerators, traveling charge guns, and powder guns. *

1.3.3 Target.

The target is usually the most important factor in hypervelocity experiments. Because of the wide variety of possible targets, a serious need exists for adequate theories to cover thin targets, thick targets, pressure vessels, etc. However, lacking a theory, the investigator must test representative samples of the many potential structures and configurations. Typical examples of these are solar cells, solar collecting panels, heat radiators for spacecraft nuclear power supplies, windows, optical lenses, rocket-engine chambers, reentry shields, and, of course, spacecraft hulls. One of the major problems concerning targets is scaling down the target to fit experimental facilities and then scaling up test results to satisfy operational conditions. One example of this

*See Proceedings of the Fourth Symposium on Hypervelocity Impact, APGC-TR-60-39, Eglin AFB, Florida, Sep 1960; and Proceedings of the Fifth Symposium on Hypervelocity Impact, Nonr-(G)-0020-62(X), Colorado School of Mines, Apr 1962

is the size problem inherent in the laboratory study of the impact flash generated by the impact of a probe or meteoroid on the lunar surface (Ref. 47).

1.3.4 Instrumentation.

The development of instrumentation for hypervelocity impact studies is as advanced as the development of environmental test equipment mentioned previously. Shadowgraph stations, velocity screens, and high-speed framing cameras have recorded projectile velocities. Flash X-ray units, framing cameras, streak cameras, and open-shutter cameras have recorded hole and crater formation, spalling, ejecta behavior, and shock wave propogation. Photomultiplier tubes, spectrographs, and microwave detection equipment have been used to monitor impact radiation. In addition, numerous devices have been developed for special applications, including pressure transducers for impulse measurements (Ref. 48), pickup wires for detecting transient response in targets (Ref. 49), and light-flash and acoustical sensors for detecting micrometeorite impacts (Ref. 50). *

*For further references, see Proceedings of the Fourth and Fifth Hypervelocity Impact Symposia; Proceedings of the National Symposium on Hypervelocity Techniques, Denver, Colorado, Oct 20-21, 1960, pub. by the Institute of Aeronautical Sciences; and Proceedings of the Second Symposium on Hypervelocity Techniques, Denver, Colorado, Mar 20-21, 1962, Plenum Press, N.Y.

The following sections of this report will review and analyze experimental and theoretical efforts in the field of hypervelocity impact, examine the phenomenological models of cratering that have been proposed, and define those areas where additional theoretical analysis and experimental efforts are needed. The primary area of concern will be the simple projectile/target model, i. e., a symmetrical, homogeneous, isotropic projectile impacting a semi-infinite, homogeneous, isotropic target. However, a summary will be made of more complicated projectile/target conditions, including nonsymmetrical projectiles (rods, discs, jets) and complex targets (thin targets, multiple-sheet targets, composites).

REFERENCES FOR SECTION 1 - INTRODUCTION

1. M. E. Van Valkenburg, W. G. Clay, and J. H. Huth, "Impact Phenomena at High Speeds," J. Appl. Phys. Vol. 27, No. 10, Oct 1956, pp. 1123-1129

2. D. Rodriquez, "Meteoroid Shielding for Space Vehicles," Aerospace Eng., Vol. 19, No. 12, Dec 1960

3. R. L. Bjork, "Meteoroids vs. Space Vehicles," ARS J., Vol. 31, No. 6, Jun 1961, pp. 803-807

4. W. Herrmann and A. H. Jones, "Survey of Hypervelocity Impact Information," Massachusetts Institute of Technology, Aeroelastic and Structures Research Laboratory, ASRL Report No. 99-1, Sep 1961

5. L. D. Jaffe and J. B. Rittenhouse, "Behaviour of Materials in Space Environments," ARS J., Vol. 32, No. 3, Mar 1962, pp. 320-346

6. E. P. Bruce, "Review and Analysis of High Velocity Impact Data," Proceedings of the Fifth Symposium on Hypervelocity Impact, Vol. 1, Part 2, Nonr-(G)-0020-62(X), Colorado School of Mines, Apr 1962

7. R. J. Eichelberger and J. W. Gehring, "Effects of Meteoroid Impacts on Space Vehicles," ARS J., Vol. 32, No. 10, Oct 1962, pp. 1583-1591

8. J. R. Davidson and P. E. Sandorff, "Environmental Problems of Space Flight Structures, II. Meteoroid Hazard," NASA TN-D-1493, Jan 1963

9. I. J. Loeffler, S. Lieblein, and N. Clough, "Meteoroid Protection for Space Radiators," ARS paper No. 2543-62 (presented at the ARS Space Power Systems Conference, Santa Monica, California, Sep 1962)

10. H. L. Martin, "The Meteoroid Hazard to Space Travel," ABMA Report DV-TN-22-59, 5 Aug 1959

11. J. E. Duberg, "The Meteoritic Hazard of the Environment of a Satellite," NASA TN-D-1248, Hampton, Virginia, May 1962 (see also D. D. Davis, "Space Environment and Its Effects on Materials," Proceedings of the NASA - University Conference on the Science and Technology of Space Exploration, Vol. 2, Chicago, Illinois, Nov 1-3, 1962, NASA SP-11)

12. E. H. Davison and P. C. Winslow, "Direct Evaluation of Meteoroid Hazard," Aerospace Eng., Vol. 21, No. 2, Feb 1962, pp. 24-33

13. E. M. Finkleman, "Optimized Protection Against Environmental Hazards in Space," Aerospace Eng., Vol. 21, No. 12, Dec 1962, pp. 41-48

14. J. B. Gayle, C. C. Dalton, H. L. Martin, and D. W. Murphee, "Review of Selected Aspects of the Meteoroid Hazard," NASA, George C. Marshall Space Flight Center, Material Damage Working Group, Rep. No. MDWG-63-1, Huntsville, Ala., 15 Feb 1963; also, "A Bibliography Concerning Aspects of The Meteoroid Hazard," Rep. No. MDWG-63-2, Huntsville, Ala., 1 Apr 1963

15. A. C. B. Lovell, Meteor Astronomy, Clarendon Press, Oxford, 1954

16. D. E. Blackwell, "The Zodiacal Light and Its Interpretation," Endeavour, Vol. 19, No. 73, Jan 1960, pp. 14-19

17. S. Chapman, "The Earth in the Sun's Atmosphere," Sci. Amer., Vol. 201, No. 4, Oct 1959, pp. 64-71

18. M. Dubin and C. W. McCracken, "Measurements of Distributions of Interplanetary Dust," Astron. J., Vol. 67, No. 5, Jun 1962, pp. 248-256

19. D. B. Beard, "Interplanetary Dust Distribution," Astrophys. J., Vol. 129, No. 2, Mar 1959, pp. 496-506

20. G. S. Hawkins and R. B. Southworth, "The Statistics of Meteors in the Earth's Atmosphere," Smithsonian Contributions to Astrophys., Vol. 2, No. 11, 1958, pp. 349-364

21. P. M. Millman, "Survey of Observations of Meteor Trails," AIAA J., Vol. 1, No. 5, May 1963, pp. 1028-33 (see also ARS paper No. 2659-62; presented at ARS 17th Annual Meeting and Space Flight Exposition, Los Angeles, Cal., Nov 13-18, 1962)

22. T. N. Nazarova, "The Investigation of Meteoric Dust by Means of Rockets and Artificial Earth Satellites," Planetary and Space Science, Vol. 11, No. 3, Mar 1963, pp. 305-309

23. I. Harris and R. Jastrow, "An Interim Atmosphere Derived from Rocket and Satellite Data," Planetary and Space Science, Vol. 1, 1959, pp. 20-26

24. C. L. Hemenway and R. K. Soberman, "Studies of Micrometeorites Obtained from a Recoverable Sounding Rocket," Astron. J., Vol. 67, No. 5, Jun 1962, pp. 256-266

25. National Aeronautics and Space Administration, The Explorer XVI Micrometeoroid Satellite, NASA Technical Memorandum X-824, Apr 1963

26. P. M. Millman, "The Meteor Radar Echo–An Observational Survey," Astron. J., Vol. 67, No. 5, Jun 1962, pp. 235-240

27. G. S. Hawkins, "Radar Determination of Meteor Orbits," Astron. J., Vol. 67, No. 5, Jun 1962, pp. 241-244

28. H. Pettersson, "Cosmic Spherules and Meteoritic Dust," Sci. Amer., Vol. 202, No. 2, Feb 1960, pp. 123-132

29. D. R. Chapman, "Recent Re-Entry Research and the Cosmic Origin of Tektites," Nature, Vol. 188, No. 4748, 29 Oct 1960, pp. 353-355

30. W. D. Crozier, "Micrometeorite Measurements – Satellite and Ground Level Data Compared," J. Geophys. Res., Vol. 66, No. 9, Sep 1961, pp. 2793-2795

31. B. Mason, "Organic Matter From Space," Sci. Amer., Vol. 208, No. 3, Mar 1963, pp. 43-49

32. E. M. Shoemaker, "Impact Mechanics at Meteor Crater, Arizona," U. S. Geological Survey, Jul 1959

33. V. E. Barnes, "Tektites," Sci. Amer., Vol. 205, No. 5, Nov 1961, pp. 58-65

34. R. S. Dietz, "Astroblemes," Sci. Amer., Vol. 205, No. 2, Aug 1961, pp. 50-58

35. E. P. Olivier, "Catalog of Hourly Meteor Rates," Smithsonian Contributions to Astrophys., Vol. 4, No. 1, 1960, pp. 1-14

36. California Institute of Technology, Annual Report, 1960, NASA Grant NsG 56-60, by H. Brown, B. C. Murray, et al, Pasadena, Calif., Jan 31, 1962

37. R. J. Parks, "Mariner II," Engineering and Science (published at the California Institute of Technology), Vol. 26, No. 1, Oct 1962, pp. 15-19

38. W. M. Alexander, "Cosmic Dust" (from "The Mission of Mariner II: Preliminary Observations,") Science, Vol. 138, No. 3545, 7 Dec 1962, pp. 1098-1099

39. F. L. Whipple, "Dust and Meteorites," Astronautics, Vol. 7, No. 8, Aug 1962, pp. 40-42 (also, ARS paper No. 2253-61, presented at the ARS Space Flight Report to the Nation, New York, Oct 9-15, 1961)

40. D. McKeown, M. G. Fox, and J. J. Schmidt, "Measurement of Surface Erosion from Discoverer 26," ARS J., Vol. 32, No. 6, Jun 1962, pp. 954-955

41. D. B. Beard, "Meteoritic Impact," ARS J., Vol. 31, No. 1, Jan 1961, pp. 87-88

42. J. W. Gehring, "Observations of the Phenomena of Hypervelocity Impact," Proceedings of the Fourth Hypervelocity Impact Symposium, Vol. 2, APGC-TR-60-39, Eglin AFB, Florida, Sep 1960

43. J. S. Rinehart, "Some Quantitative Data Bearing on the Scabbing of Metals Under Explosive Attack," J. Appl. Phys., Vol. 22, No. 5, May 1951, pp. 555-560

44. K. R. Becker, R. W. Watson, and F. C. Gibson, "Hypervelocity Impact Phenomena," Bureau of Mines, Explosives Research Laboratory, Quarterly Reports to the Ballistic Research Laboratory, Auth. No. 4086, 1961-1963

45. C. R. Nysmith and J. L. Summers, "Preliminary Investigation of Impact on Multiple-Sheet Structures, Etc.," NASA TN-D-1039, Sep 1961

46. J. S. Curtis and J. W. Gehring, "Projection Techniques" (paper presented at the Symposium on Structural Dynamics Under High Impulse Loading, Dayton, Ohio, Sep 17-18, 1962)

47. J. W. Gehring and D. W. Sieck, "A Study of the Phenomena of Impact Flash and Its Relation to the Reaction of the Lunar Surface to the Impact of a Lunar Probe," ARS paper No. 2476-62 (presented at the ARS Lunar Missions Meeting, Cleveland, Ohio, Jul 17-19, 1962)

48. R. J. Eichelberger and G. E. Hauver, "Solid State Transducers for Recording of Intense Pressure Pulses," Les Ondes de Detonation, Centre National de la Recherche Scientifique, Paris, 1962, pp. 363-382

49. J. T. Frasier and B. G. Karpov, "Hypervelocity Impact Studies in Wax," Proceedings of the Fifth Hypervelocity Impact Symposium, Vol. 1, Part 2, Nonr-(G)-0020-62(X), Colorado School of Mines, Apr 1962

50. W. M. Alexander and O. E. Berg, "Microparticle Hypervelocity Impacts from Ranger I," Proceedings of the Fifth Hypervelocity Impact Symposium, Vol. 1, Part 2, Nonr-(G)-0020-62(X), Colorado School of Mines, Apr 1962

51. C. W. McCracken, W. M. Alexander, and M. Dubin, "Direct Measurements of Interplanetary Dust Particles in the Vicinity of the Earth," Nature, Vol. 192, 4 Nov 1961, pp. 441-442

52. F. L. Whipple, "On Meteroids and Penetration" (paper presented at the Interplanetary Missions Conference of the American Astronautical Society, Jan 1963)

53. P. M. Millman and M. S. Burland, "Magnitude Distribution of Visible Meteors" (paper presented at the 96th meeting of the American Astronomical Society, New York, 1956)

54. F. G. Watson, Between the Planets, The Blakiston Company, Philadelphia, Pa., 1941

SECTION II

REVIEW OF EMPIRICAL APPROACHES

The phenomenon of cratering in semi-infinite metal targets has been treated in more detail, both empirically and theoretically, than any other phase of hypervelocity impact. This section of the report will deal with empirical treatments and applications of this phenomenon; an analysis of the theoretical aspects of crater formation will be given in the next section.

There are at least twenty empirical and semi-empirical relationships describing the cratering process in semi-infinite targets. No doubt each of these accurately describes the results obtained in a particular projectile-target-velocity impact, but the number of relationships testifies to the inability of any one of them to fit all velocity ranges and projectile-target combinations. Some are enough alike that they need not be described separately. Therefore, the six relationships that most effectively demonstrate the differences between the many relationships reviewed have been selected for this discussion.

It has been established that in the hypervelocity region the shape of the crater tends to be hemispherical, and that the crater dimensions will scale linearly with the diameter, or equivalent spherical diameter, of the projectile. Beyond these points of agreement there is little similarity between the six relationships. These six are as follows:

(1) $$\frac{p}{d} = \left(\frac{3}{4\pi k}\right)^{1/3} \left(\rho_p V^2\right)^{1/3}$$ Atkins (Ref. 1) (2.1)

p = depth of penetration
d = diameter of projectile
k = 690 joules/cm^3 for Al vs. Al
ρ_p = density of projectile, gm/cm^3
V = velocity of projectile, cm/sec

(2) $\frac{p}{d} = k \left(\rho_p V\right)^{1/3}$ Bjork (Ref. 2) (2.2)

where p = depth of penetration

d = diameter of projectile

k = 0.878 for Al vs. Al, = 0.488 for Fe vs. Fe

ρ_p = density of projectile, gm/cm^3

V = velocity of projectile, km/sec

(3) $\frac{p}{d} = 2.25 \left(\frac{\rho_p}{\rho_t}\right)^{2/3} \left(\frac{V}{C}\right)^{2/3}$ Charters & Summers (Ref. 3) (2.3)

where p = depth of penetration

d = diameter of projectile

ρ_p = density of projectile

ρ_t = density of target

V = velocity of projectile

C = sonic velocity in target material

(4) $\frac{p}{d} = 0.795 \times 10^{-3} \left(\frac{\rho_p V^2}{B}\right)^{1/3}$ Eichelberger & Gehring (Ref. 4) (2.4)

where p = depth of penetration

d = diameter of projectile

ρ_p = density of projectile, gm/cm^3

V = normal component of velocity of projectile, cm/sec

B = hardness of target material, Bhn

(5) $\frac{p}{d} = k_1 \left(\frac{\rho_p}{\rho_t}\right)^{2/3} \log_e \left(1 + \frac{\rho_p^{2/3} \rho_t^{1/3} V^2}{k_2 H_t}\right)$ Herrmann & Jones (Ref. 5) (2.5)

where p = depth of penetration

d = diameter of projectile

k_1 = constant (about 0.6 for most materials)

ρ_p = density of projectile, gm/cm^3

ρ_t = density of target, gm/cm^3

V = velocity of projectile, km/sec

k_2 = constant (about 4 for most materials)

H_t = hardness of target, Bhn

(6) $$\frac{p}{d} = \gamma\left(\frac{\rho_p}{\rho_t}\right)^{1/2}\left(\frac{V}{C}\right)^{2/3}$$ Loeffler, Lieblein & Clough (Ref. 6) (2.6)

where p = depth of penetration

d = diameter of projectile

γ = constant (1.5 to 2.5 for most materials)

ρ_p = density of projectile

ρ_t = density of target

V = velocity of projectile

C = sonic velocity in target material $= \sqrt{\frac{E_t\, g}{\rho_t}}$

Bruce (Ref. 7), in a thorough review of existing experimental data applicable to the impact of high velocity particles with semi-infinite targets, arrived at the following empirical relation:

$$\frac{p}{d} = 1.96\left(\frac{\rho_p}{\rho_t}\right)^{1/2}\left(\frac{v}{C}\right)^{2/3} \qquad (2.7)$$

Since this expression is almost identical to that developed by Loeffler, et al., it will not be treated separately in this report.

The above relationships have all been normalized with respect to p/d, depth of penetration/diameter of projectile. Figure 2.1 is a comparative plot of the six empirical penetration laws for the following case:

A) Projectile – 2017 Aluminum, $\rho_p = 2.80$ gm/cm^3

B) Target – 2024-T3 Aluminum, $\rho_t = 2.77$ gm/cm^3

$B, H_t = 120$ Bhn

$C_t = 5.1$ km/sec

C) Normal Impact – $\alpha = 0^o$

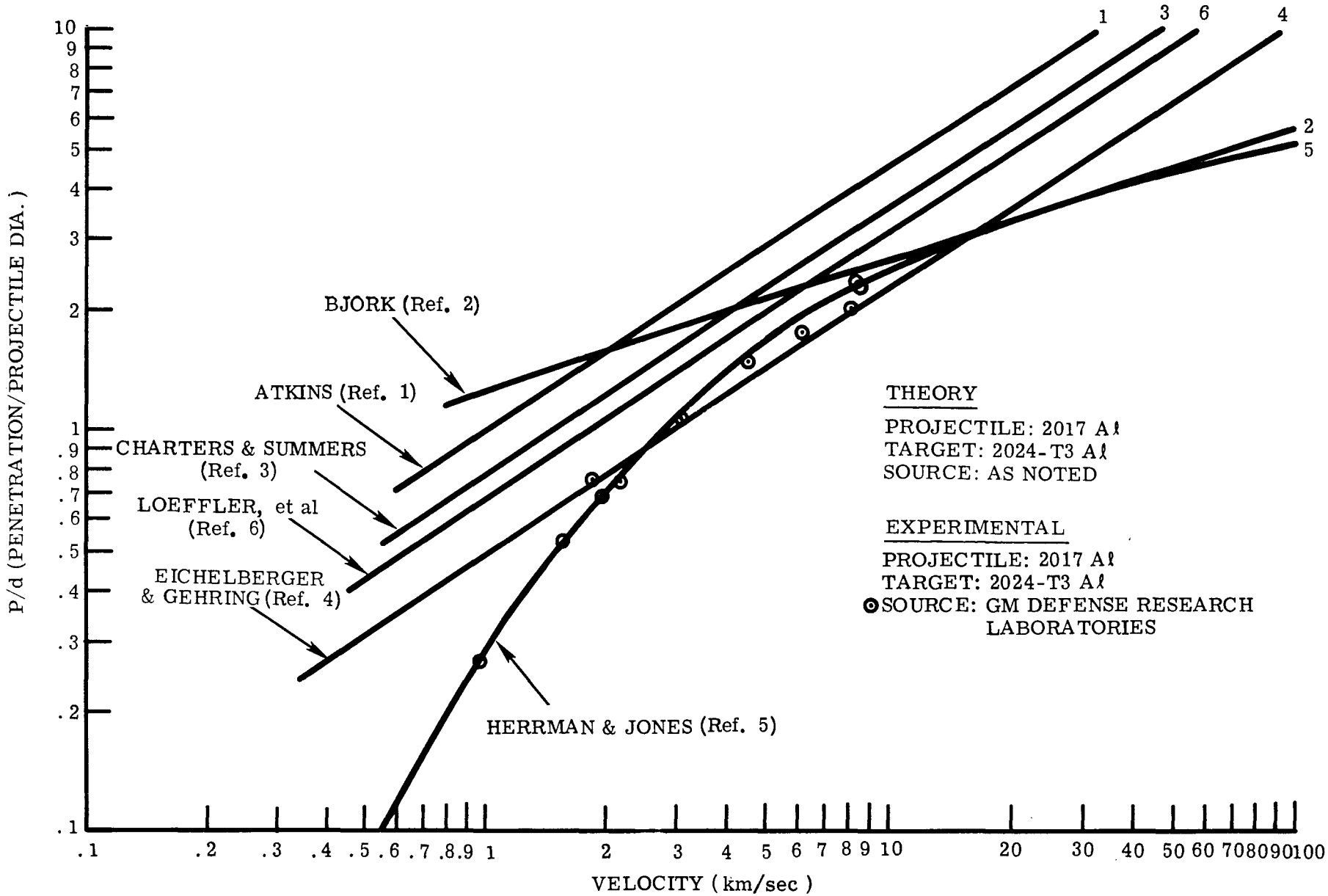

Fig. 2.1 Empirical Penetration Laws for Aluminum Projectiles and Targets

Also shown on Fig. 2.1 is a series of data points obtained by Maiden, et al., (Ref. 8). These points are for 1/8-in. diameter aluminum spheres impacting semi-infinite aluminum targets. The relationships of the empirical curves to the data points can be summarized as follows:

(1) Atkins, Charters & Summers, and Loeffler, et al.

These three curves can be expressed as $p/d = k\,(V)^{2/3}$, where k = .99 for Atkins, k = .764 for Charters, and k = .678 for Loeffler. All three curves have about the same slope as the data points in the range of 2–9 km/sec but are conservative in that the predicted p/d will range from 25 to 100 percent higher than actually observed in experiments. Below 2 km/sec, the fit of curves to data points becomes quite poor; this is to be expected since this level is definitely below the hypervelocity region. Above 9 km/sec, the lack of experimental points does not permit any definite conclusions, but it does appear that the curves will continue to be conservative.

(In a later paper (Ref. 9), Charters and Summers use a combination of Eq. 2.3 and a simple model of the impact process to derive another relationship. This new formula shifts the emphasis from the speed of sound to the strength of the target material and is given by

$$\frac{p}{d} = 0.50 \left(\frac{\rho_p}{\rho_t}\right)^{1/3} \left(\frac{\rho_p V^2}{2 S_t}\right)^{1/3} \qquad (2.8)$$

where S_t is assumed to be a constant deformation strength of the material. Unfortunately, the values of S_t are not well known for the conditions of hypervelocity impact. However, Charters and Summers suggest that an impact experiment be conducted and, from Eq. 2.8 and the measured crater depth, a value for S_t be derived. This value can then be used to predict damage in the same target material but under different impact conditions. The derivation of Eq. 2.8 is treated in detail in Section 3.3.)

(2) Eichelberger & Gehring

This curve can also be expressed as $p/d = k\,(V)^{2/3}$, where k = .490, and has about the same slope as the data points in the range of 2–9 km/sec; however, the fit with the data points is much better, having a maximum

deviation on the order of ± 15 percent. Above 9 km/sec, the data points might continue to follow a $(V)^{2/3}$ slope, but data points in the 20–40 km/sec range are needed to verify or reject this hypothesis. (Eichelberger & Gehring's Eq. 2.4 was derived from the relationship $V = 4 \times 10^{-9} E/B$, where V is crater volume in cm^3, E is projectile kinetic energy in ergs, and B is target hardness in standard Bhn. This relationship applies to meteoroid impact conditions where velocities can be expected to range from 10 to 70 km/sec; hence, Eq. 2.4 is subject to the same conditions. At lower impact velocities, a factor T which is a measure of the primary penetration phase of crater formation (see Sections 3 and 4D) becomes important and should be added. T is proportional to $(\rho_p / \rho_t)^{1/2}$ but is essentially independent of velocity; therefore, as velocity increases, the contribution of T to the total penetration becomes negligible.

(3) Bjork

This curve, which can be expressed as $p/d = k (V)^{1/3}$ where k = 1.24, is based on momentum considerations and is extremely conservative below 8 km/sec; but there is a definite trend of the data points toward this curve above 8 km/sec. Again, however, experimental data in the range of 20–40 km/sec is needed to verify or dispute this trend. (Note that Bjork's equation, usually regarded as theoretical, is considered here because the constant involved is a function of both projectile and target material and so has some empirical basis.)

(4) Herrmann & Jones

This curve, which can be expressed $p/d = k_1 \log_e (1 + k_2 V^2)$, where k_1 = .604 and k_2 = .593, shows very good agreement with experimental results in the 1–9 km/sec range. This might be expected, since this curve is truly an empirical one and is based primarily on a large number of data points rather than on the application of momentum or energy considerations to a limited number of data points. Between 9 and 100 km/sec this curve agrees very closely with Bjork's curve, but, again, experimental verification is lacking.

2.1 EFFECT OF VELOCITY

The question of whether the penetration of the target is related to the energy, to the momentum, or to some other function of the velocity of the projectile remains unanswered.

Clearly the relationship of Bjork is one of momentum, while the relationships established by Charters and Summers, Atkins, Eichelberger and Gehring, and Loeffler, et al., are related to the projectile's energy. The relationship of Herrmann and Jones may be expanded in series form as,

$$p/d = k_1 \left[x - \frac{1}{2} x^2 + \frac{1}{3} x^3 - \cdots \right] \qquad (2.9)$$

$$\text{where } x = \frac{\rho_t V^2}{k_2 H_t}$$

This equation does not appear to indicate much as to the physical significance of either energy or momentum of the projectile. As discussed in Herrmann and Jones' paper and shown above, this relationship seems to fit the existing data points at relatively low velocities as well as the points for very high velocities calculated by Bjork. Thus it would seem that the fit might be good over a wide range of velocities, even though the physical significance is evidently missing.

The data of Eichelberger and Gehring indicate that there is little variation in the linear volume/energy relationship to velocities of 12 km/sec. At this point, the data are approaching the meteoric velocities of primary concern.

2.2 EFFECT OF TEMPERATURE

It has been shown that target strength can affect crater size. The strength of the target is, of course, a function of its temperature. In these relationships, the effect of temperature of the target material is included (excepting the Bjork and Atkins formulas, although they contain a "constant" which may vary as a function of temperature), in the Brinell hardness number or wave velocity, both of which are reduced at elevated temperature. In general, the empirical relationships show that the penetration will be inversely proportional to either the two-thirds power of the wave velocity or the one-third power of the hardness of the target.

In their paper, Eichelberger and Gehring have summarized a series of experiments which show that the crater volume appears to increase approximately in proportion to a factor $\theta = T/T_{melting}$, where T is temperature. With aluminum targets, for example, they find that at 700°F the crater volume will be about seven times that at room temperature, indicating a penetration ratio $\left(P_T/P_o\right)$ of about 1.9. If the above empirical corrections for wave velocity and hardness are applied to a similar target, the following results are obtained:

2024-T3 ALUMINUM TARGET

Wave Velocity, C	Target Hardness, H
$E_o = 10.6 \times 10^6$ psi	$H_o = 120$ Bhn
$E_T = 5.0 \times 10^6$ psi*	$H_T = 20$ Bhn*
$E_o/E_T = 2.1$	$H_o/H_T = 6.0$
$C_o/C_T = (E_o/E_T)^{1/2} = 1.45$	$P_T/P_o = (H_o/H_T)^{1/3} = \underline{1.8}$
$P_T/P_o = (C_o/C_T)\ 2/3 = \underline{1.3}$	

* Estimated for 700°F

E = Modulus of elasticity

P = Depth of penetration

Subscript o = Room temperature

Comparing these calculated values of P_T/P_o with the experimentally determined values, it is seen that closer agreement is realized with a correction based on target hardness than on wave velocity. (See Section 4E for a discussion of target strength and temperature.)

2.3 EFFECT OF TARGET STRENGTH

The effect of target strength is partially included in paragraph 2.2, a discussion of the effects of temperature. Of the relationships selected, the only ones which include the effect of target strength by considering hardness are the Eichelberger

and Gehring formula and the Herrmann and Jones formula. It is obvious that the others will be unable to differentiate between various degrees of work-hardening or heat-treatments (for example) where the sound velocity remains essentially constant. (See Section 4E for a discussion of target strength and temperature.)

2.4 EFFECT OF TARGET DENSITY

The formulas of Charters and Summers, Loeffler, et al., and Herrmann and Jones are unique insofar as the density of the target material appears as a discrete term. The formulas of Atkins and Bjork carry constants which are undoubtedly based on target parameters, but here the effects of density cannot be separately determined.

In the relationships given by Charters and Summers, Herrmann and Jones, and Loeffler, et al., as well as in the data obtained by Maiden, et al., (Ref. 10) the exponent attached to the target-density term varies from -. 80 to -. 50, a change which can result in a variation in penetration/projectile diameter of up to $\pm$ 9 percent for a target density of 3 gm/cc.

2.5 EFFECT OF PROJECTILE PARAMETERS

As noted, all the listed relationships dictate that the penetration will be proportional to the projectile diameter. Also, all these relationships show that penetration (normalized with respect to projectile diameter) is proportional to projectile density. However, they do not agree on the influence of projectile density (i. e., the exponent) which ranges from 1/3 for Atkins, Bjork, and Gehring and Eichelberger, to 2/3 for Charters and Summers, and Herrmann and Jones. For a projectile density of 3 gm/cc, this disagreement can cause a variation in penetration/projectile diameter of $\pm$ 18 percent. (See Section 4F for a detailed discussion of projectile configurations.)

2.6 PRACTICAL APPLICATIONS

As an illustration of the practical applications of the empirical penetration laws, the minimum skin thicknesses required for various spacecraft missions will be determined. The empirical law of Bjork and that of Eichelberger and Gehring

will be used for the following reasons: (1) Bjork's is typical of those laws based on momentum considerations, and Eichelberger and Gehring's is typical of those laws based on energy considerations; (2) these two laws bracket extrapolated penetration data in the velocity range to be covered, 15 – 30 km/sec; (3) both laws lend themselves to relatively straightforward mathematical interpretation and manipulation.

The determination of spacecraft design parameters will be based on a method followed by Collier (Ref. 11): First, the critical thickness required to prevent perforation will be found as a function of perforation rate; and second, the minimum thickness required to give a particular probability level of no perforation will be found as a function of mission variables, i. e., time, spacecraft area, and target or objective. It should be noted here that the minimum thickness thus determined will be on the low side, since spalling and other effects peculiar to thin targets will not be taken into account. (See Sections 4A and 4C of this report for a detailed discussion of these phenomena.)

2. 6. 1 The determination of critical thickness requires that certain variables be defined and assumptions made, as follows:

(1) Spacecraft shall be aluminum, giving for the penetration laws,

$$p = 1.09\ (mV)^{1/3} \qquad \text{Bjork} \qquad (2.10)$$

$$p = 0.43\ (mV^2)^{1/3} \qquad \text{Eichelberger and Gehring} \qquad (2.11)$$

where p = depth of penetration, cm

m = mass of particle, gm

V = velocity of particle, km/sec

(The use of 1. 09 as the constant in Bjork's equation implies a meteoroid density of 2. 7 gm/cm^3, since this constant is based on analysis of an aluminum/aluminum impact. Eichelberger and Gehring's equation, however, is independent of projectile density. It should be noted here that the equations of Charters and Summers, Herrmann and Jones, and Loeffler, Lieblein and Clough, when modified to include projectile mass as a distinct term, are <u>not</u> independent of projectile density which continues to appear as a separate term.)

(2) The meteoroid flux ϕ in number of particles of mass m, or greater, per square-meter-second shall be taken as,

Pessimistic, $\phi = 10^{-13} \times \frac{1}{m}$ (2.12)

(from Fig. 1.1)

Optimistic, $\phi = 10^{-15} \times \frac{1}{m}$ (2.13)

(from Fig. 1.1 and Ref. 12)

(The meteoroid flux ϕ is assumed to be uniform with respect to both time and space.)

(3) The mass/velocity distribution for meteroids (based on Refs. 11, 13) shall be taken as follows:

Mass (gm)	10^{-12}	10^{-10}	10^{-8}	10^{-6}	10^{-4}	10^{-2}	10^{0}
Velocity (km/sec)	16	18	20	22	24	26	28

(4) It is assumed that the spacecraft surface is spherical and that all impacts are normal to the surface.

By calculating depth of penetration p for a given mass/velocity combination (using Eqs. 2.10 to 2.13), the curves given in Fig. 2.2 can be obtained. These curves define the average perforation rate for a particular value of skin thickness. As would be expected, for a given skin thickness the rate of perforation is less for the optimistic flux rate, $10^{-15} \times \frac{1}{m}$, than for the pessimistic flux rate, $10^{-13} \times \frac{1}{m}$. Also, as can be inferred from Fig. 2.1, the rate of perforation is less for Bjork's than for Eichelberger and Gehring's relationship; however, the velocity range and mass/velocity distribution chosen for this example have made the differences between the two laws small enough to be insignificant.

2.6.2 The minimum thickness required to give a particular probability level of no perforation can now be determined by applying a statistical model to the results given in Fig. 2.2. A Poisson distribution will be assumed for the example being considered,

$$p\ (a/H) = \frac{r^a}{a!}\ e^{-r} \qquad (2.14)$$

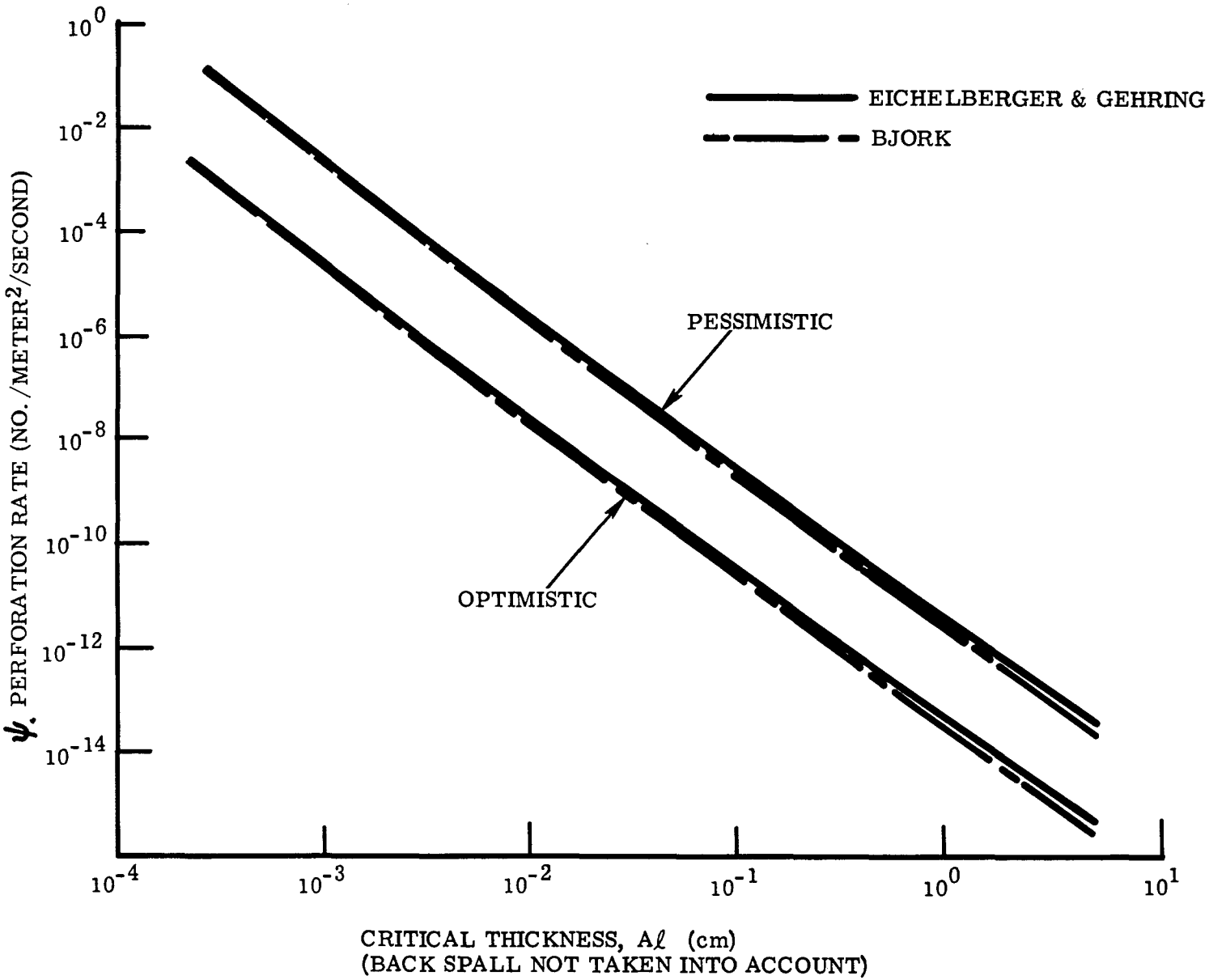

Fig. 2.2 Perforation Rate vs. Critical Thickness

where p (a/H) = the probability of a occurrences under a given set H of assumed propositions.

r = xn = chance of event or rate of event, x, times the number of trials or duration of trials, n

Letting a = O (no perforation)

x = ψ (perforation rate)

n = AT (area of spacecraft times duration of mission)

This can be put in the form

$$p(o) = e^{-\psi \quad AT} \tag{2.15}$$

The assumption of a Poisson distribution is reasonable since, although there is small chance of an event occurring in any one trial (i. e., the perforation rate is low), there are so many trials (i. e., the time involved is relatively long) that there is a good probability that the event may occur (Ref. 14).

Applying Eq. 2.15 to the curves in Fig. 2.2 (averaging Bjork's and Eichelberger and Gehring's curves since the differences in critical thicknesses are relatively small for the particular set of conditions being considered), and assuming an arbitrary yet reasonable range for AT, the curves given in Fig. 2.3 can be obtained. As would be expected, the minimum thickness required for a given mission (i. e., the value of AT) increases with the increasing probability of no perforation and is less for an optimistic meteoroid flux than for a pessimistic meteoroid flux. This example can be carried one step farther by tabulating the minimum skin thicknesses (neglecting spall effects) required for specific spacecraft/mission parameters. Such a tabulation is given in Tables 2.I (optimistic meteoroid flux) and 2.II (pessimistic meteoroid flux). The three missions listed are based on the application of the following requirements to Fig. 2.3.

(1) Moon: Spacecraft surface area = 100 square meters
Transit time (round trip) = 4.6 days (Ref. 15)

(2) Venus: Spacecraft surface area = 100 square meters
Transit time (round trip) = 300 days (Ref. 15)

(3) Mars: Spacecraft surface area = 100 square meters
Transit time (round trip) = 520 days (Ref. 15)

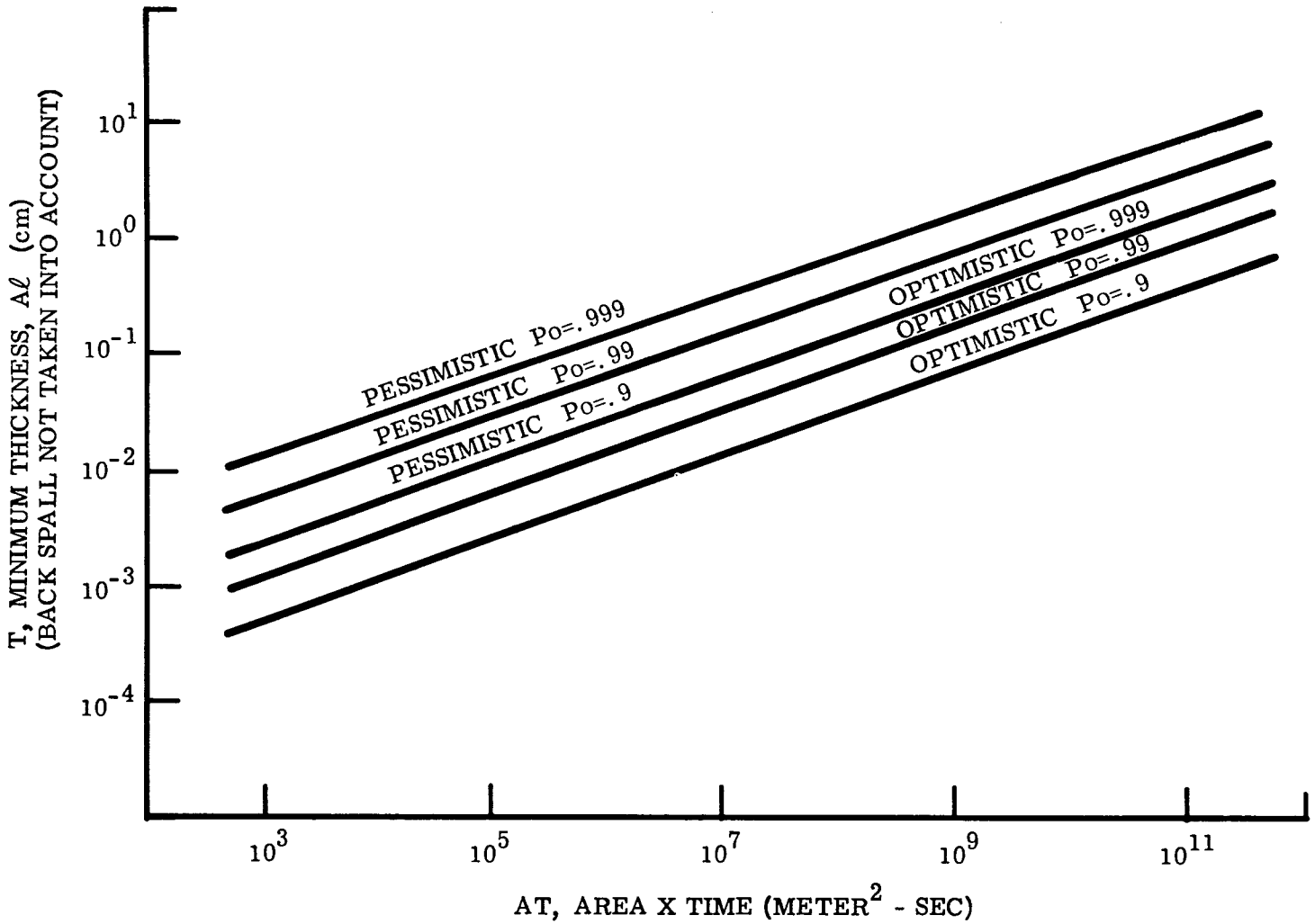

Fig. 2.3 Minimum Skin Thicknesses, Aluminum vs. Spacecraft Design Parameters

Table 2.I

SPACECRAFT SKIN THICKNESSES, ALUMINUM, FOR VARIOUS MISSIONS
(OPTIMISTIC METEOROID FLUX)

	Probability of No Perforations Optimistic Meteoroid Distribution $10^{-15} \times \frac{1}{m}$		
Mission Round Trip	.9	.99	.999
Moon	0.022 cm	0.052 cm	0.10 cm
Venus	0.10 cm	0.25 cm	0.44 cm
Mars	0.13 cm	0.30 cm	0.55 cm

Table 2. II
SPACECRAFT SKIN THICKNESSES, ALUMINUM,
FOR VARIOUS MISSIONS (PESSIMISTIC METEOROID FLUX)

	Probability of No Perforations Pessimistic Meteoroid Distribution $10^{-13} \times \frac{1}{m}$		
Mission Round Trip	.9	.99	.999
Moon	0.10 cm	0.23 cm	0.47 cm
Venus	0.44 cm	1.0 cm	2.1 cm
Mars	0.55 cm	1.3 cm	2.5 cm

The values listed in Tables 2. I and 2. II show that, for the particular conditions used in this example, the minimum aluminum skin thicknesses range from 0. 022 cm (0. 009 in.) for a lunar round trip under optimistic conditions, to 2. 5 cm (0. 98 in.) for a round trip to Mars under pessimistic conditions. All of the results given are for the case of a single-hulled, aluminum (2024-T3 or equivalent) vehicle with thin-target effects neglected; however, corresponding values for other configurations and materials could be obtained by appropriate selection of penetration equations and the constants used in these equations.

REFERENCES FOR SECTION 2 - EMPIRICAL APPROACHES

1. W. W. Atkins, "Hypervelocity Penetration Studies," Proceedings of the Fourth Symposium on Hypervelocity Impact, Eglin Air Force Base, Fla., APGC-TR-60-39, Vol. 1, Sep 1960

2. R. L. Bjork, "Meteoroids vs. Space Vehicles," ARS J., Vol. 31, No. 6, Jun 1961, pp. 803-807

3. A. C. Charters and J. L. Summers, "High-Speed Impact of Metal Projectiles in Targets of Various Materials," Proceedings of the Third Symposium on Hypervelocity Impact, Armour Research Foundation, Chicago, Feb 1959

4. R. J. Eichelberger and J. W. Gehring, "Effects of Meteoroid Impacts on Space Vehicles," ARS J., Vol. 32, No. 10, Oct 1962, pp. 1583-1591

5. W. Herrmann and A. H. Jones, "Correlation of Hypervelocity Impact Data," Proceedings of the Fifth Symposium on Hypervelocity Impact, Colorado School of Mines, Nonr-(G)-0020-62(X), Vol. 1, Part 2, Apr 1962

6. I. J. Loeffler, Seymour Lieblein, and N. Clough, "Meteoroid Protection for Space Radiators," ARS paper No. 2543-62 (presented at the ARS Space Power Systems Conference, Santa Monica, Calif., Sep 1962)

7. E. P. Bruce, "Review and Analysis of High-Velocity Impact Data," Proceedings of the Fifth Symposium on Hypervelocity Impact, Vol. 1, Part 2, Nonr-(G)-0020-62(X), Colorado School of Mines, Apr 1962

8. C. J. Maiden, J. W. Gehring and A. R. McMillan, "Investigation of Fundamental Mechanism of Damage to Thin Targets by Hypervelocity Projectiles," Semi-Annual Report, Contract ARPA Nonr-3891 (00)(X), General Motors Corporation, GM Defense Research Laboratories, Report No. TR63-208, Mar 1963 (work reported in this paper was presented at the Sixth Hypervelocity Impact Symposium, Cleveland, Ohio, Apr 30 – May 2, 1963

9. A. C. Charters and J. L. Summers, "Some Comments on the Phenomena of High-Speed Impact," Proceedings of the Decennial Symposium, White Oak U. S. Naval Ordnance Laboratory, 1959

10. C. J. Maiden, et al, "On Investigation of Spalling and Crater Formation by Hypervelocity Projectiles," Proceedings of the Fourth Symposium on Hypervelocity Impact, Vol. 3, APGC-TR-60-39, Eglin Air Force Base, Fla., Sep 1960

11. K. I. Collier, "The Range and Sources of Uncertainty in Current Meteoroid Damage Estimates," Master of Science Thesis, No. GA/Mech 62-1, School of Engineering, Air Force Institute of Technology, Aug 1962

12. W. M. Alexander, "Cosmic Dust" (from "The Mission of Mariner II: Preliminary Observations,") Science, Vol. 138, No. 3545, 7 Dec 1962, pp. 1098-1099

13. F. L. Whipple, "The Meteoritic Risk to Space Vehicles," Vistas in Astronautics, Vol. 2, M. Alperin, ed., Pergamon Press, New York, Feb 1958 (also, Proceedings of the VIII International Astronautical Congress, Springer-Verlag, Vienna, 1957)

14. H. Jeffreys, Theory of Probability, Clarendon Press, Oxford, 1961, p. 68

15. Staff Report of the Select Committee on Astronautics and Space Exploration, "Space Handbook: Astronautics and Its Applications," House Document No. 86, 86th Congress, 1st Session, Washington, D. C., 1959

SECTION III

PHENOMENOLOGICAL MODELS AND THEORETICAL APPROACHES

3.1 INTRODUCTION

This section will review the basic phenomena of hypervelocity impact, including the fundamental observations of crater formation and the detailed phenomenological model which can be derived therefrom. An attempt will be made to relate several selected experimental and theoretical approaches to the basic model and to describe the extent to which each approach covers the basic phenomena. The many physical observations of crater formation are discussed and synthesized into a model of the process, detailed to represent physical reality instead of being merely a mathematically tractable approach.

Early investigators of the hypervelocity impact phenomena, such as Opik, 1936 (Ref. 1), Grimminger, 1948 (Ref. 2), Pugh, et al., 1948 (Ref. 3), Rostocker, 1953 (Ref. 4), and Goranson, et al., 1955 (Ref. 5), used an empirical approach based upon hypothetical considerations. Opik treated the projectile impact according to the basic principles of mechanics; that is, the projectile was deformed in its entirety immediately after impact, as described by Bernoulli's equations for the pressures generated at the interface and in accordance with the conservation of radial momentum. Opik's treatment was based upon an infinite wave velocity in the projectile – not a physical reality, of course. In addition, it has since been shown that there exists a variation in linear momentum with time after impact wherein $M_p + M_{ejecta} = M_{total}$. On the other hand, Grimminger considered the use of a basic drag equation to be dependent upon the resistance of the target material to a projectile that is not deformed by the impact and penetration – again, a situation which is physically invalid.

More accurate approaches to the phenomena were made by Pugh, Rostocker, and Goranson, all of whom treated the target and the projectile as incompressible

fluids wherein the flow was assumed to be in a steady state when viewed from a frame of reference moving with the penetration velocity. From the basic conservation equations, each was able to determine the stagnation pressure at the interface. This treatment assumed that the penetrations ceased when the pressure reached the dynamic yield point of the target material. (Unfortunately, however, this dynamic yield point was not known under the conditions of impact.)

In addition, for the case of a very short projectile, i. e., a sphere, it is questionable that the assumption of steady state hydrodynamics is applicable, since it has been shown that the penetration does not cease as soon as the projectile has been consumed by the target, and that a hypervelocity projectile imparts to the target material a kinetic energy which must be dissipated within it. The energy is spent in the form of kinetic energy of the ejecta from the target and in thermal energy within the target from attenuation of the shock that is transmitted through the target material. This flow of the target material after the projectile has been consumed is commonly known as secondary penetration, or cavitation. In shaped-charge jet penetrations, the secondary flow is of small consequence; whereas, in hypervelocity projectile impact, the secondary flow forms the major part of the crater. Hence, the assumptions made in these early treatments led to very large errors. Later treatments by Gilvarry and Hill, 1956 (Ref. 6), Cook, 1959 (Ref. 7), and Staniukovich, 1962 (Ref. 8) used essentially a one-dimensional shock analysis together with the appropriate equations of state to compute the extremely high pressures and temperatures created at the interface. These high pressures were then related to the heats of fusion and heats of vaporization of the material, and the so-called "explosion hypothesis" was born. Here again, these treatments were based upon an incorrect physical model, and the empirical relationships derived therefrom were not borne out by the results of crater measurements obtained experimentally.

In still another analytic approach, Zaid, 1962 (Ref. 9) formulated the equations of motion for the case of an undeformed projectile penetrating a deformable target. This model of an expanding fluid zone just ahead of the projectile could be applicable immediately after impact but would be valid for only a fraction of a microsecond, i. e., until the pressures rose to exceed the yield strengths of both the projectile and target materials.

Still later, Bjork in 1958 (Ref. 10), and Walsh and Tillotson in 1963 (Ref. 11), used a high-speed digital computer to make computations of the craters produced by hypervelocity impact. The differential equations used by Bjork were based on the nonsteady compressible hydrodynamics that govern compressible fluid flow. However, the equations that were used do not take into account the shear strength and viscous forces of the projectile, nor do they take into account the shear and viscous resistance of the target to secondary flow after the projectile has been "used up".

Since many of the experimental observations of the phenomena of crater formation can be explained by each of several theoretical models, claims have been made as to the certainty of each approach. While these claims are often correct for a specific instance, the model usually handles only one or two of the more numerous physical processes involved. These complex physical processes and the problems associated with the mathematical equations required for their solutions cannot be ignored by simplifying assumptions.

A critical look into the detailed physical model encompassing many modes of crater formation and into the theoretical approaches that have already been undertaken to cover certain modes will aid in the planning of future research and will help single out the pertinent physical parameters which should be measured. An inquisitive look at the detailed model of the cratering process should reveal the assumptions made by, and the critical parameters considered by, each investigator. It is also necessary to note those areas of unanimity concerning the general character of craters and the mechanism of their formation. When these critical examinations are made, a more phenomenological approach to the problem will no doubt be necessary, so that the theoretical model described can be used on its own merit when making comparisons with experimental data.

Therefore several fundamental observations of crater formation, the model derived therefrom, and the extent to which the theoretical efforts describe the total phenomena are presented for examination.

3.2 MODEL OF CRATER FORMATION IN SEMI-INFINITE TARGETS

3.2.1 First Phase of Impact Cratering

A model evolved from the combined theoretical and experimental studies of many researchers is illustrated schematically in Fig. 3.1 (Ref. 12). The process is dynamically illustrated (Fig. 3.2) with selected frames of a Beckman & Whitley camera record of the impact of a projectile on an aluminum target. The projectile can be seen approaching the target at a velocity greatly in excess of the wave propagation velocity in either the impacting particle or the target material. Immediately after the projectile contact with the target material, the first phase, or transient state (in which the pressure at the interface pertains to a plain one-dimensional impact, that is, the megabar range) begins.

Shock waves propagate a short distance from the contact surface in both the projectile and the target, and then rarefactions released at the boundary of the projectile start a lateral flow of both materials. During the first phase, an impact flash is observed to last for only a very brief period (approximately 1 microsecond, as seen in the B&W camera frames of Fig. 3.2). During the initial stages of the process, some fusion and ionization of both the projectile material and target material occur. Although neither phenomenon has been observed to have a detectable effect on the correlations obtained, several significant observations should be noted.

The appearance of an intense flash of light upon impact of the projectile is a result of the conversion of mechanical energy to electromagnetic energy (Refs. 13-16). Most certainly the energy of the projectile is expended in a number of possible reactions, among which are the generation of heat, the initiation of radiation (possibly over the spectrum from gamma rays to microwaves), and the mechanical work done in forming the impact crater. Although the experiments of Refs. 13 and 15 were concerned with monitoring only that portion of the energy which appears as visible light, it is reasonable to assume that the magnitude of the radiated visible light will be a function of the energy of the impacting projectile.

Since the target reacts to the impact in a manner dictated by the magnitude of the pressure pulse, it may also be reasonable to relate the intensity of impact flash to the properties of the shocked materials after collision. However, a process

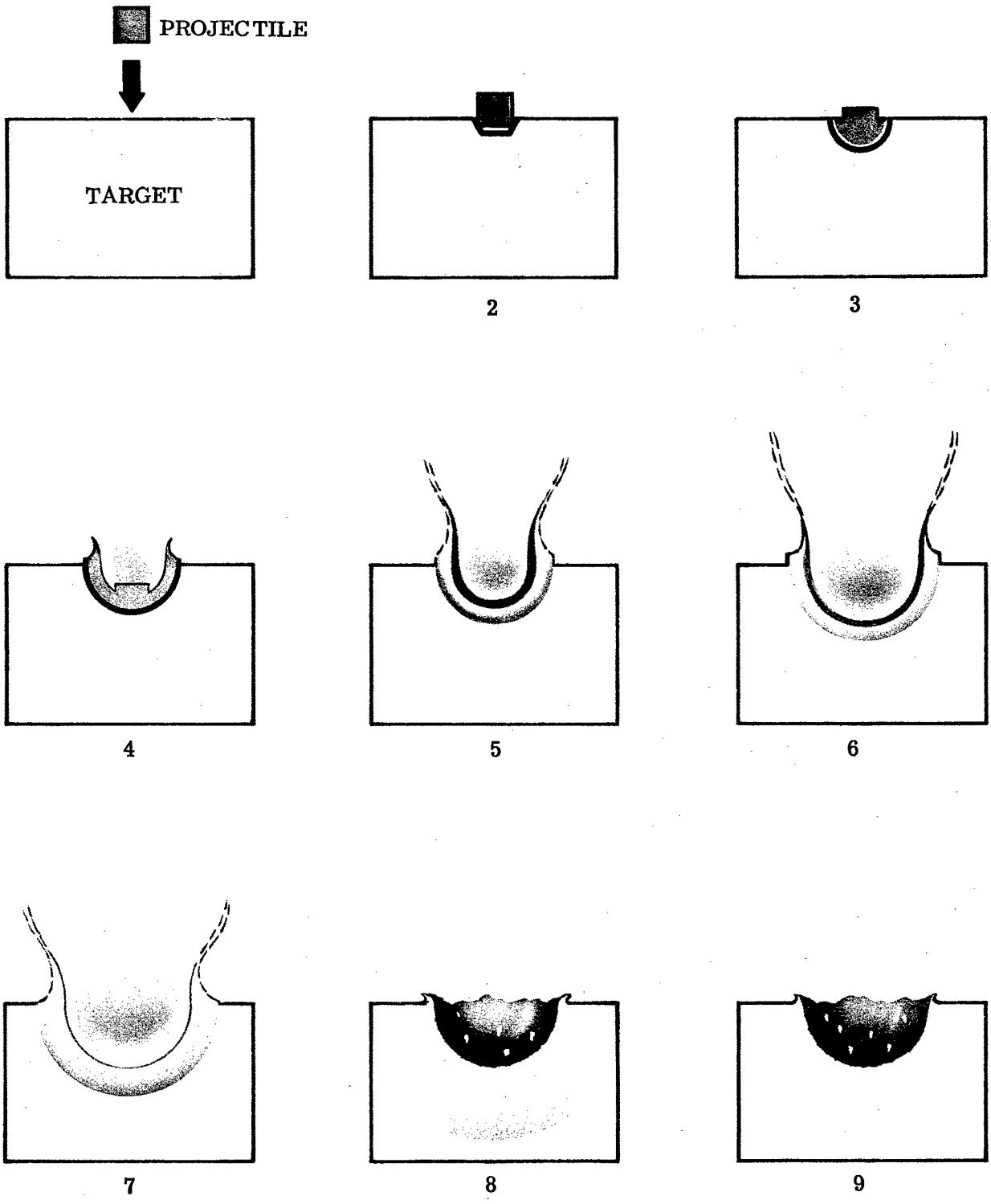

Fig. 3.1 Schematic of Projectile and Target Behavior on Impact of Solid Projectile with Thick Target

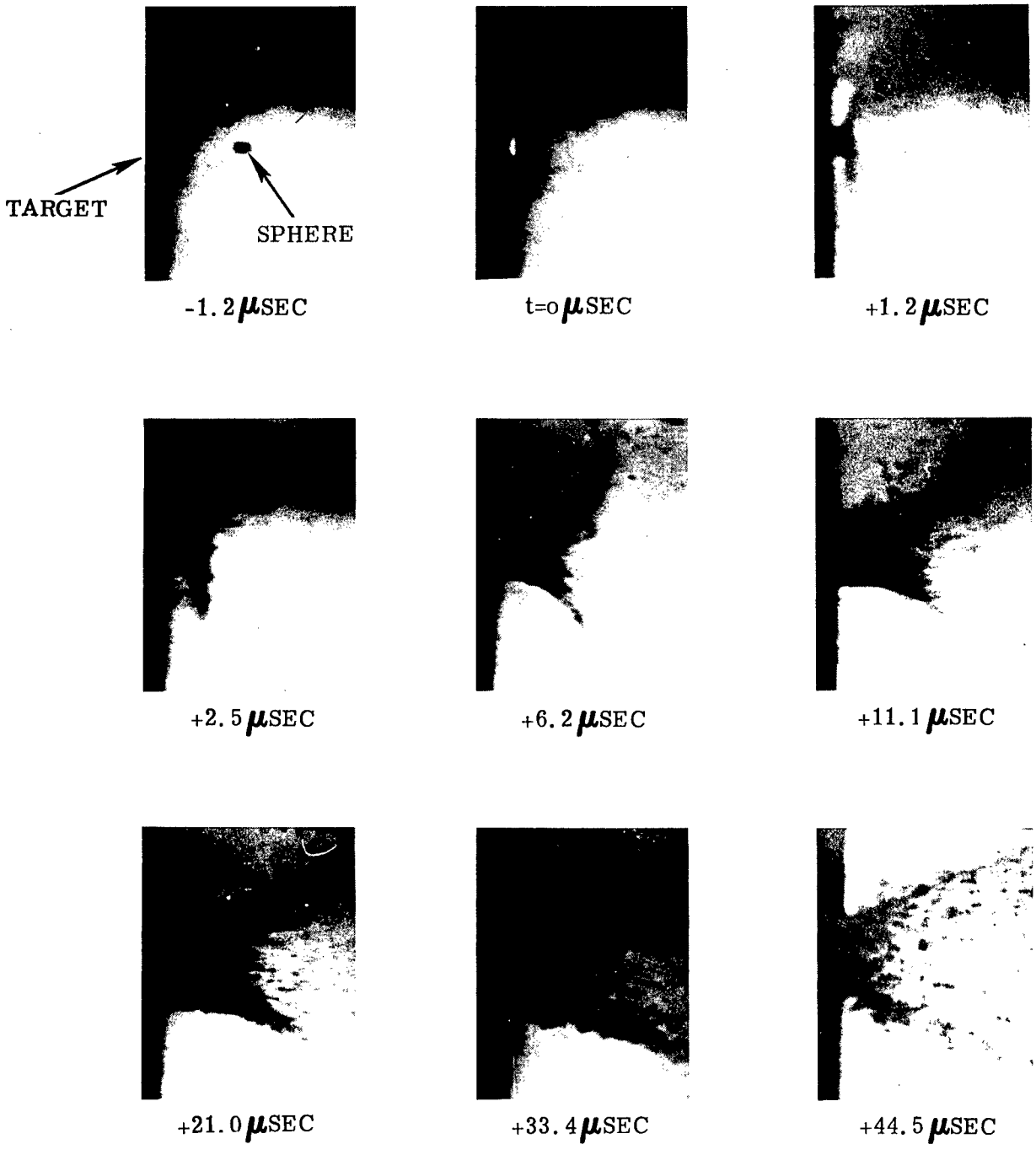

Fig. 3.2 Framing Camera Sequence of a 1/8-In. Glass Sphere Impacting a Cast Aluminum Block at 7.0 km/sec

by which luminosity is derived from the rapid application of pressure is not yet available. Consequently, a causal relationship between an impact-generated pressure and luminous radiation cannot be established by these experiments. (Of a more complex nature and much more difficult to define is the excitation energy of atoms under compression and the multiple electron problem in which electrons of different binding energies react in many different ways.)

An empirical relationship established (Ref. 15) from the phenomena permits estimates to be made of the intensity of an impact flash. The equation in its present form, however, can account for only variations in the target and projectile materials (by use of a constant for each of the possible combinations) and appears as,

$$L_p = Cav^n \qquad (3.1)$$

where L_p = peak luminosity (visible)

a = presented area of projectile on target surface

v = velocity of projectile

n = velocity exponent

C = a constant

Equation 3. 1 illustrates several important factors concerning impact flash. First, peak luminosity is proportional to projectile area, not to projectile mass (and, therefore, not to projectile momentum or kinetic energy). Second, peak luminosity is strongly influenced by impact velocity, since the exponent n varies from 3 to 9, depending on projectile and target properties. Third, the constant C is also a function of projectile and target properties (with target properties being more important than those of the projectile). Finally, it should be noted that there is no allowance in Eq. 3. 1 for either pressure or composition of surrounding gas. Measurements of impact flash have shown that peak luminosity is invariant with either composition or pressure for air and helium at pressures less than 10 mm Hg.

The variation of luminosity with time is shown for three impact conditions in Fig. 3. 3. It can be seen that peak luminosity is reached in less than a microsecond in all cases, but the subsequent time decay of the luminosity is strongly influenced by projectile and target materials.

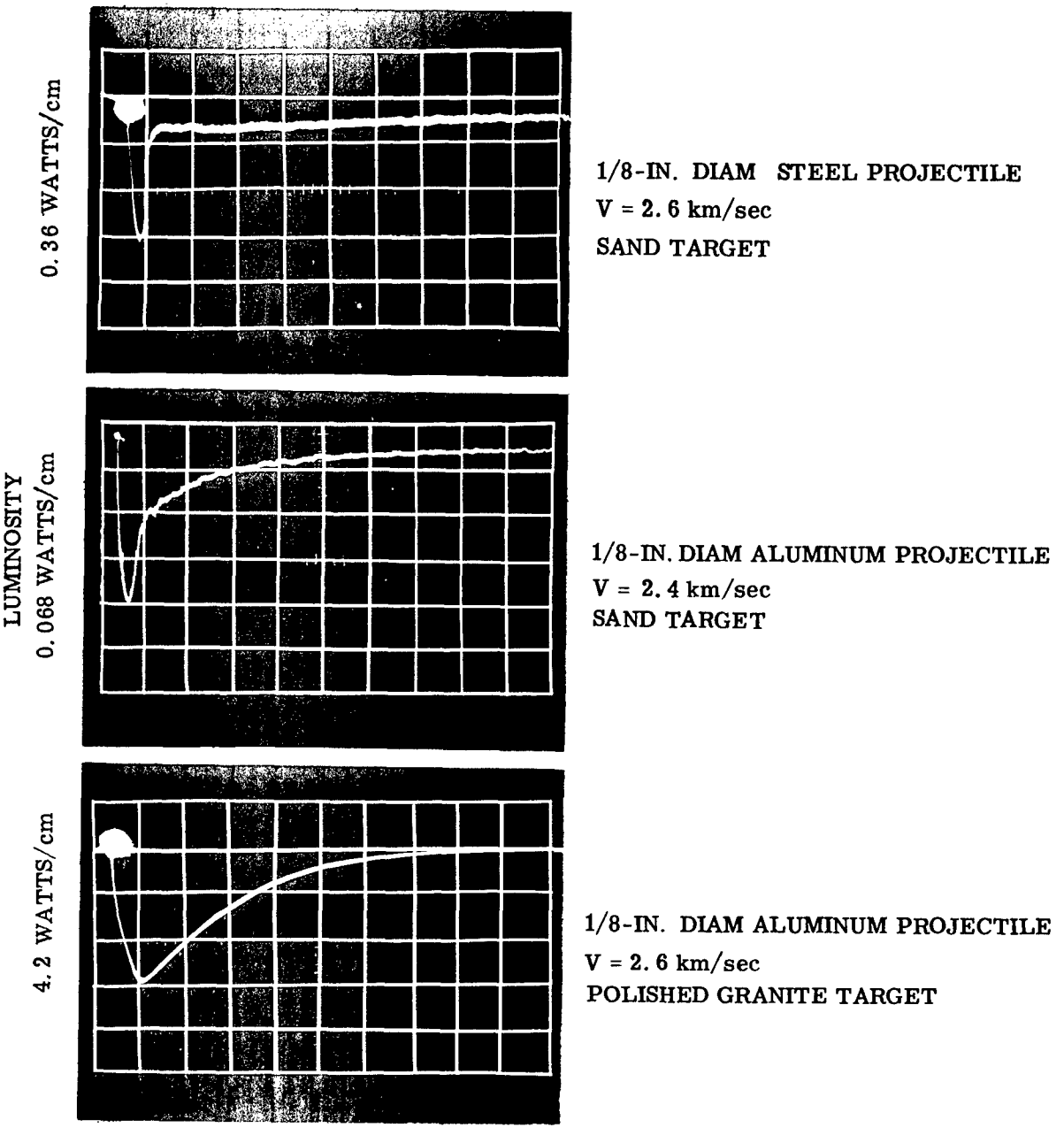

Fig. 3.3 Typical Photomultiplier Traces for Impacts of Various Projectile/Target Combinations

In examining this first transient stage of the cratering process during which the impact flash occurs, it is possible that several investigators considered the analogy of the cratering process to be identical to that formed by an equivalent mass of high explosive detonated in contact with the surface of the target, or to the analogy of crater size being a function of the heat required to remove a unit mass of target material. Cook and Stanukovich related the energy of the impacting projectile to that of an equivalent mass of high explosive from which the initial pressure on the front of the shock wave could be computed and the sharp drop in pressure with increasing distance from the point of initiation could be estimated. The mechanism of cratering includes vaporization and melting of target material, processes which cease when the energy density at the shock front becomes less than a certain value which had to be predicted empirically.

In similar fashion, other investigators, including Whipple (Ref. 17), Lavrentyev (Ref. 18), and Langton (Ref. 19), assumed a thermal penetration process in which the penetration takes place by melting or vaporization of the projectile and the target. In these assumptions, the heats of vaporization and the latent heats of fusion were used to limit the mass of material that could be removed by the kinetic energy of the incoming projectile. Although these approaches resulted in empirical relationships which were capable of predicting the final crater parameters for certain specific instances, they were found to be invalid for general use. In addition, the assumption that a single-valued physical process is the sole cause of the final crater has been seen by many experimenters to be incorrect. Also, neither the explosive analogy nor the thermal analogies for crater formation take into account either the primary penetration of the deforming projectile or the elastic/plastic recovery of the crater in the final stages.

Reviewing the model which covers the first phase of penetration described above, it is evident that the different properties of the impacting projectile and the impacted target are important during the first stage of crater formation. In the first, or transient stage, the impact velocity and the Hugoniot properties are the only significant parameters in establishing the pressures acting on the projectile and the target.

3.2.2 Second Phase of Impact Cratering

During the second, steady state stage, the densities and compressibilities of the projectile and target material as well as the velocity and the dimensions of the projectile all enter into any evaluation of the intensity and the duration of the pressure pulse produced. This second stage, commonly called the primary penetration stage, is that period during which the projectile acts as a causative force while being used up in a fluid flow process. The lateral dimensions relative to length of the projectile will determine the length of time required to achieve an equilibrium condition that is typical of the second stage. If the projectile length is small compared to the smallest lateral dimension, the steady regime will be unimportant; the energy will be dissipated during the transient regime and a broad, shallow crater will be obtained instead of the classical hemisphere. During this transient stage, shock waves are propagated from the contact surface into both the projectile and the target. At the same time, the pressure is released at the boundary of the projectile, initiating lateral flow of both materials.

With projectiles whose length is significantly greater than their lateral dimensions, the process of the steady state stage is far more important and the crater formation resembles that of shaped-charge jet penetration. These phenomena have been experimentally verified in Refs. 3 and 20. During this second stage, the region of compressed material is confined to a thin shell with extremely high energy density adjacent to the crater surface. This phenomenon was shown schematically in the third and fourth illustrations of Fig. 3.1. To reiterate, the projectile is used up as a causative force during the second stage.

The duration of the steady state regime can be estimated (Refs. 3, 12, 20) from hydrodynamic considerations,

$$t = \frac{\ell}{v}\left[1 + \left(\frac{\rho_p}{\rho_t}\right)^{\frac{1}{2}}\right] \qquad (3.2)$$

where t = time

ℓ = length of projectile

v = impact velocity

ρ_p = density of projectile

ρ_t = density of target

Both compressibility and strength are neglected in this simple formula, but it provides useful orders of magnitude. For example, a meteoroid 1 mm in length striking a body of equal density at a velocity of 40 km/sec would produce a steady state regime lasting only 0. 05 microseconds and would penetrate a distance of 1 mm into the body during that time.

3. 2. 3 Third Stage of Impact Cratering

After the impacting body has been completely deformed and has been removed as a causative force from the system, the shock wave continues to expand and with it the crater. This is the third, or cavitation, stage of crater formation. Although the rate of crater expansion and the intensity and velocity of the shock decrease, the crater surface undergoes a more rapid decrease in velocity. Therefore, the thickness of the shell of compressed target material increases. These phenomena have been experimentally verified in Ref. 12.

During the second and third stages of crater formation, shear deformation takes place parallel to the walls of the expanding crater. The flow velocity is so high that the projectile material and the target material are both ejected from the crater with considerable velocity. It is only at relatively low speeds that the pellet material is found plated or scattered as small particles over the surface of the final crater. The amount of shear that occurs at extremely high strain rates is responsible for the classification of target materials into two groups – ductile and frangible.

The ductile materials flow for a much longer time after impact, apparently because of the decrease in their resistance to deformation at extreme strain rates (Ref. 12). This behavior is not clearly understood, but it is similar to that used in some new impact extrusion processes. The frangible materials include the long chain polymers, silicous materials, and stones; in addition to their brittleness, they share a common monotonic increase in resistance to deformation with increasing strain rate– even at the very high strain rates involved in hypervelocity impact. As a result, the crater stops expanding in lucite earlier than in aluminum despite the relative magnitudes of their static shear strength.

This peculiarity of ductile materials has been one of the main sources of difficulty in formulating a complete theory. Hydrodynamic calculations, which

yield accurate predictions for the initial stages of the process, fail to predict final crater dimensions correctly because they take no account of the stage in which high strain-rate properties affect material flow. Since it is during this stage that a significant fraction of crater expansion takes place, calculation and experiment disagree in regard to depth of penetration and crater volume.

In developing the theoretical aspects of the third, or cavitation stage, the profiles of the pressure wave developed during the first two stages are of importance (Ref. 21, 22). In practice, as long as the pressures are high enough, the hydrodynamic approximation is accurate. (The resistance of the target material is significant only during the waning stages of the pressure pulse.) The cavitation stage of the process becomes so dominant in very-high-speed impacts on ductile materials that neither the density, compressibility, nor even the dimensions of the projectile can be detected in empirical correlations. At low impact velocities (6. 6 km/sec), however, the data in Section 4F (Figs. 4F. 2, 4F. 3) show that both the density and the shape of the projectile influence the crater volume and the shape of the crater.

In summary, therefore, the third or cavitation stage continues until the energy density behind the shock wave becomes too small to overcome the intrinsic resistance to deformation of the material, at which point the shock wave continues to expand as a low-intensity plastic and/or elastic wave (the crater may shrink somewhat from plastic and elastic recovery). In brittle materials, the tensile stresses produced by reflection of the shock wave from free surfaces will produce fracture and spall that may, in extreme cases, entirely obscure the form of the crater. These processes occur during the fourth, and final, stage of crater formation.

3. 2. 4 Fourth Stage of Impact Cratering

The fourth stage of crater formation is characterized by the reaction of the target material after the stress wave has been attenuated to a level that no longer causes flow or gross plastic deformation of the target material. Although this stage of crater formation is not considered in most theoretical approaches, experiments have been conducted to illustrate the three known reactions ((1) elastic/plastic recovery of the crater, (2) possible brittle spalling around the surface of the crater, (3) recrystallization of the metal in an area beneath the visible crater).

In the case of the elastic/plastic recovery of the crater, Kineke (Ref. 23) has shown that in the case of a target of 1100-F aluminum, the instantaneous crater depth and diameter reached a given maximum, then, in the final stages, the crater dimensions diminished; this would indicate that some recovery of the crater had occurred. The instantaneous crater dimensions were measured from sequential radiographs – in some instances, the final crater depth or diameter was as much as 20 percent less than the maximum reached during its formation. Much work remains to be done in describing the phenomena of crater recovery, particularly in estimating the amount of recovery for specific materials. Although a detailed analysis has not been carried out, it has been postulated that the compressed shell of material under the crater will undergo recovery to the degree allowed by

$$R = f\left[\frac{\sigma_y}{E}(\nu)\right] \tag{3.3}$$

where

σ_y = dynamic yield stress of the target material

E = dynamic Young's Modulus

ν = Poisson's ratio

In another set of experiments, flash radiographs were taken of incipient craters in both lucite and soft aluminum (Refs. 21, 23, 24) at periodic intervals during crater formation. The radiographs of the aluminum targets are enlightening in that they show the phenomena described earlier – the development of a hemispherical crater, the formation of the lip, etc. Careful measurement of the pictures, however, shows that the final crater size is less than the maximum size reached during the period of crater formation. These results are confirmatory evidence of the suspected elastic recovery of the target material under conditions of extremely high strain rates.

The pictures of the crater forming in lucite are of more immediate interest as they show that the process of crater formation in a very brittle material is not intrinsically different from that prevailing in the ductile aluminum – that is, the crater is formed in the same hemispherical fashion, although without the lip characteristic of ductile materials. At the same time, however, the initiation and propagation of cracks in the plastic target material demonstrate why the final craters observed in such frangible materials are so drastically different

from those observed in ductile materials. The effects of reflected tension waves upon materials that have relatively low tensile strength produce extensive spalling and fracture, both of which lead to the removal of a large amount of material from a layer near the surface. As a consequence, the diameter of the crater is increased although the depth is not. The process of crater formation itself is, however, no different from that observed in the ductile material.

Many investigators have studied the third reaction observed during the fourth stage of impact cratering – the recrystallization of an "affected region" surrounding the actual crater. (This phenomenon may also occur during the third or cavitation stage of crater formation.) This "affected area" is significant for at least two reasons: First, energy that is not accounted for in the theoretical approaches is consumed in the material transformation process; second, for engineering or structural strength considerations, the affected region could have markedly different mechanical properties which would lead to total damage far in excess of that described by the immediately visible crater. Although it is not possible at this time to describe analytically the phenomena of shock compression recrystallization, or to take into account the many variables of dynamic deformation and energy absorption, Glass and Pond (Ref. 25) have calculated and made experimental measurements of the ratio of affected area to actual crater volume and have found that the ratio increased with increasing energy of the impacting projectile. Thus, it is indicated that at meteoroid impact velocities with significantly high impact energy, the volume of the affected area might be an order of magnitude larger than the actual volume of the crater.

3.3 THEORIES OF CRATER FORMATION

To quantitatively describe the process of crater formation, three basic approaches to the problem have been made under the much-used categorical titles of blast wave theory, hydrodynamic theory, and visco-plastic theory.

Blast Wave Theories

In formulating an approximate model based on the blast wave analogy, Rae, et al. (Ref. 26), Davids, et al. (Ref. 27), and Heyda (Ref. 28) assumed that the impacting projectile drives a hemispherical shock wave into a semi-infinite medium. In so doing, the shock compression is assumed to be adiabatic, the

target compressible, and the equation of state of the target to be that of a perfect gas with constant specific heat ratio γ. Thus it is implied that the shock radius (R_s) must be proportional to a power of the time ($R_s \propto t^N$), since the collision of projectile and target occurs as an instantaneous release of energy and momentum. The blast wave theory has the limitation that it applies only to the period during which the material can be treated as a perfect gas. Also, the first and second stages of crater formation described previously are completely neglected.

In developing the blast wave analogy, the hemispherical shock wave results in an axisymmetric flow that can be described by the equations of motion of an inviscid, compressible fluid. Since the changes in state are adiabatic, the entropy is constant along a particle path; consequently, the pressure developed is a function of density alone (pressure = zero ahead of the advancing shock). Therefore,

$$S = f\left(\frac{P}{\rho^{\gamma}}\right) \tag{3.4}$$

where S is the entropy, P the pressure, and ρ the density. In a self-similar solution, variations of the radius of the crater r and the time of formation t depend upon the ratio of

$$\eta = \frac{r}{R_s(t)} \tag{3.5}$$

provided that the shock radius is proportional to some power of time

$$R_s = At^N \tag{3.6}$$

where A is a constant.

Through the process of an iterative solution for N as a function of γ and by approximating the crater volume $r(\eta)$, a value of N was determined to be 0.375. This value of N allows for the conservation of the total energy of the system but not of the total momentum.

By solving the basic equations of motion for a spherically symmetric expanding shock wave first derived by Taylor (Ref. 29), and by specifying that the total

energy of the system is equal to the kinetic energy of the impacting projectile E, the following equation can be derived,

$$R_s(t) = \left(\frac{25}{8\pi I_1(\gamma)} \frac{Et^2}{\rho_o}\right)^{\frac{1}{5}} \tag{3.7}$$

where $I_1(\gamma)$ is the energy density at the shock.
This equation can be used to describe the shock propagation in a specific medium.

In order to determine the size of a crater which could result from a given impact, it is necessary to define the intensity level at which the blast wave solution is stopped. Although Refs. 26-28 used different values of shock intensity as the cutoff point, their results agree basically. From Eq. 3.7 the shock radius as a function of time can be written in the form

$$R_s = A t^{\frac{2}{5}} \tag{3.8}$$

and the shock velocity as

$$\dot{R}_s = \frac{2}{5} A \left(\frac{A}{R_s}\right)^{\frac{3}{2}} \tag{3.9}$$

where $\dot{R}_s = C$ = cutoff point.

The radius of the crater is, therefore,

$$R_c = A\left(\frac{2A}{5C}\right)^{\frac{2}{3}} = \left(\frac{1}{2\pi I_1} \frac{E}{\rho_o C^2}\right)^{\frac{1}{3}} \tag{3.10}$$

Or, by converting E for a spherical projectile,

$$\frac{R_c}{d} = \left(\frac{1}{24 I_1} \frac{\rho_p}{\rho_o}\right)^{\frac{1}{3}} \left(\frac{V}{C}\right)^{\frac{2}{3}} \tag{3.11}$$

where ρ_p is projectile density and V is impact velocity.

Since $\gamma(v)$ is roughly the same for a wide variety of materials, C can be re-written as

$$C = \sqrt{\frac{\gamma+1}{2}\frac{P}{\rho_o}} \tag{3.12}$$

which gives

$$\frac{R_c}{d} = \left(\frac{1}{12 I_1}\frac{\rho_p V^2}{(\gamma+1)P}\right)^{\frac{1}{3}} \tag{3.13}$$

Although the validity of the empirical relationship in Eq. 3.13 is in apparent agreement with some experimental crater results, the treatment applies only to the assumption of a perfect gas and takes no account of plastic flow, elastic recovery, or subsequent fluid motion of any material which may be lying behind the shock at the instant of cutoff. In addition, the determination of final crater size depends upon the selection of a final cutoff point C which could introduce appreciable error in some target media.

Two other quantitative theories of crater formation which, because of their similarity, are discussed jointly are those of Charters and Summers (Ref. 30), and Luttrell (Ref. 31). The momentum of a uniformly expanding hemispherical shell composed of both the projectile and the target material is assumed to be equal to the projectile momentum by analogy with the ballistic pendulum

$$M_{fs}\,\mu_{fs} = M_p v_p \tag{3.14}$$

where M_{fs} = mass of fluid shell, μ_{fs} = velocity of fluid shell, and M_p and v_p are the mass and velocity of the projectile, respectively.

The kinetic energy of the projectile is then compared to the kinetic energy of the fluid shell by using the hydraulic analogy of shaped charge penetration (correct only for the case of a projectile and target of the same material) for which

$$\mu_{fs} = \frac{1}{2} v_p \tag{3.15}$$

and

$$\frac{1}{2} M_{fs}\,\mu_{fs}^2 = \frac{1}{2} M_p v_p^2 \tag{3.16}$$

The kinetic energy of the fluid shell is assumed to be used in the work of deformation in the incipient crater.

$$\frac{1}{2} M_{fs} \mu_{fs}^2 = \int_o^p S \, 2\pi r^2 dr \tag{3.17}$$

where S = the deformation stress, p the maximum crater depth, and r the radius of the crater. By integration with constant S

$$S = \frac{3 M_p v_p^2}{8\pi p^3} \tag{3.18}$$

By taking into account the experimental data for hemispherical craters and rearranging the terms, the penetration equation is then

$$\frac{p}{d} = \frac{1}{2}\left(\frac{\rho_p}{\rho_t}\right)^{\frac{1}{3}}\left(\frac{\rho_p v_p^2}{2S}\right)^{\frac{1}{3}} \tag{3.19}$$

or

$$S = \frac{1}{16} \frac{\rho_p^2}{\rho_t} \frac{v_p^2}{\left(\frac{p}{d}\right)^3} \tag{3.20}$$

Luttrell uses static stress values for the value S, while Charters and Summers suggest that S should be measured by experiment at least once for every target material and that this measured value should then be used as a constant in the equation for each specific material.

Here again the theoretical approach ignores the first and second stages of crater formation and assumes a single physical process for the entire mechanism of crater formation. It also assumes a constant deformation stress for a given material – valid only for a completely fluid impact model in which the deformation stress is zero. For the case of metal targets, however, it has been shown that the deformation stress changes radically under dynamic loads of varied intensity (Ref. 32).

Hydrodynamic Theories

Since the pressures generated in hypervelocity impact are usually several orders of magnitude greater than the shear strengths of the projectile and target materials, many investigators have attempted to treat both the projectile and target as inviscid fluids, thus neglecting the possible effects of shear strength. The

theories developed have assumed the resistance of the target to penetration to be entirely dependent on the inertial forces required to accelerate the target material and have been called hydrodynamic theories. Under such an assumption, Bjork (Ref. 10) and Walsh and Tillotson (Ref. 11) noted that the behavior of the material can be described by an entropic equation of state that correlates energy, pressure, and specific volume but neglects viscosity and heat condition. The equations of motion used by Bjork are

$$\rho \frac{\partial v}{\partial t} + \rho \bar{v} \cdot \text{grad}\, \bar{v} + \text{grad}\, P = 0 \tag{3.21}$$

$$\frac{\partial \rho}{\partial t} + \bar{v} \cdot \text{grad}\, \rho + \rho \,\text{div}\, \bar{v} = 0 \tag{3.22}$$

$$\rho \frac{\partial e}{\partial t} + \rho \bar{v} \cdot \text{grad}\, e + P \,\text{div}\, \bar{v} = 0 \tag{3.23}$$

$$P = f(\rho, e) \tag{3.24}$$

where $\bar{v}$ = fluid velocity vector

P = pressure

e = specific internal energy

ρ = density

t = time after impact

Since the problem has not been solved analytically, it was necessary to use numerical techniques. For simplicity, the projectile was taken as a right circular cylinder, and the initial impact conditions were described with the pressure, internal energy, and velocity of the target equal to zero.

Walsh and Tillotson used a similar set of equations to solve numerically the set of finite difference equations corresponding to the appropriate hydrodynamic equations of compressible fluids. The Eulerian form of the differencing equations are solved by dividing the Eulerian space into a finite number of small cells through which the mass moves and interacts according to the conservation equations and the equation of state of the material. This computational scheme, first introduced as the Particle-in-Cell (PIC) model by Evans and Harlow at Los Alamos (Ref. 33), permits pictorial printouts of the mass distribution and velocity field as well as providing data for the pressure, density, velocity, and specific internal energy for each cell.

Neither Bjork, nor Walsh and Tillotson, considered terms of viscosity or heat conduction. Thus, by the exclusion of second derivatives, simple linear scaling laws should apply. This assumption, based upon experimental data shown by Eichelberger and Gehring (Ref. 12) for projectiles of masses ranging from 10^{-11} to 10.0 gms, appears reasonable. On the other hand, terms of viscosity and strength must eventually be added to the equations in order to determine the point at which the flow is no longer hydrodynamic. In Bjork's approach, the hydrodynamic model was used to describe the entire interaction so that strength effects had to be artificially introduced to arrest the flow and limit the crater size. This treatment led to the conclusion that crater volume was proportional to projectile momentum. Calculations made for aluminum-on-aluminum and iron-on-iron impacts at 5, 20, and 72 km/sec (Ref. 34) could be described by the empirical relations,

$$p = 1.09\,(mv)^{1/3} \text{ for Al vs. Al} \tag{3.25}$$

$$p = 0.606\,(mv)^{1/3} \text{ for Fe vs. Fe} \tag{3.26}$$

where p = depth of penetration, cm
m = projectile mass, gm
v = velocity, km/sec

These relationships showed fair agreement with experimental results at the single velocity of 5 km/sec; however, a review of the bulk of experimental evidence (Fig. 2.1) indicates that crater volume is proportional to projectile kinetic energy.

Walsh and Tillotson terminated the hydrodynamic solution at a pressure of one megabar and resorted to a combination of theoretical and experimental results to develop the following expression:

$$\frac{p}{d} = k\left(\frac{v_o}{c_o}\right)^{0.62} \tag{3.27}$$

where p, d are standard dimensions for the crater and projectile
v_o = impact velocity
$c_o = \left(\frac{\partial P}{\partial \rho}\right)^{1/2}_s$ (at $P = 0, \rho = 0$)
k = dimensionless constant that depends on strength properties

The velocity exponent, 0.62, is given as independent of the metal being considered.

Walsh and Tillotson emphasize that the hydrodynamic approximation alone may become invalid in the latter stages of the crater formation process because the influence of strength, thermal conduction, and viscosity can no longer be neglected. However, they demonstrate how results of a single impact experiment can be used, together with the hydrodynamic theory, to establish a general expression for crater depth.

Visco-Plastic Theories

In attempting to cope with the problem of the limiting effects of material strengths, several theoretical models have been explored by Chou (Ref. 35), Riney and Chernoff (Ref. 36), Wilkens and Giroux (Ref. 37), Glass and Pond (Ref. 25), and Fugelso (Ref. 38). These models have often been classified as visco-plastic theories, or, as in the latter two cases (Refs. 25, 38), as metallurgical approaches which consider, primarily, material properties and high strain-rate effects. Glass and Pond developed for metal targets a cratering theory based on material properties. Two factors of prime importance in determining final crater volume are the theoretical shear strength of the material and the true stress-strain curve for the material. These two factors are, in turn, influenced by residual stresses, preferred orientations, temperature, and alloying additions. Although Glass and Pond conclude that crater volume will be proportional to projectile energy, there is no one equation that will take all variables into account – not unless all properties of materials and their behavior under all conditions encountered in the impact process can be accounted for in one expression.

Fugelso used equations of motion based on dislocation theory to predict plastic deformation under conditions of impulsive loading. The model thus developed gives total deformation of the target in terms of elastic distortion and the motion of dislocations under the applied stress. The magnitude of the deformation is determined by the magnitude of the stress (which may be a function of impact velocity) and its duration (which may be a function of projectile geometry and material and of target material).

Chou, who has applied a theory of visco-plastic flow to the perforation of thin plates (Ref. 35), assumes that the projectile shears a plug out of the plate and that fragmentation of the projectile and plug take place after the shear process

is complete. The assumption of a material viscosity other than zero permits shear stresses to be transmitted through the plate even during plastic flow of the material. Chou's analysis is strictly qualitative; a quantitative solution would require knowledge of viscosity coefficients and compressibility effects which could be used in an equation having the form

$$\tau = \mu \frac{\partial v}{\partial x} \tag{3.28}$$

where τ = the viscous stress

μ = the coefficient of viscosity

$\frac{\partial v}{\partial x}$ = the velocity gradient

Riney and Chernoff (Ref. 36) have formulated a visco-plastic model that assumes a fluid impact but differs basically from the hydrodynamic approach because a "viscosity factor" and a "dynamic yield stress" are included. These factors take into account the inertial, viscous, and plastic effects that influence the cratering process. Riney and Chernoff define the mechanism of crater formation in terms of cavitation, with the final crater size determined by (1) the shape and amplitude of the pressure wave established during the second phase of cratering, and (2) the resistance of the target material to flow. Flow of the target material continues until the amplitude of the wave decreases below the "intrinsic" yield strength of the material.

The early work of Riney and Chernoff was based upon a one-dimensional, Lagrangian treatment of a two-body collision in which the materials, stressed beyond their yield strengths, act as Newtonian viscous liquids. The pressure p acting on the materials will be a function of the material density ρ and the shock velocity μ by the simple Rankine-Hugoniot relationship

$$p = f(\rho, \mu) \tag{3.29}$$

and the material resistance to shear will have the form of a Bingham visco-plastic model given by

$$\tau = \left(\mu_0 + \frac{\tau_0}{|D|}\right) D \tag{3.30}$$

where τ = shearing stress

μ_0 = static viscosity

τ_0 = yield value of the shearing stress

$|D|$ = a constant

D = strain rate

$\left(\mu_0 + \frac{\tau_0}{|D|}\right)$ = coefficient of viscosity

In the solution, the decay of pressure with time was considered and values of μ_0 and τ_0 were varied to approximate a value of τ equal to the unknown dynamic shear yield strength.

More recently, Riney (Ref. 39) has used the Particle-in-Cell method (Ref. 33) of handling the hydrodynamic phase of cratering in a manner similar to that of Bjork and Walsh. In addition, a series of visco-plastic equations was developed to bridge the transition from the hydrodynamic to the visco-plastic regime. A flow-resistant coefficient was introduced as

$$\mu(D) = \eta_0 + \frac{S_0}{\sqrt{D^{2+\epsilon}}} \tag{3.31}$$

where D^2 = second invariant of the deformation strain tensor

S_0 = static yield shear stress of the target material

η_0 = viscosity factor

$\eta(D)D^2 = \tau_1^2$ = the deformation of the material

Thus, the material is considered rigid if stressed below its yield strength; and if stressed above its yield strength, the material behaves as a Newtonian fluid. The factor ϵ is introduced into the equation to account for the moving surface of separation between the rigid and fluid regions of the medium.

The technique of introducing flow-resistant coefficients to account for the stresses in the visco-plastic regime which follows the strictly hydrodynamic regime is also being explored by Wilkens and Giroux (Ref. 37); however, as the analytical efforts of Riney, and Wilkens and Giroux, are still being developed, their results are not yet available.

3.4 SUMMARY

This section of the report has been directed toward describing the theoretical approaches to the phenomena of hypervelocity impact cratering and to noting the extent to which each theory covers the basic phenomena. The many physical observations of crater formation have been discussed and synthesized into a model of the cratering process which consists of four phases or modes of cavitation.

(1) The transient phase– a luminous flash occurs and the pressures rise to levels at which fluid flow of the projectile and target begins
(2) The primary penetration phase– approximately described by steady state hydrodynamic flow of both projectile and target material to the point at which the projectile is consumed as a causative force
(3) The cavitation phase– in the early stages hydrodynamic flow occurs, and in the later stages visco-plastic and basic material properties act to retard the cavitation process
(4) The recovery phase– the crater undergoes plastic and elastic rebound, peripheral spalling occurs, and phase changes in the solid state may occur in an area beneath the actual crater

Lack of a priori knowledge of the dynamic yield point of specific materials prohibits this model from independently predicting the crater volume in an untested material. It does not, however, prevent an accurate description of the progress of the shock field in the material after the primary penetration stage but before the crater recovery stage. The experimental observations of the process do not permit acceptance of the theory that the pellet explodes upon impact, nor does analysis of the stress field demand the assumption of a constant deformation stress or static stress field. Although the model does not require that the final crater be hemispherical in profile, there is little doubt from the observations and from the analysis of the expanding stress field that a hemisphere will result, provided that the following two conditions are met: (1) the impact occurs at hypervelocity, and (2) the material is ductile (so that spalling will not occur around the pheriphery).

REFERENCES FOR SECTION 3 - THEORETICAL APPROACHES

1. E. Opik, "Researches on the Physical Theory of Meteor Phenomena: I. Theory of the Formation of Meteor Craters," Acta et Comm. Univ. Tartuensis, 1936

2. G. Grimminger, "Probability That a Meteorite Will Hit or Penetrate a Body Situated in the Vicinity of the Earth," J. Appl. Phys., Vol. 19, No. 10, Oct 1948, pp. 947-956

3. E. M. Pugh, G. Birkhoff, D. P. MacDougall, and G. Taylor, "Explosives With Lined Cavities," J. Appl. Phys., Vol. 19, No. 6, Jun 1948, pp. 563-582

4. N. Rostocker, "The Formation of Craters by High Speed Particles," Meteoritics, Vol. 1, 1953

5. R. W. Goranson, D. Bancroft, B. L. Burton, T. Blechar, E. E. Houston, E. F. Gittings, and S. A. Landeen, "Dynamic Determination of the Compressibility of Metals," J. Appl. Phys., Vol. 26, No. 12, Dec 1955, pp. 1472-1479

6. J. J. Gilvarry and J. E. Hill, "The Impact of Large Meteorites," Astrophys. J., Vol. 124, 1956, p. 610-622

7. M. A. Cook, "Mechanism of Cratering in Ultra-High Velocity Impact," J. Appl. Phys., Vol. 30, No. 5, May 1959, pp. 725-735; also, The Science of High Explosives, Reinhold Publishing Co., New York, 1958

8. K. P. Staniukovich, "Elements of Impact Theory for Solid Bodies Having High (Cosmic) Speeds," ARS J., Russian Supplement, Vol. 32, No. 9, Sep 1962, pp. 1459-1473

9. M. Zaid, "Penetration by Hypervelocity Projectiles," Proceedings of the Fifth Symposium on Hypervelocity Impact, Vol. 1, Part 1, Nonr-(G)-0020-62(X), Colorado School of Mines, Apr 1962

10. R. L. Bjork, "Effects of a Meteoroid Impact on Steel and Aluminum in Space," The Rand Corporation, Report TR P-1662, 16 Dec 1958

11. J. M. Walsh and J. H. Tillotson, "Hydrodynamics of Hypervelocity Impact," General Dynamics Corporation, General Atomic Division, Report GA-3827, 22 Jan 1963 (work reported in this paper was presented at the Sixth Hypervelocity Impact Symposium, Cleveland, Ohio, Apr 30 - May 2, 1963)

12. R. J. Eichelberger and J.W. Gehring, "Effects of Meteoroid Impacts on Space Vehicles," ARS J., Vol. 32, No. 10, Oct 1962, pp. 1583-1591

13. W. W. Atkins, "Flash Associated with High Velocity Impact on Aluminum," J. Appl. Phys., Vol. 26, No. 1, Jan 1955, pp. 126-127

14. A. C. Charters, "High Speed Impact," Sci. Amer., Vol. 203, No. 4, Oct 1960, pp. 128-140

15. J. W. Gehring and D. W. Sieck, "A Study of the Phenomena of Impact Flash and Its Relation to the Reaction of the Lunar Surface to the Impact of a Lunar Probe," ARS Paper No. 2476-62; J. W. Gehring, "An Investigation of the Phenomena of Impact Flash and Its Potential Use as a Hit Detection and Target Discrimination Technique" (paper presented at the Sixth Hypervelocity Impact Symposium, Cleveland, Ohio, Apr 30 - May 2, 1963); J. W. Gehring and A. C. Charters, "Meteoroid Impact on the Lunar Surface" (paper presented at the Lunar Surface Materials Conference, Boston, Massachusetts, May 21-23, 1963)

16. R. W. MacCormack, "Investigation of Impact Flash at Low Ambient Pressures" (paper presented at the Sixth Hypervelocity Impact Symposium, Cleveland, Ohio, Apr 30 - May 2, 1963)

17. F. L. Whipple, "The Meteoritic Risk to Space Vehicles," Vistas in Astronautics: 1958, Pergamon Press, New York, 1958, pp. 115-124

18. M. A. Lavrentyev, "The Problems of Piercing at Cosmic Velocities," NASA TT F-40, May 1960 (translated from "Artificial Earth Satellites," No. 3, Academy of Sciences, Moscow, USSR, 1959)

19. N. H. Langton, "The Thermal Dissipation of Meteorites by a Bumper Screen," Bericht Uber den V. Internationalen Astronautischen Kongres, Aug 1954

20. R. J. Eichelberger, "Experimental Test of the Theory of Penetration by Metallic Jets," J. Appl. Phys., Vol. 27, No. 1, Jan 1956, pp. 63-68

21. J. W. Gehring, "Observations of the Phenomena of Hypervelocity Impact," Proceedings of the Fourth Symposium on Hypervelocity Impact, Vol. 2, APGC-TR-60-39, Eglin Air Force Base, Florida, Sep 1960

22. J. M. Walsh, M. H. Rice, R. G. McQueen, and F. L. Yarger, "Shock Wave Compressions of Twenty-Seven Metals," Phys. Rev., Vol. 108, 15 Oct 1957, pp. 196-216 (see also R. G. McQueen and S. P. Marsh, "Equation of State for Nineteen Metallic Elements from Shock Wave Measurements to Two Megabars," J. Appl. Phys., Vol. 31, No. 7, Jul 1960)

23. J. H. Kineke, "Observations of Crater Formation in Ductile Materials," Proceedings of the Fifth Symposium on Hypervelocity Impact, Vol. 1, Part 2, Nonr-(G)-0020-62(X), Colorado School of Mines, Apr 1962

24. J. W. Gehring, "High-Speed Radiographic and Optical Techniques Applied to Hypervelocity Impact Studies," Proceedings of the Fifth International Congress on High-Speed Photography, Society of Motion Picture and Television Engineers, 1962

25. C. M. Glass and R. B. Pond, "A Metallurgical Approach to the Hypervelocity Problem," Proceedings of the Fourth Symposium on Hypervelocity Impact, Vol. 3, APGC-TR-60-39, Eglin Air Force Base, Florida, Sep 1960; also, "Energy Balances in Hypervelocity Penetration" (paper presented at the Sixth Hypervelocity Impact Symposium, Cleveland, Ohio, Apr 30 — May 2, 1963)

26. W. J. Rae, H. A. Scheetz and H. P. Kirchner, "A Study of Meteoroid Impact Phenomena," Cornell Aeronautical Laboratory Reports Nos. RM-1655-M-2, Jun 1962, and RM-1655-M-3, Sep 1962; also, W. J. Rae and H. P. Kirchner, "A Blast-Wave Theory of Crater Formation in Semi-Infinite Targets" (paper presented at the Sixth Hypervelocity Impact Symposium, Cleveland, Ohio, Apr 30 — May 2, 1963)

27. N. Davids, Y. K. Huang, and W. Jaunzemis, "Some Theoretical Models of Hypervelocity," Proceedings of the Fifth Symposium on Hypervelocity Impact, Vol. 1, Part 1, Nonr-(G)-0020-62(X), Colorado School of Mines, Apr 1962

28. J. F. Heyda, "Shock Front Variation in Time for High Speed Impact Into Water" (paper presented at the Sixth Hypervelocity Impact Symposium, Cleveland, Ohio, Apr 30 — May 2, 1963)

29. G. I. Taylor, "The Formation and Enlargement of a Circular Hole in a Thin Plastic Plate," Quarterly J. of Mechanics and Applied Mathematics, Vol. 1, 1948

30. A. C. Charters and J. L. Summers, "Some Comments on the Phenomena of High Speed Impact," Proceedings of the Decennial Symposium, White Oak U. S. Naval Ordnance Laboratory, 26 May 1959

31. J. L. Luttrell, "A Hypervelocity Impact Model for Completely Deforming Projectiles" (paper presented at the Sixth Hypervelocity Impact Symposium, Cleveland, Ohio, Apr 30 – May 2, 1963)

32. Proceedings of the Conference on the Properties of Materials at High Rates of Strain, Institution of Mechanical Engineers, Westminster, S. W. 1, England, Apr 30 – May 2, 1957 (see, e. g., papers by Costello, Cottrell, Maiden, and Minshall)

33. M. W. Evans and F. H. Harlow, "The Particle-in-Cell Method for Hydrodynamic Calculations," Los Alamos Scientific Laboratory, LA-2139, Nov 1957

34. R. L. Bjork, "Meteoroids vs. Space Vehicles," ARS J., Vol. 31, No. 6, Jun 1961, pp. 803-807

35. P. C. Chou, "Visco-Plastic Flow Theory in Hypervelocity Perforation of Plates," Proceedings of the Fifth Symposium on Hypervelocity Impact, Vol. 1, Part 1, Nonr-(G)-0020-62(X), Colorado School of Mines, Apr 1962

36. T. D. Riney and P. R. Chernoff, "Inertial, Viscous and Plastic Effects in High Speed Impact," Proceedings of the Fifth Symposium on Hypervelocity Impact, Vol. 1, Part 1, Nonr-(G)-0020-62(X), Colorado School of Mines, Apr 1962

37. M. L. Wilkens and R. Giroux, "Calculations of Stress Waves in Solids" (paper presented at the Sixth Hypervelocity Impact Symposium, Cleveland, Ohio, Apr 30 – May 2, 1963)

38. L. E. Fugelso, "A Theoretical Study of Dynamic Plastic Deformation Under Impact Loads," Proceedings of the Fifth Symposium on Hypervelocity Impact, Vol. 1, Part 1, Nonr-(G)-0020-62(X), Colorado School of Mines, Apr 1962

39. T. D. Riney, "Visco-Plastic Solution of Hypervelocity Impact Cratering Phenomena" (paper presented at the Sixth Hypervelocity Impact Symposium, Cleveland, Ohio, Apr 30 — May 2, 1963)

SECTION IV

ENGINEERING CONSIDERATIONS

4.0 INTRODUCTION

Sections 2 and 3 of this report have been concerned with the simple projectile/target model, i.e., the case of a solid equiaxial projectile impacting a semi-infinite target. This model may be inadequate from the viewpoint of the design engineer, because many of the design problems associated with reentry vehicles, spacecraft, space radiators, solar panels, etc., do not lend themselves to treatment by such a simple model. Therefore, this section will be concerned with the practical aspects, or engineering considerations, that are associated with a useful theory of hypervelocity impact. These engineering considerations will be treated under the following six headings:

4A. Thin Targets (including composites, laminates and fillers)
4B. Pressure Vessels and Stressed Structures
4C. Spalling
4D. Oblique Impact
4E. Target Strength and Temperature
4F. Projectile Configurations

4A. THIN TARGETS

One of the most important aspects of hypervelocity impact is that of perforation, or penetration, of thin targets at hypervelocities. Numerous references in which the analysis of meteoroid impact on space vehicles was discussed (Refs. 1-9) have appeared in the literature. Even the definition of the problem is not complete, for some investigators regard spacecraft and satellites as basically thin targets because of the relatively thin materials used in their construction, while other investigators are of the opinion that spacecraft and satellites should be classed as thick targets because most meteoroids are very small. This is academic, however, for the meteoroid hazard does exist

regardless of meteoroid size. Hence, a complete understanding of thin target behavior under conditions of hypervelocity impact is of prime importance to the spacecraft design engineer.

4A.1 A Model of Thin Target Behavior

The term "thin target" can be broadly interpreted to include any target which is perforated or whose free-surface effects influence the damage resulting from hypervelocity impact. In the restricted sense, the term thin target is used to refer to any target which is perforated and where the mechanism of perforation is similar to the "primary" phase of penetration in a semi-infinite target.

In the attempt to develop a theoretical description of the mechanism of thin target perforation and projectile breakup, a number of theories have been advanced. Some theories (Ref. 10) have been concerned with low-velocity (less than 2.0 km/sec) projectiles, while others have been based on an incorrect physical model and vague assumptions. On the other hand, several approaches which are based primarily on experimental observations have established the following facts concerning impact on thin targets: (1) both the target and the projectile flow upon impact, (2) material is ejected from both sides of the thin target, and (3) a thin shield is effective because it causes the projectile to break up, spreading the fragments over a relatively large surface area on the backup plate. The perforation of a thin target by a projectile is comparable to the "primary" phase of penetration into a thick target, and the projectile is a continuous source of energy throughout the period of perforation (see Refs. 6, 11). (It may be noted that this mechanism applies only under conditions of hypervelocity impact; at very low impact velocities, material strength becomes a much more important factor and different penetration mechanisms are operative.)

These facts are summarized in Fig. 4A.1, a schematic illustration of projectile and target behavior during hypervelocity impact. An experimental demonstration of the same target/projectile behavior is given in Fig. 4A.2, which is a framing-camera sequence of a spherical projectile perforating a thin target. Flow of the projectile and target is obvious, material is ejected from both sides of the thin target, or bumper plate, and the projectile has been broken up and the fragments spread out.

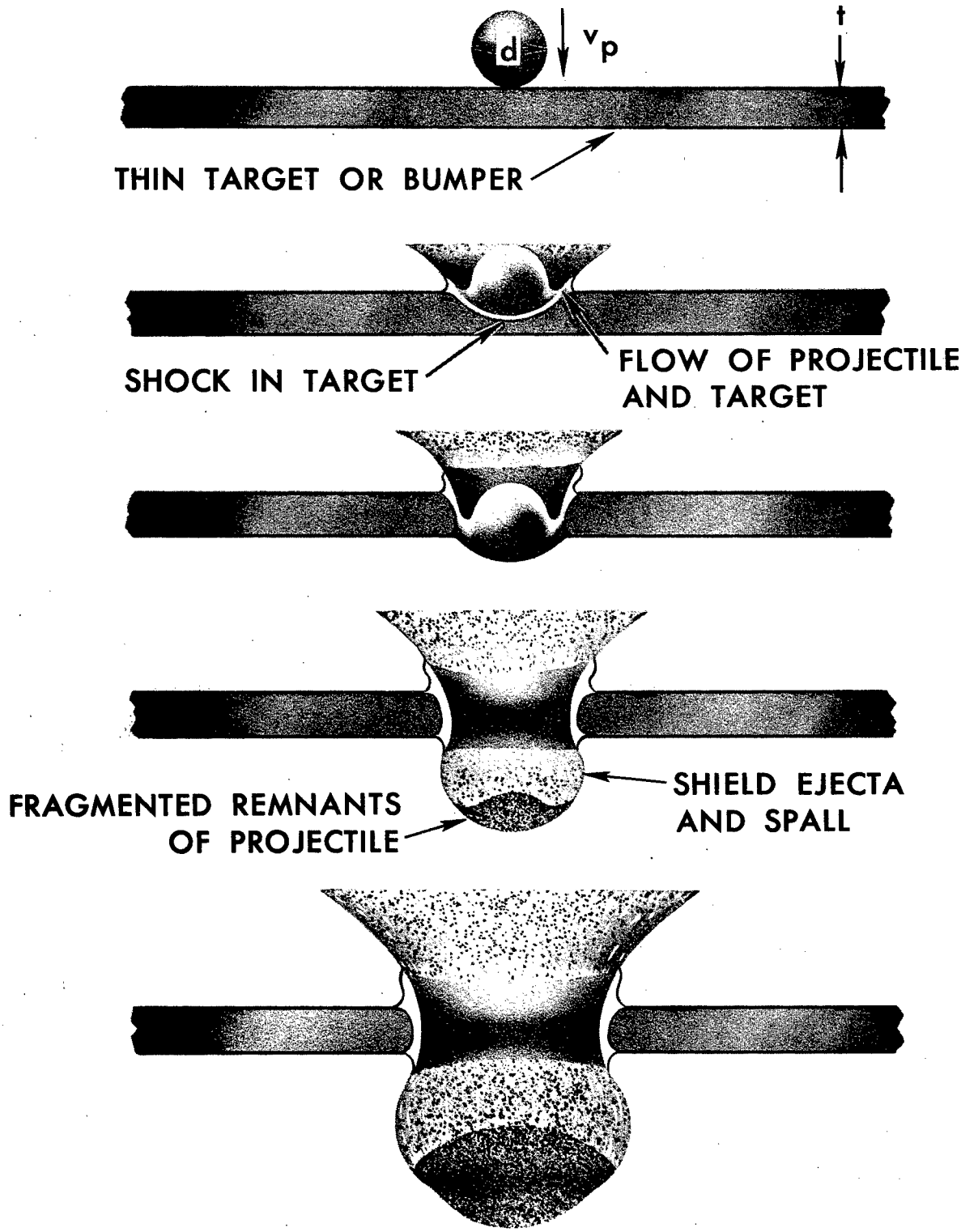

Fig. 4A.1 Projectile and Target Behavior on Impact of Solid Sphere with Thin Target

PROJECTILE: 0.125-IN.-OD SOLID
SILVER SPHERE, 0.18 gm

TARGET: 0.063-IN. 2024-T3 Al
2-IN. SPACING
0.250-IN. 2024-T3 Al

VELOCITY = 3.7 km/sec

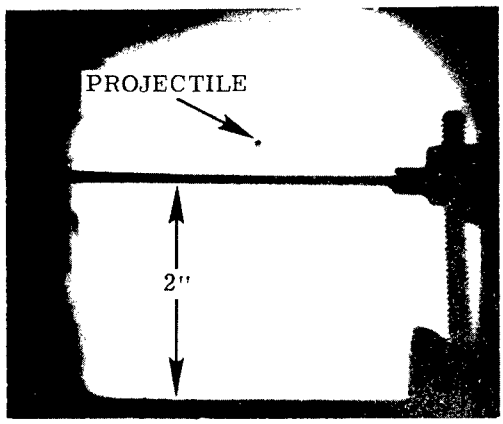

-1.7 μS

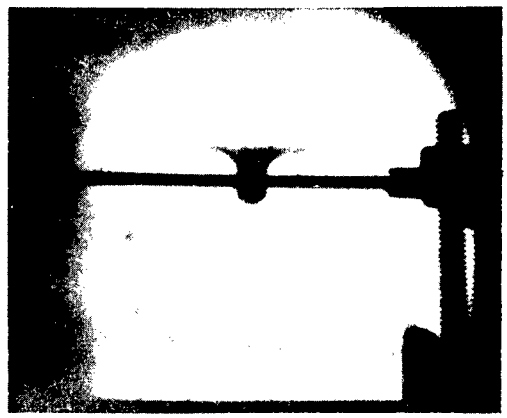

+1.7 μS

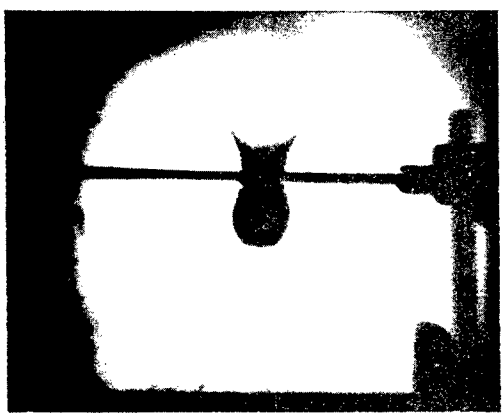

+5.2 μS

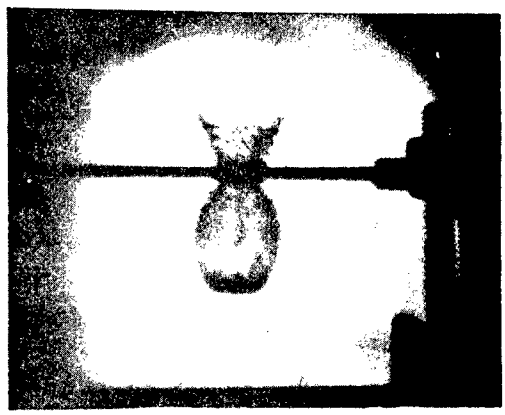

+8.7 μS

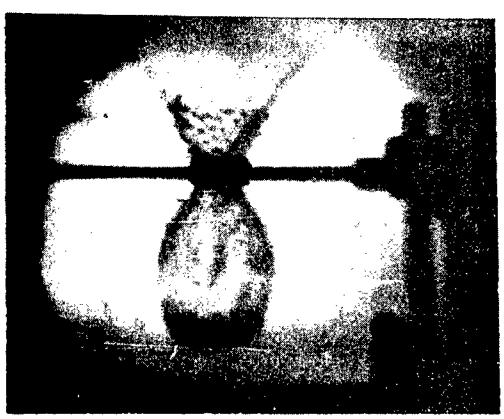

+12.2 μS

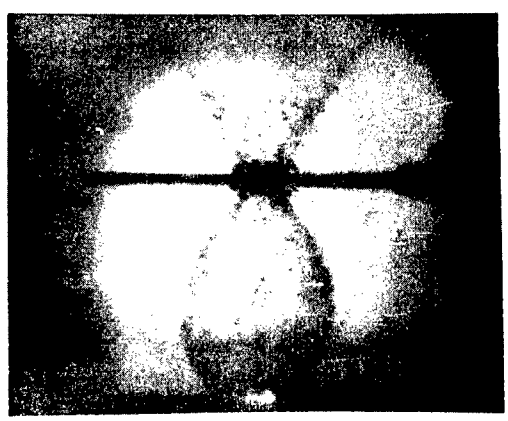

+15.7 μS

Fig. 4A.2 Framing Camera Sequence of Sphere Impacting a Multiple-Sheet Target

The damage to spaced targets by a projectile is shown in Fig. 4A.3. The projectile has been completely broken up and, together with the ejecta from the thin shield, or bumper plate, has impacted the backup plate over a relatively large area. Of particular interest here is the spall that has come off the rear of the backup plate. This spall, caused by the intense shock wave resulting from the high momentum of the debris that impacted the backup plate, indicates that the shield concept may not be of advantage under all conditions; i.e., the damage capacity of the spall behind a thin plate might, in some cases, be more severe than when no bumper is used.

Some basic qualitative conclusions on the behavior of thin targets are illustrated in Fig. 4A.4 which shows a series of flash X-ray pictures of impacts under various conditions. The thin target, or shield, has effectively fragmented the projectile, spread the fragments over a large area (relative to the original projectile area), and reduced the velocity of many of the fragments normal to the backup plate. It can be seen that the effectiveness of the shield increases with thickness. However, the total momentum of the debris from the shield may be greater with a thicker shield; and, therefore, the tendency for spall from the rear of the backup plate may also be greater.

4A.2 Some Experimental and Theoretical Observations on Thin Target Behavior

A number of experimental and theoretical research studies on thin target impact phenomena have been conducted (Refs. 3, 7, 10-26). A summary of the conclusions drawn from nine of these investigations, together with pertinent comments on these conclusions, is given below.

4A.2.1 Becker, Watson, and Gibson (Ref. 21) carried out a detailed study of behind-target effects for normal and oblique impact of thin targets. Principal conclusions were as follows:

(1) For normal impact, the percentage of spall fragments found in any given element of solid angle behind the target is independent of velocity.

(2) The average mass of a spall particle of either projectile or target material depends markedly on target thickness but is relatively independent of velocity.

TARGET: 0.063-IN. 2024-T3 Aℓ
2-IN. SPACING
0.250-IN. 6061-0 Aℓ

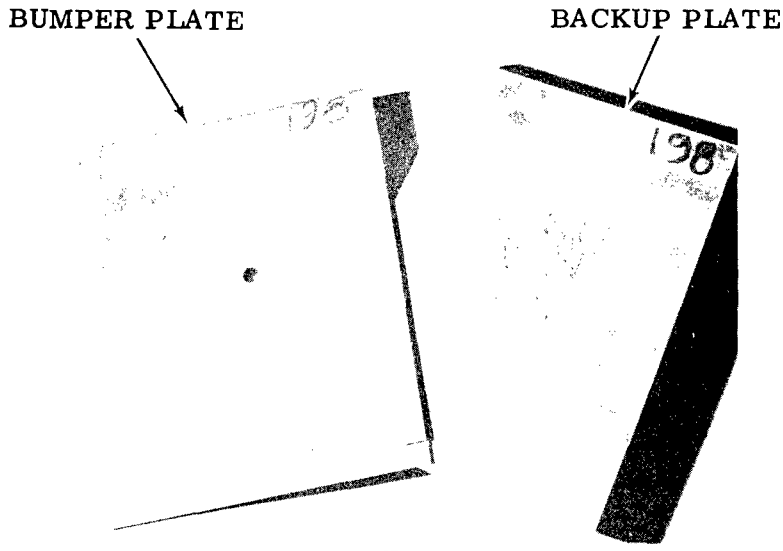

FRONT VIEW

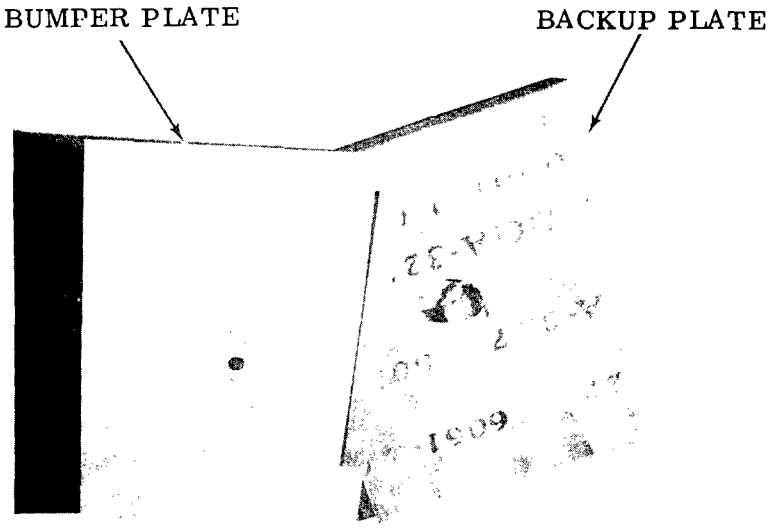

REAR VIEW

Fig. 4A. 3 Multiple-Sheet Target Impacted by 3/16-In. Aluminum Sphere at 5. 4 km/sec

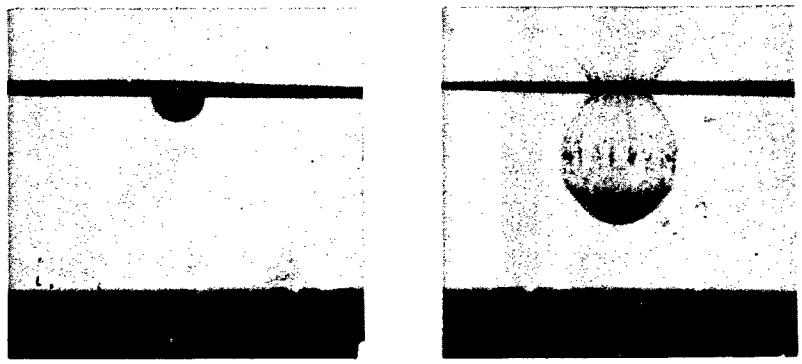

TIME AFTER IMPACT: 1 μs 4 μs

SHIELD THICKNESS = 0.010 IN.

TIME AFTER IMPACT: 3 μs 8 μs 12 μs

SHIELD THICKNESS = 0.038 IN.

Fig. 4A.4 X-Ray Pictures of 3/16-In. Aluminum Spheres Impacting Copper Shields at 6.1 km/sec

(3) Within the limits of scale sizes tested, the percentage of the total number or total mass of spall particles found in a given space behind the target is independent of the projectile size.

The approach taken by Becker, et al., to the problem of ejecta from the rear of a thin target is a good one, but their conclusions are based on limited experimental conditions, particularly that of impact velocity. The validity of their conclusions with respect to a general model of thin target behavior is not established.

4A. 2. 2 Humes, Hopko, and Kinard (Ref. 13) conducted a study of the effectiveness of thin shields in protecting semi-infinite backup plates. They concluded that impact damage can be reduced by using a properly selected bumper shield. Their results for one-target combination (Fig. 4A. 5) give total penetration in a bumper-protected target and a semi-infinite target as a function of impact velocity, using 1/16-in. -diameter copper spheres. Figure 4A. 5 also gives data based on experiments conducted at GM DRL, using 1/8-in. -diameter aluminum spheres. For the velocity range covered, both sets of data show that damage to a bumper-protected target reaches a maximum at a low velocity, i. e., about 2. 5 km/sec. However, the GM DRL, data shows that the damage tends to level off at about 8. 0 km/sec; and it is possible that at still higher velocities, the curve will swing up again and exceed the maximum shown at 2. 5 km/sec. The significant differences in p/d ratio for a given velocity for the two sets of data are the results of differences in projectile size and material.

4A2. 3 Lull (Ref. 7) performed a theoretical treatment of the protective ability of a thin shield with some quantitative results based on meteoroid observation data. Lull's model of operation of a thin shield is as follows:

(1) An elastic collision is assumed. (Evaluation of the mechanism does not require any great reliance on hydrodynamic theory or on the data and extropolations of hypervelocity cratering.)

(2) The projectiles will completely penetrate the thin shield.

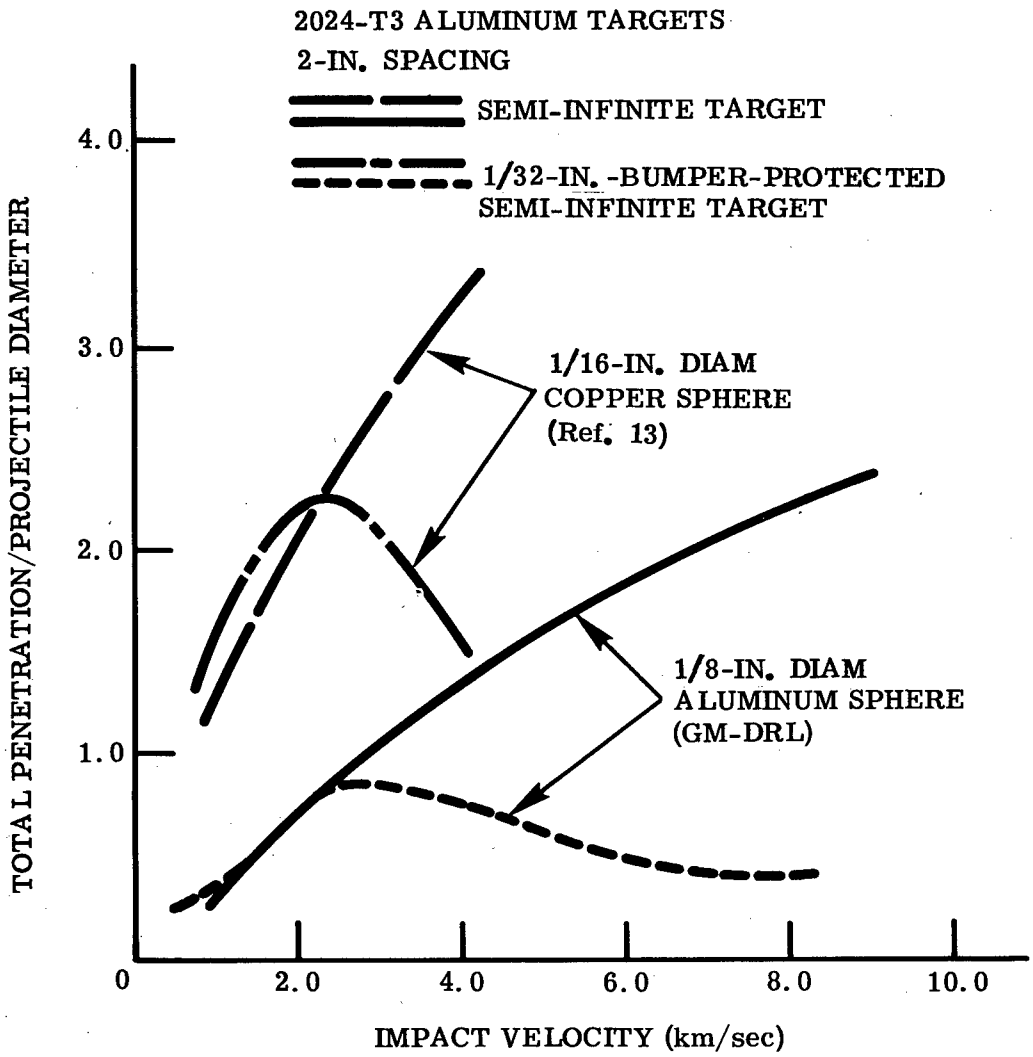

Fig. 4A.5 Total Penetration in a Bumper-Protected Target and Semi-Infinite Target vs. Impact Velocity

(3) After impact with the thin shield, the projectile behaves as an exploding pellet, ("exploding" does not mean vaporization but rather expansion of the debris in all directions).

(4) The fragmented projectile expands and spreads out over a large enough area to permit the second shield to absorb the momentum without appreciable damage.

The principle qualitative conclusions reached by Lull are: (1) the energy (or momentum) density on the backup plate can be reduced to any required level by increasing the spacing between the plates and (2) bumper plate effectiveness is directly proportional to bumper mass/unit area. Lull also concludes that the proposed model might be extrapolated to meteoritic velocities. Although Lull's model seems to fit experimentally observed phenomena in some of its major points, his last conclusion is subject to re-appraisal in view of the experimental results of the past two years. (For a more detailed review of Lull's model, see Ref. 11.)

4A.2.4 Maiden (Ref. 11) conducted an experimental and theoretical study of the protective ability of thin shields. In developing a theoretical model of thin target perforation, Maiden considered a right-circular cylinder impacting a thin shield (Fig. 4A.6). The estimated wave pattern shortly after impact (Fig. 4A.6a.) shows that two shock waves, S_1 and S_2, have propagated away from the interface I, and that the finite size of the projectile has resulted in rarefaction waves, R_1 and R_2, being transmitted towards the axis of symmetry. In Fig. 4A.6b, the shock S_2 has reflected from the back face of the shield. To satisfy the boundary condition of zero pressure, the shock is reflected as a rarefaction wave, R_3. The resultant particle velocities behind R_3 cause the profile of the back face of the shield to be as shown. As the process continues, this "bubble" grows through the addition of material from both the shield and projectile (see the upper left-hand picture in Fig. 4A.4).

From a physical viewpoint, the rarefactions R_1, R_2, and R_3, generated to satisfy boundary conditions, can be looked upon as tension waves. Hence, fracture will occur if the net tensile stress exceeds the fracture stress at any point in the projectile or shield. In addition, rarefactions will be produced to satisfy boundary conditions at any new fracture surfaces, and these can lead to

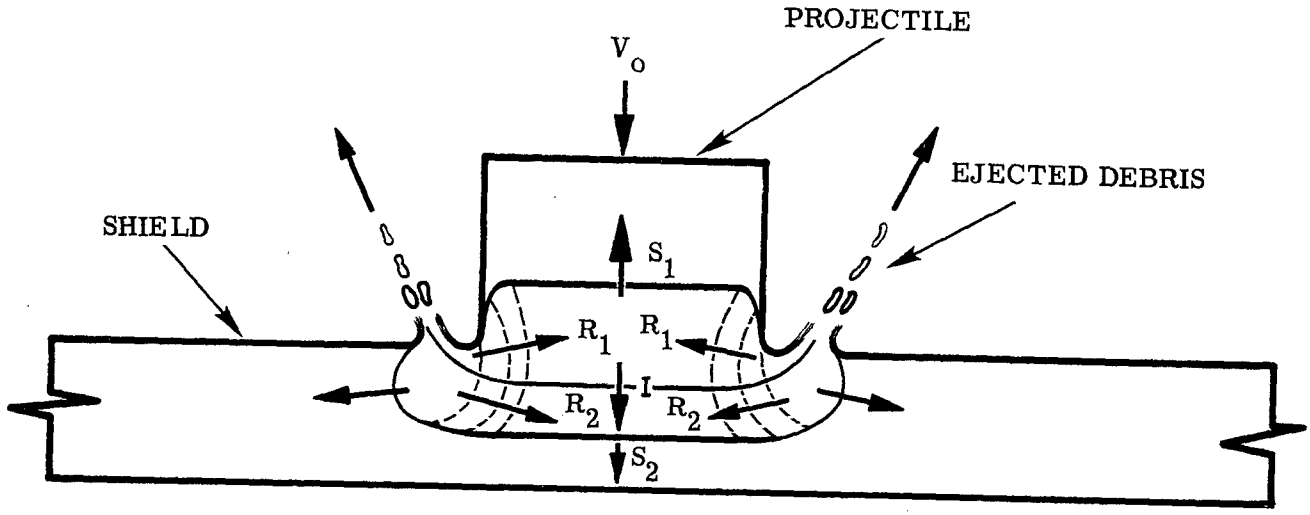

Fig. 4A. 6a Estimated Wave Patterns in a Projectile and Shield Soon After Impact (from Ref. 11)

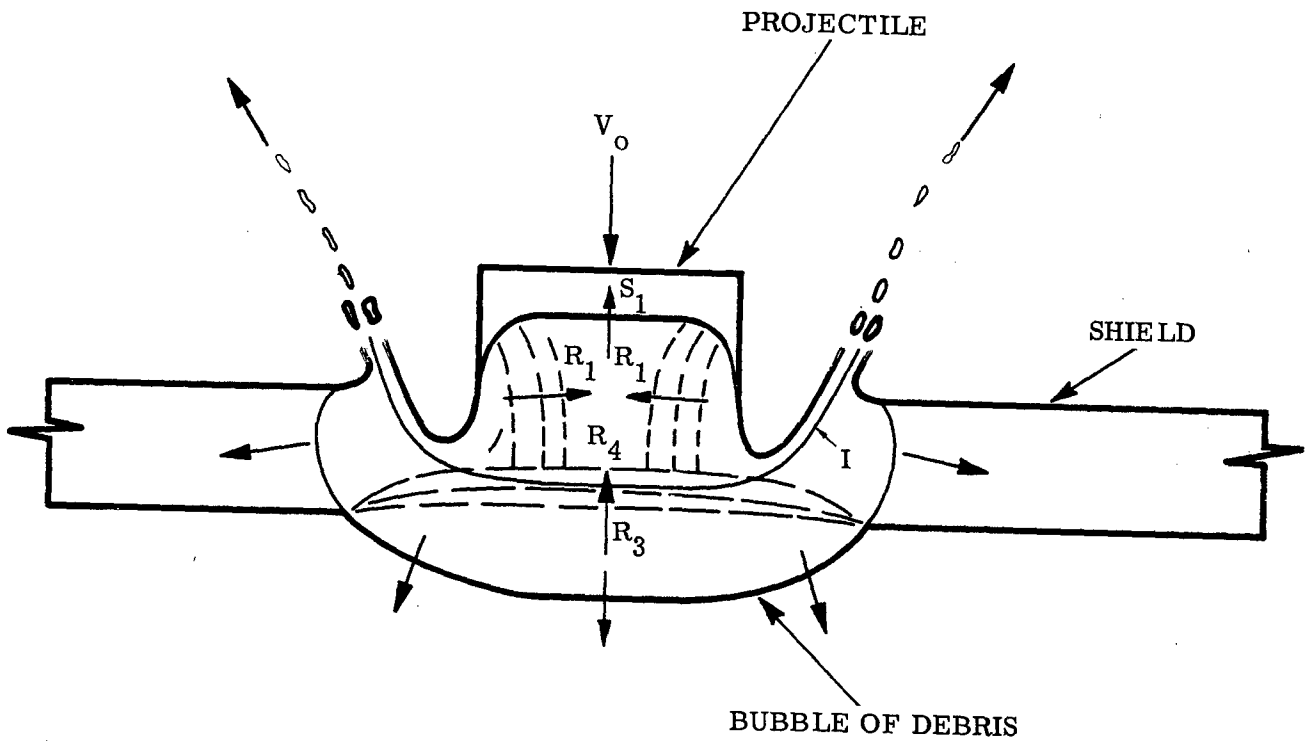

Fig. 4A. 6b Estimated Wave Pattern After The Shock Has Reflected From The Bottom Face of Shield (from Ref. 11)

further fractures. Thus, the whole process of fracture of a projectile and shield can be interpreted as a multiple spalling phenomenon which starts at the free surfaces.

The conclusions arrived at by Maiden can be summarized as follows:

(1) The effectiveness of a shield is reduced as it is made thinner, because the spread of the fragments decreases while the velocities of the fragments tend to approach the velocity of the original projectile. Conversely, as a shield is made thicker, its effectiveness increases (up to an optimum thickness for which the total depth of penetration, including shield thickness, will be minimum).

(2) For various shield materials with equal weight per unit area, and a shield-weight/projectile-weight ratio (per unit area) of about 0.13, aluminum, magnesium, titanium, copper, and gold shields proved equally effective. However, for shield-weight/projectile-weight ratios higher than 0.13, the shields become more effective as the initial impact pressure increases (for a given projectile and velocity, a high impact pressure is obtained with high density and low compressibility shield material).

(3) For impact pressures up to about 4×10^{10} dynes/cm^2 (about 3.5 km/sec), there is incomplete fragmentation of an aluminum projectile, and the total depth of penetration, including shield thickness, is no less (and may be more) than with a semi-infinite target. Above this point, the total depth of penetration will decrease if the shield thickness is within an optimum range (of values) that is a function of velocity and materials.

In general, Maiden's conclusions are compatible with the model suggested in Fig. 4A.1. The results indicate that impact data for velocities in the lower range (11 – 30 km/sec) of meteoroid velocities would be of great value in the development of a complete thin target theory.

4A.2.5 Nysmith and Summers (Ref. 12, 23) conducted an evaluation of the effectiveness of multiple-sheet structures for increasing the penetration resistance of spacecraft. They concluded that the penetration resistance of a structure can be increased, at a constant weight per unit area, as follows:

(1) Increasing the number of sheets while keeping the total sheet thickness constant

(2) Increasing the spacing between successive sheets

(3) Filling the space between the sheets with a low-density material

(4) Concentrating the available structural weight in the rear sheet and making the front sheet only thick enough to shatter the projectile completely

Conclusions (1) through (3) are illustrated in Fig. 4A. 7, which is based on Nysmith and Summers' early work (Ref. 12) at relatively low velocities (less than 5.0 km/sec) and which gives impact velocity (the velocity at which the plate, or plates, will just resist penetration, i.e., the ballistic limit) as a function of the number of sheets. More recent studies (Ref. 23) at velocities up to 7.3 km/sec have substantiated these conclusions and have also shown that in the transition and high-velocity-impact regions, the effects of target spacing become more noticeable than at low velocities.

4A. 2.6 Rolsten, Hunt, and Wellnitz (Ref. 3) carried out a detailed experimental and analytical study of the general problem of meteoroids impacting spacecraft. Explosive accelerators and a light-gas gun were used to accelerate steel, copper, glass, and nylon projectiles to velocities up to 28, 600 feet/second. Semi-infinite and multiple-sheet targets were of aluminum, titanium, steel, magnesium, magnesium-lithium, and glass; and fillers and pressurized vessels were evaluated. The principal conclusions concerning a thin bumper plate were as follows:

(1) The effectiveness of a bumper plate depends primarily on its mass and not on its strength or toughness.

(2) Optimum thickness of the bumper plate is a function of projectile mass (size) and velocity.

(3) Two plates provide more protection than a single plate of the combined thickness.

(4) Within limits, the thinner the bumper, the greater the spacing required for maximum protection.

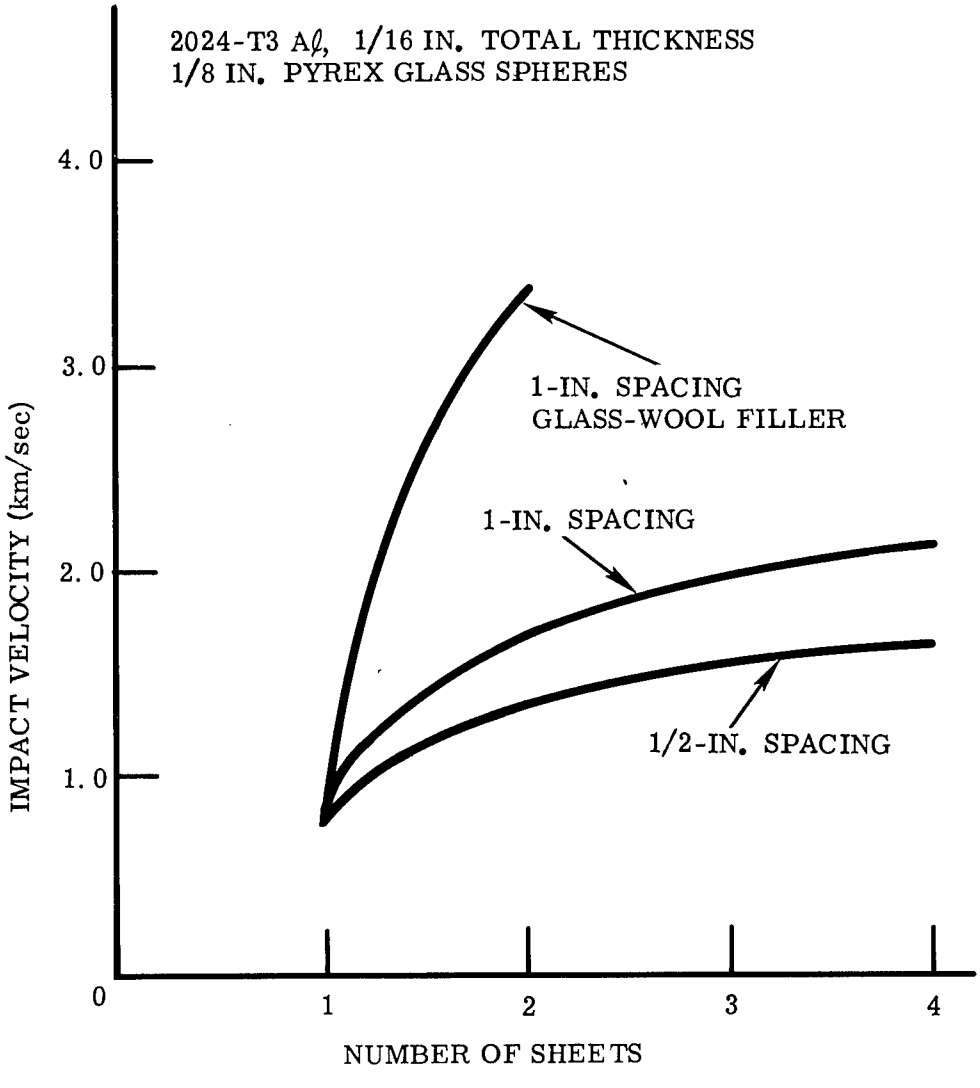

Fig. 4A.7 Impact Velocity vs. Number of Sheets Required to Prevent Perforation (from Ref. 12)

The above conclusions are in general agreement with those reached by other investigators, and the overall results are presented by Rolsten, et al., to serve as a guideline for the spacecraft design engineer.

4A.2.7 Vitali, Becker, and Watson (Ref. 22) conducted an investigation of perforation of targets of finite thickness by projectiles at 3.2 km/sec. Results are given in a series of graphs which can be summarized as follows:

(1) For very thin targets, crater entrance diameter increases from a value slightly greater than the projectile diameter to the diameter of crater in a semi-infinite target, as illustrated in Fig. 4A.8.

(2) As target thickness increases, the total mass of spall ejected from the rear of a thin target increases to a maximum at some target thickness and then begins to decrease, returning eventually to zero as target thickness continues to increase (Fig. 4A.9). Also shown in Fig. 4A.9 is the fact that the total mass of spall depends strongly on bumper plate material.

The general conclusion arrived at by Vitali, et al., is that damage to thin targets which are impacted by a high-velocity projectile is similar to that produced by shaped-charge jets; however, as the authors themselves emphasize, this conclusion is tentative, and more detailed test results will be required to support it. (This conclusion is similar to that depicted in Fig. 4A.1 and discussed in Section 3, where the projectile is deformed and partially destroyed during penetration in the manner described for penetration of a shaped-charge jet.)

4A.2.8 Bull (Ref. 27) carried out a theoretical study of the use of bumpers for protection from meteoroids. An impact model is described that assumes ideal fluid behavior for projectile and target materials, and the strong shock approximation is used, i.e., the density ratio is assumed to have reached a limiting value. The model is described in detail in two phases: (1) The initial shock mechanisms and states along the lines of conventional, one-dimensional hydrodynamic shock propagation are established; (2) the propagation of the initial planar fronts and the explosion-like expansion flow of the vaporized pellet material are analyzed. Impact pressures and temperatures are

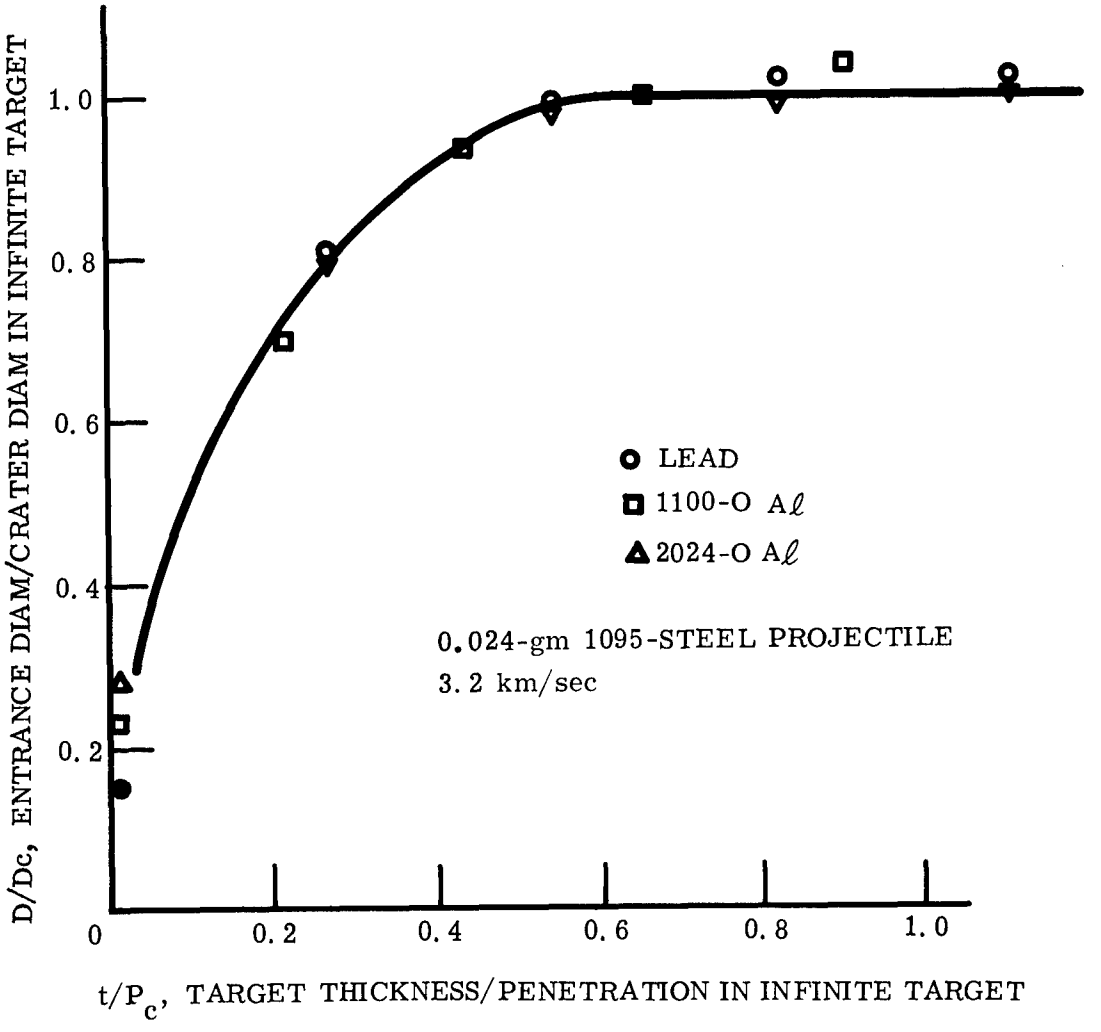

Fig. 4A.8 Thin Target Entrance Diameter vs. Target Thickness, Normalized to Semi-Infinite Target Results (from Ref. 22)

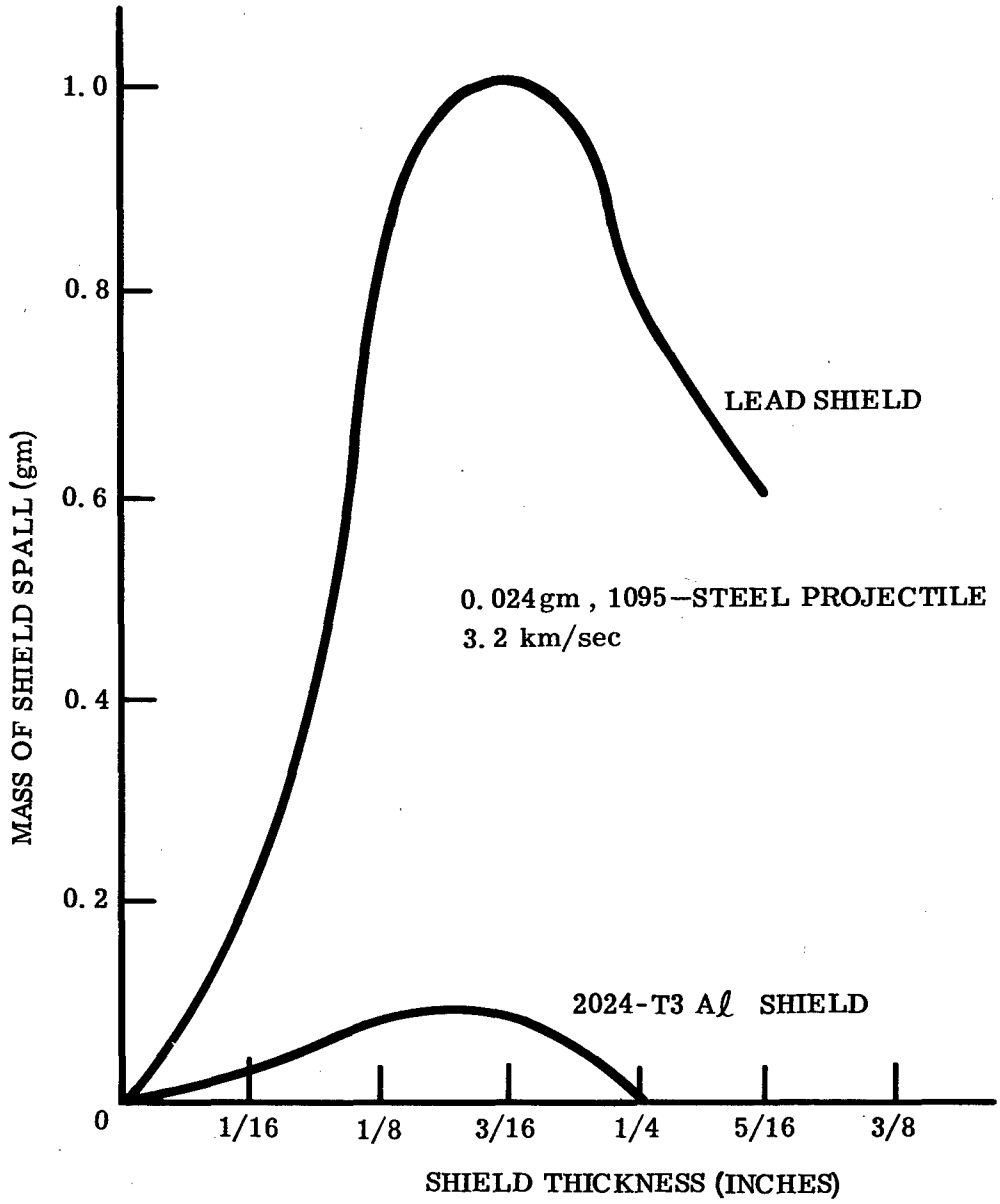

Fig. 4A.9 Recovered Spall Mass Behind Lead and Aluminum Shields (from Ref. 22)

calculated as functions of impact velocity, and the radial flow of material from the rear face of the bumper is considered.

4A.2.9 McMillan (Ref. 25) studied the effect on the damage to thin targets by changing the target radius, as shown in Fig. 4A.10. For a wall thickness of 0.446 inches, the depth of penetration is substantially decreased as the inside diameter is decreased from infinite (flat target) to 0.50 inches. Below 0.50 inches, little change in penetration is observed. The ability of the circular target shape to sustain impact damage stems from the fact that shock propagation through the circular section is affected by more free surface. Consequently, the rarefaction waves which act to diminish the intensity of the transient pulse react more quickly, thus weakening the shock and diminishing its ability to perforate the target or to cause spall.

4A.3 Composites, Laminates, and Fillers

Although composites, laminates, and fillers are not thin targets, per se, they are included in this section because they are often used in conjunction with thin targets. The following definitions will apply to this discussion.

Composite: compounded of two or more homogeneous materials which are mixed in such a way that any given volume of the structure, of adequate size, has the same composition as any other volume of equal size. For example, a uniform mixture of steel spheres in a matrix of plastic.

Laminate: adjacent layers of the same or different materials either with or without a bonding agent between the layers. For example, a steel shield bonded to a plastic structure.

Filler: a homogeneous material, usually of low bulk density, that uniformly fills the space between adjacent plates. For example, glass-wool batting between aluminum sheets.

In general, the experimental and theoretical efforts devoted to composites, laminates (Ref. 25), and fillers (Ref. 26) have been relatively small. Most of the published literature has been concerned either with low velocities, which makes it of little use to the hypervelocity investigator, or has been classified, which severely limits its dissemination. In one set of experiments, however, the behavior of a glass-wool filler was investigated by Nysmith and Summers

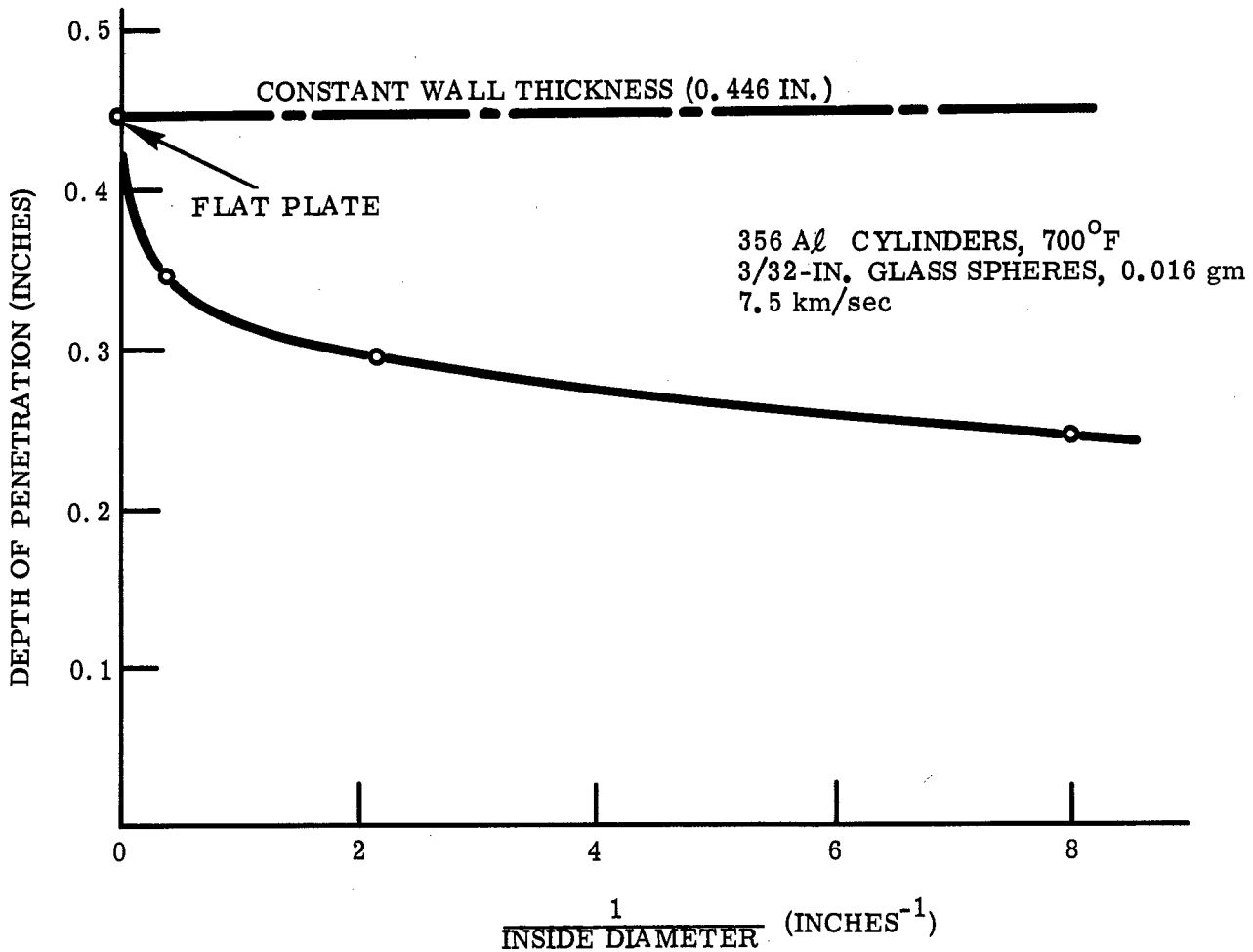

Fig. 4A.10 Depth of Penetration vs. Target Diameter – Constant Wall Thickness

(Ref. 12, Fig. 4A. 7) who found that at velocities of less than 4 km/sec the filler was effective in reducing damage by spall to backup targets (under their test condition). A more detailed study of fillers was made by Rolsten, et al., (Ref. 3) who concluded that energy-absorbing fillers can significantly reduce the weight-per-unit-area of a meteoroid protection system.

The ability of a laminate to eliminate spall from the rear of a relatively thick target (Fig. 4A. 11 – based on Gehring and Lieblein (Ref. 8) who studied the potential vulnerability to meteoroid impact of various space radiator designs.) Among the designs studied were thick-walled, cast-aluminum tubes, one of which utilized a tough, ductile inner liner. Without the laminate, or liner, the pressure wave generated by the impacting projectile has caused a substantial piece of spall to be separated from the inside wall; whereas, with a liner, the liner has dimpled but prevented any spall from being separated from the tube. (See Section 4C and Fig. 4C. 2.)

The effects of laminates on spall and penetration in flat targets are shown in Fig. 4A. 12 (Ref. 25). All four targets shown are of equal weight per unit area. The aluminum/polyethylene laminate was most effective in eliminating the ejection of spall (the aluminum has perforated and spalled but the polyethylene has contained the debris). The aluminum/copper laminate was most effective in eliminating spall from the aluminum, although the copper was severely deformed and spalled. The copper/aluminum laminate provided the poorest protection in terms of depth of penetration and spall. The main point illustrated in Fig. 4A. 12 is that there is not any one laminated structure that will provide maximum protection; rather, the type of protection required (allowable depth of penetration or spall) will determine the combination of materials and thicknesses.

4A. 4 Summary

It should be emphasized that the conclusions cited above are based on the particular test conditions described in the respective reports and are not intended to apply to all encounter conditions.

There is general agreement in both experimental and theoretical investigations that one or more thin sheets placed in front of a principal target will reduce damage to that target. It is also generally agreed: that the thin target

ALUMINUM TUBES, 700° F

3/32-IN. DIAM GLASS SPHERE, 7.6 km/sec

NO LINER

HS-25 LINER (0.02 IN.)

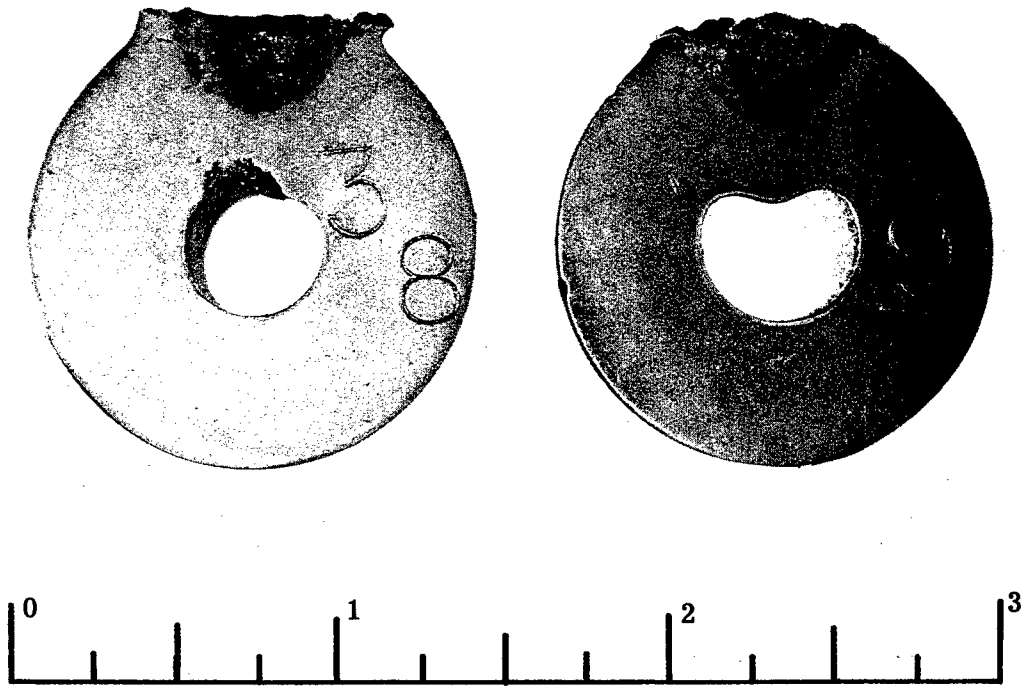

Fig. 4A.11 Effect of Liner on Spall – Cylindrical Target

ALL TARGETS EQUAL WEIGHT PER UNIT AREA, 3.4 gm/cm^2
1/8-IN. 2017 ALUMINUM SPHERES, 0.047 gm
7.4 km/sec

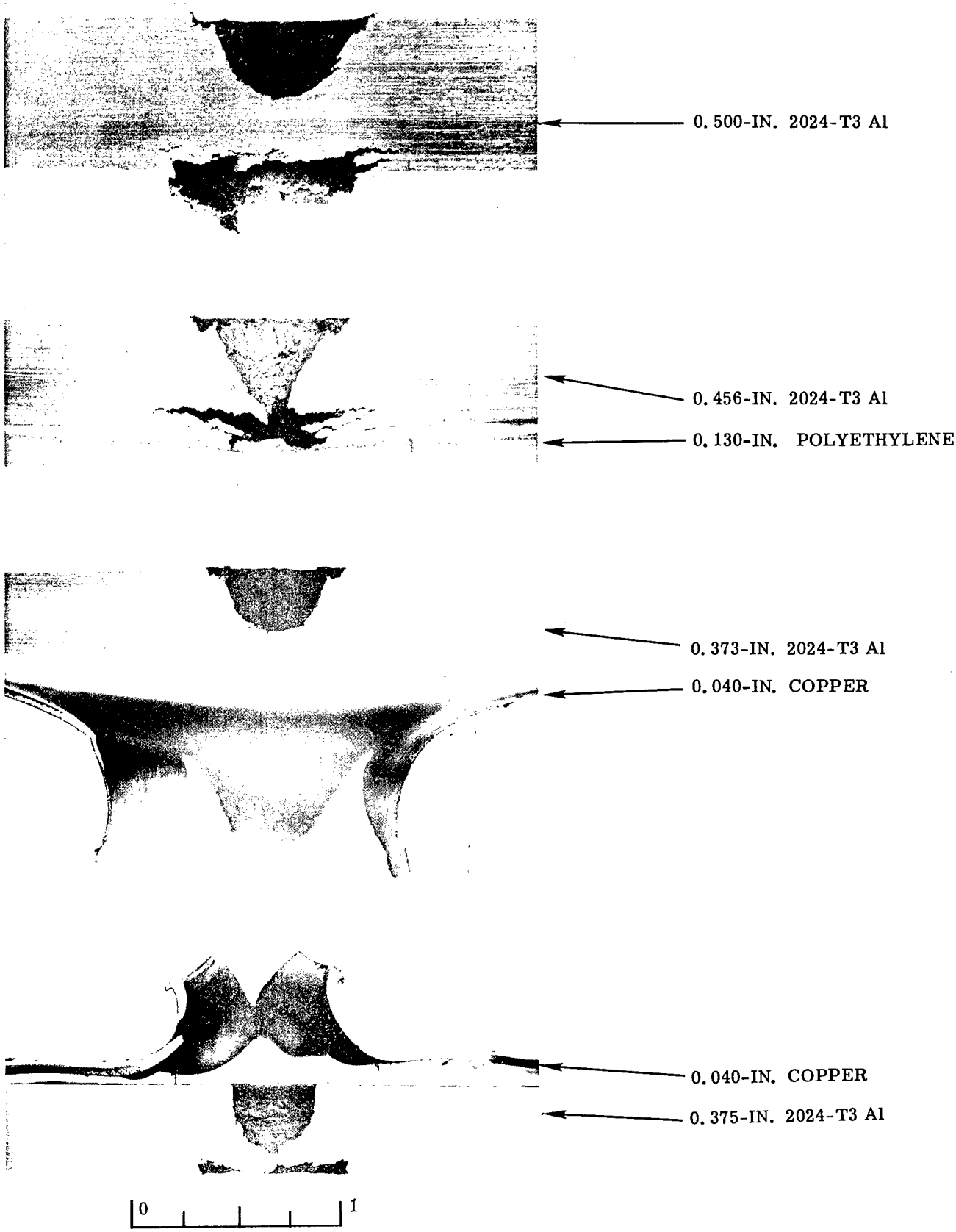

Fig. 4A.12 Effects of Laminates on Spall and Penetration – Flat Targets

mechanism is basically one of breaking up the projectile, causing the fragments to spread out over a large area (relative to the original projectile area), and reducing the velocity of the fragments normal to the principal target; that increasing the spacing between the shield and the principal target increases the effectiveness of the mechanism; that increasing shield mass per unit area, or density, increases the effectiveness; that the strength of the shield material has relatively little effect; that composites, laminates, and fillers can be of advantage in developing low-weight-per-unit-area meteoroid protection systems; and that shield effectiveness is a function of projectile mass and velocity and, to a lesser degree, material.

There is not general agreement (as might be expected as a result of the widely varying test conditions) on the quantitative aspects of protection by thin targets. In particular, extrapolation of test results at relatively low velocities (less than 8 km/sec) to meteoroid velocities (11 – 72 km/sec) has resulted in a broad range of estimates of shield design parameters required for protection on specific space missions. Of course, a substantial portion of the range of estimates can be attributed to the uncertainty in meteoroid distribution estimates, discussed in Section 1.

REFERENCES FOR SECTION 4A - THIN TARGETS

1. R. J. Eichelberger and J. W. Gehring, "Effects of Meteoroid Impacts on Space Vehicles," ARS J., Vol. 32, No. 10, Oct 1962, pp. 1583-1591
2. F. L. Whipple, "The Meteoric Risk to Space Vehicles," Vistas in Astronautics, Permagon Press, 1958, pp. 115-124
3. R. F. Rolsten, H. H. Hunt, and J. N. Wellnitz, "Study of Principles of Meteoroid Protection," General Dynamics/Astronautics Report No. A.E. 62-0413, Apr 1962
4. S. F. Singer, "The Effect of Meteoric Particles on a Satellite," Jet Propulsion, Vol. 26, No. 12, Dec 1956
5. J. J. Volkoff, "Protection Requirements for the Resistance of Meteorite Penetration of Interplanetary Spacecraft," AIAA Paper No. 63059-63 (presented at the AIAA Electric Propulsion Conference, Colorado Springs, Colo., Mar 11-13, 1963)
6. R. L. Bjork, "Meteoroids Versus Space Vehicles," ARS J., Vol. 31, No. 6, Jun 1961
7. D. B. Lull, "Analysis of Impact of Hypervelocity Pellet with a Thin Shield," Arthur D. Little, Inc., Memorandum No. 62509-1, 29 Dec 1959
8. J. W. Gehring and S. Lieblein, "Preliminary Results on Effects of Hypervelocity Impact on Space Radiator Tubes," ARS Paper No. 2544-62 (presented at the ARS Space Power Systems Conference, Santa Monica, California, Sep 1962)
9. J. R. Davidson and P. E. Sandorff, "Environmental Problems of Space Flight Structures, II. Meteoroid Hazard," NASA TN-D-1493, Jan 1963
10. B. Paul and M. Zaid, "Normal Perforation of a Thin Plate by Truncated Projectiles," Journal of The Franklin Institute, Vol. 265, No. 4, Apr 1958, pp. 317-335

11. C. J. Maiden, J. W. Gehring, and A. R. McMillan, "Investigation of Fundamental Mechanism of Damage to Thin Targets by Hypervelocity Projectiles," General Motors Corporation, GM Defense Research Laboratories Semi-Annual Report, Contract ARPA Nonr-3891 (00) (X), GM DRL Report No. TR63-208, Santa Barbara, Calif., Mar 1963 (work reported in this paper was presented at the Sixth Hypervelocity Impact Symposium, Cleveland, Ohio, Apr 30 - May 2, 1963)

12. C. R. Nysmith and J. L. Summers, "Preliminary Investigation of Impact on Multiple-Sheet Structures, Studies of Meteoroid Hazard to Space Flight and Application to the Design of Space Vehicles," NASA TN-D-1039, Sep 1961

13. D. Humes, R. N. Hopko, and W. H. Kinard, "An Experimental Investigation of Single Aluminum Meteor Bumpers," Proceedings of the Fifth Symposium on Hypervelocity Impact, Vol. 1, Part 2, Nonr-(G)-0020-62(X), Colorado School of Mines, Apr 1962 (See also "An Experimental Investigation of the Effectiveness of Single Aluminum Meteoroid Bumpers," by D. H. Humes, NASA TN-D-1039, May 1963)

14. A. C. Charters and G. S. Locke, Jr., "A Preliminary Investigation of High Speed Impact; The Penetration of Small Spheres into Thick Copper Targets," NACA RM-A58B26, 1958

15. J. L. Summers, "Investigations of High-Speed Impact; Regions of Impact at Oblique Angles," NASA TN-D-94, 1959

16. W. Kinard, C. H. Lambert, Jr., D. R. Schryer, and F. W. Casey, Jr., "Effects of Target Thickness on Cratering and Penetration of Projectiles Impacting at Velocities to 13,000 ft/sec," NASA Memo 10-18-58L, 1958

17. A. E. Olshaker, Jr., "Experimental Investigation in Lead of the Whipple Meteor Bumper," J. Appl. Phys., Vol. 31, No. 12, Dec 1960, pp. 2118-2120

18. W. Herrmann and A. H. Jones, "Survey of Hypervelocity Impact Information," Massachusetts Institute of Technology, Aeroelastic and Structures Research Laboratory, ASRL Report No. 99-1, Sep 1961

19. R. K. Becker and R. Vitali, "Spatial Distribution of Fragments Behind Thin Targets," Fundamentals of Shape Charges, Chapter III, Carnegie Institute of Technology, Pittsburgh, Pa., Oct 31, 1961

20. R. W. Watson, "The Perforation of Thin Plates by High Velocity Fragments," Proceedings of the Fifth Symposium on Hypervelocity Impact, Vol. 1, Part 2, Nonr-(G)-0020-62(X), Colorado School of Mines, Apr 1962

21. K. R. Becker, R. W. Watson, and F. C. Gibson, "Hypervelocity Impact Phenomena," Bureau of Mines, Explosives Research Laboratory Quarterly Report to the Ballistic Research Laboratory, Auth. No. 4086, Aug 1962

22. R. Vitali, K. R. Becker, and R. W. Watson, "Perforation of Finite Targets by High Velocity Projectiles," Proceedings of the Fifth Symposium on Hypervelocity Impact, Vol. 1, Part 2, Nonr-(G)-0020-62(X), Colorado School of Mines, published Apr 1962

23. C. R. Nysmith and J. L. Summers, "An Experimental Investigation of the Impact Resistance of Double-Sheet Structures at Velocities to 24,000 Feet/Second," NASA TN-D-1431, Oct 1962

24. J. O. Funkhouser, "A Preliminary Investigation of the Effect of Bumpers as a Means of Reducing Projectile Penetration," NASA TN-D-802, Apr 1961

25. A. R. McMillan, "An Investigation of the Penetration of Hypervelocity Projectiles into Composite Laminates" (paper presented at the Sixth Hypervelocity Impact Symposium, Cleveland, Ohio, Apr 30-May 2, 1963)

26. S. J. Pepitone and B. W. Reynolds, "Meteoroid Protection System for Space Vehicles," AIAA paper No. 2895-63 (presented at the AIAA Launch and Space Vehicle Shell Structures Conference, Palm Springs, Calif., Apr 1-3, 1963)

27. G. V. Bull, "On The Impact of Pellets With Thin Plates, Theoretical Considerations - Part I," Technical Report Under NASA Contract No. NAS5-664, Arthur D. Little, Inc., Report No. 63270-03-01, Jan 1962

4.B PRESSURIZED VESSELS AND STRESSED STRUCTURES

The impact of meteoroid particles on those space vehicles that have components which are highly pressurized with fluid or gas of varying temperatures have reportedly (Refs. 1-3) caused catastrophic ruptures. Typical pressurized vessels in space vehicles which may encounter meteoroids are power plants, space radiators (Ref. 4), fuel tanks, and storage bottles. Since it is impossible to control meteoroids in space, the designer must choose a safeguard that can protect the system from impact by the largest meteoroid it is likely to encounter during its time of exposure.

When a high-speed particle strikes the surface of a pressurized vessel, one of two things will usually happen: First, the projectile may completely perforate the vessel, spewing particle fragments and spall into the inner material and increasing the internal pressure; or (in the case of a very thin-walled vessel) the projectile may perforate both the front and rear surfaces of the container; second, the projectile may not perforate but may generate a shock wave into the internal fluid, setting up a compression wave in the fluid. In both cases, the internal pressure will be increased; when the internal pressure exceeds the hoop-tensile-strength of the container, the pressure vessel will fail.

For example, in the case of a structure which has a very thin wall, such as a pressurized missile-propellant tank, it was observed by Rolsten, Hunt, and Wellnitz (Ref. 2), and Stepka and Morse (Ref. 3) that the chances of catastrophic failure are high. Rolsten, et al., cite the case of impact of a liquid-pressurized, thin-walled vessel by a projectile. As illustrated in Fig. 4B.1, there was catastrophic failure of the vessel wall, attributed to the stored energy from the hoop-tension stresses. On the other hand, in the case of a liquid-pressurized, thick-walled vessel, the probability that catastrophic failure will occur is lower.

GM Defense Research Laboratories conducted a test where a 1/8-in.-diameter glass sphere was impacted against a sphere of 2024-T3 aluminum (16 in. in diameter and 1/4 in. thick) at 7.0 km/sec. The aluminum sphere contained water at a pressure of 800 psi. Figure 4B.2 shows that there was no catastrophic failure – instead, the result was a clean perforation. However, if the projectile had been larger, or the thickness of the structure reduced, the chances of a catastrophic failure would have been greater. Also, the failure

IMPACT VELOCITY = 5.2 km/sec

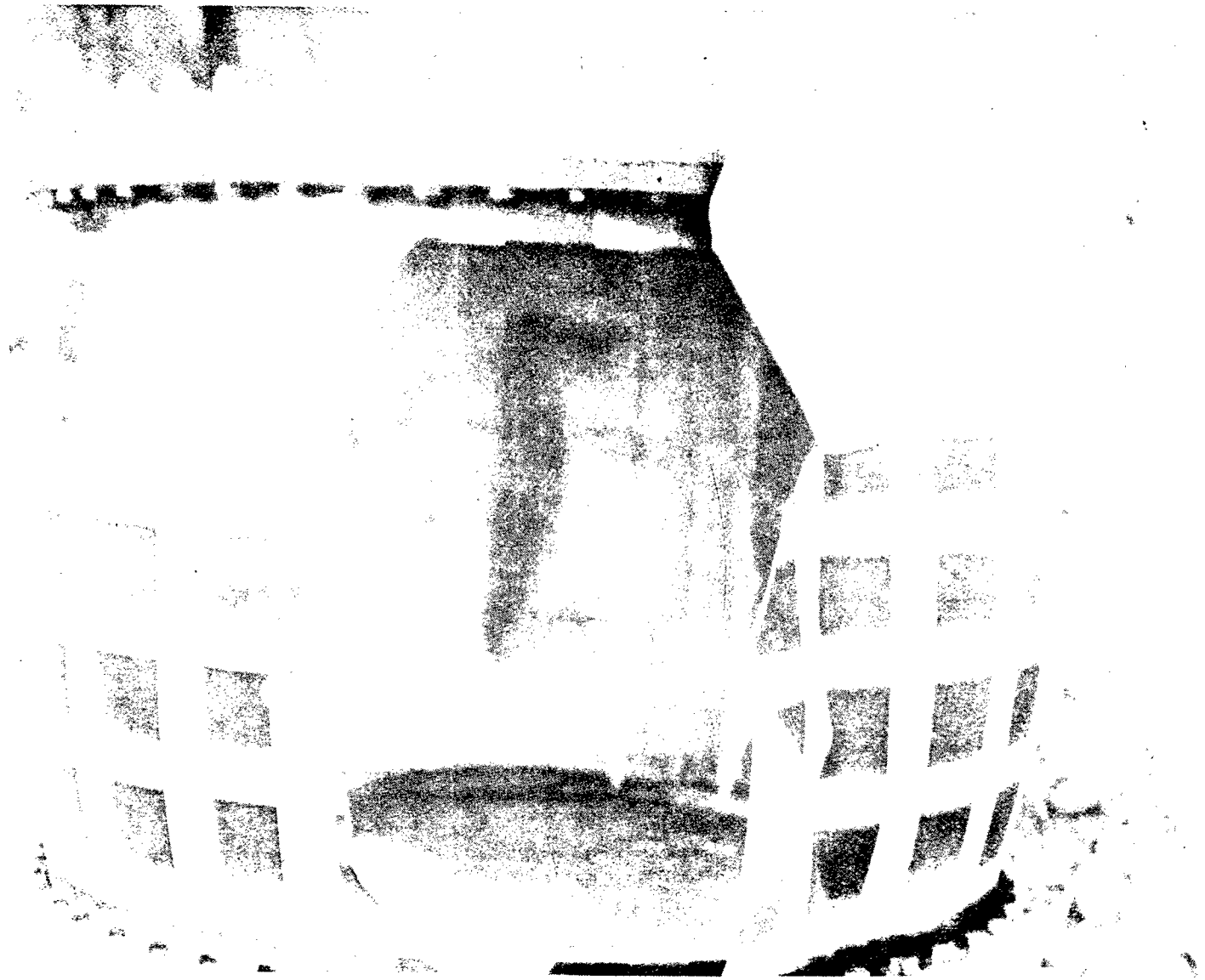

Fig. 4B.1 Impact Damage to Thin-Walled, Liquid-Pressurized Vessel (from Ref. 2)

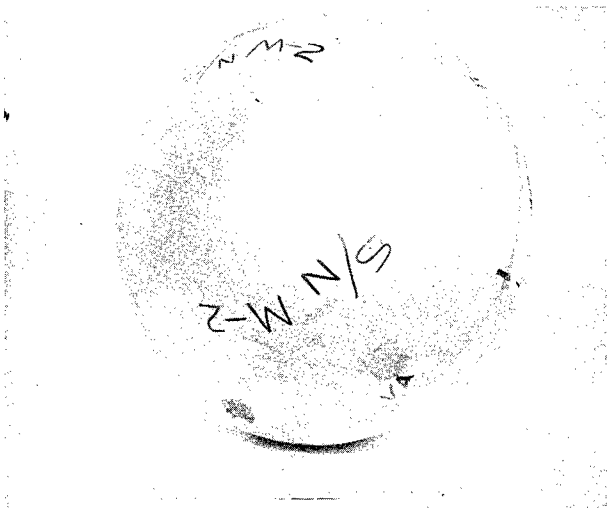

16-IN.-DIAM SPHERE
1/4-IN. THICK

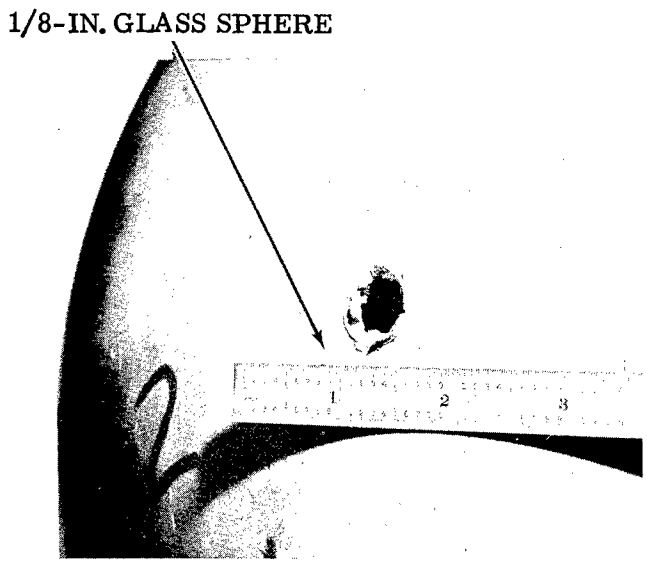

SPHERE CONTAINED WATER AT 800 PSI
BEFORE IMPACT AT 7.0 km/sec

Fig. 4B.2 Impact Damage to Thick-Walled, Liquid-Pressurized Vessel

mechanisms under conditions of gas pressurization, where shock propogation to the rest of the vessel would be significantly different, could have been different in each case. Some results of experimental work on pressure vessels can be found in the classified literature (Kreyenhagen, Mortensen, and Zimney, Ref. 5).

Another problem is that the high temperature associated with an impact flash created by the impact of a high-speed particle against a fluid-rich pressurized space vehicle may cause it to burn or explode. An astronaut may experience shock, concussion, or disastrous decompression (Ref. 6).

The frictional removal or change of temperatures of structural material as the result of repeated impacts can contribute to failure by either (1) reducing the net area of the structure, thus increasing the stress level, or (2) reducing the strength of the material by uncontrolled heat treating, so that failure of the structure could result from a shorter critical crack length.

In conclusion, catastrophic failure depends upon the structure of the material, stress level, internal pressure of the medium, type of internal fluid, area of hole, compression wave behavior in the material, and reactivity between the medium and structural material.

REFERENCES FOR SECTION 4B

PRESSURE VESSELS AND STRESSED STRUCTURES

1. R. H. Kemp, "Flow and Fracture Problems in Aerospace Vehicles," Proceedings of the NASA-University Conference on the Science and Technology of Space Exploration, Vol. 2, Chicago, Illinois, Nov 1-3, 1962, NASA SP-11

2. R. F. Rolsten, H. H. Hunt, and J. N. Wellnitz, "Study of Principles of Meteoroid Protection," General Dynamics/Astronautics Report No. AE 62-0413, Apr 1962

3. F. S. Stepka and C. R. Morse, "Preliminary Investigations of Catastrophic Fracture of Liquid-Filled Tanks Impacted by High-Velocity Particles," NASA TN-D-1537, May 1963

4. J. W. Gehring and S. Lieblein, "Preliminary Results on Effects of Hypervelocity Impact on Space Radiator Tubes," ARS Paper No. 2544-62 (presented at the ARS Space Power Systems Conference, Santa Monica, California, Sep 1962)

5. K. N. Kreyenhagen, R. B. Mortensen, and H. S. Zimney, "Impact Effects Against Propulsion Systems (U)," Proceedings of the Fifth Symposium on Hypervelocity Impact, Vol. 2, Nonr-(G)-0020-62(X), Colorado School of Mines, Apr 1962

6. M. Kornhauser, "Satellite Pressure Losses Caused by Meteoroid Impacts," ARS J, Vol. 30, No. 5, May 1960, pp. 475-479

4C. EFFECTS OF SPALLING

When a particle strikes a plate at high velocity, it forms a crater in the front surface of the plate and starts a strong compressive shock (see Section 3). This shock, attenuated as it travels through the plate, is generally reflected off the rear surface (or any free surface) as a tension wave. If the plate is thin enough, or if the initial shock is strong enough, the reflected tension wave will be so intense that a portion of the free surface of the plate may be ejected with a momentum sufficient to damage other parts of the structure (Refs. 1-9). This phenomenon, called spalling, can be defined as fracture resulting from reflection of a decaying shock wave from a free surface. Spalling can occur even when the plate is not perforated (Fig. 4C.1). The diameter of the spall is usually two or three times the thickness of the plate; the thickness of the spall is usually in the range of 1/10 to 1/2 the thickness of the plate. The following formula (Ref. 2) can be used for computing spall thickness.

$$t = \frac{\sigma_c}{\sigma_o} \quad \frac{\lambda}{2} \qquad (4C.1)$$

where

t = spall thickness

σ_c = critical stress necessary to fracture the material

σ_o = maximum stress of the compressive wave

λ = length of the pulse

The velocity v of the spall is given by

$$v = \frac{2\sigma_o - \sigma_c}{\rho_t} \qquad (4C.2)$$

where

ρ_t = density of material

Table 4C.I (Ref. 3) gives the critical normal fracture stress of several materials determined experimentally.

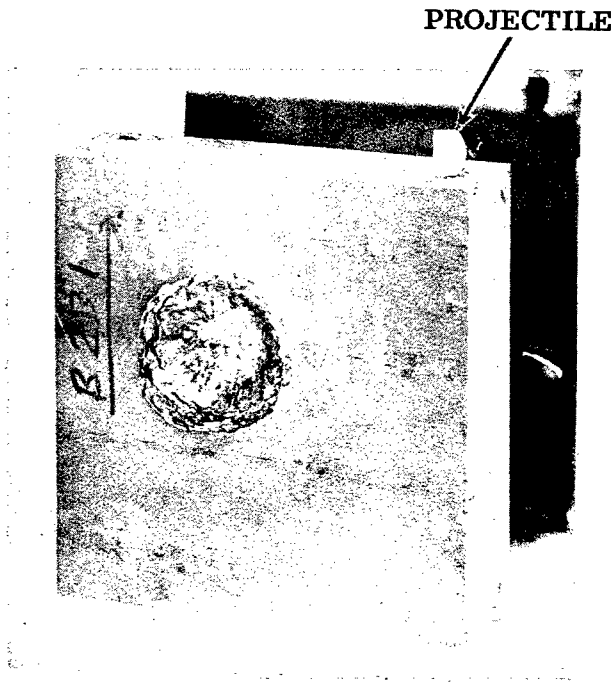

FRONT VIEW

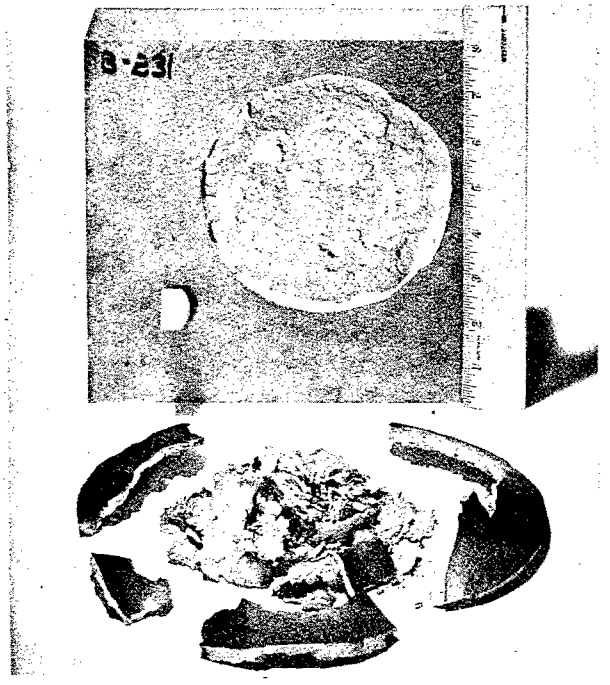

REAR VIEW

TARGET: 2.0-IN. 2024-T3 ALUMINUM
PROJECTILE: 4.14-gm POLYETHYLENE

VELOCITY: 7.9 km/sec

Fig. 4C.1 Back Spall from Thick Target

Table 4C.I

CRITICAL NORMAL FRACTURE STRESS
OF SEVERAL MATERIALS

Metal	Critical Normal Fracture Stress (lb/sq in.)
4130 Steel	440,000
Copper	415,000
Brass	310,000
1020 Steel	180,000
2024-T4 Aluminum	140,000

The calculation of spall thickness and velocity is difficult because neither the magnitude nor the shape of the compressive pulse are well defined for given conditions of impact.

It is possible to reduce spall by using laminates of properly selected materials (Ref. 2). The pertinent property of a material is its acoustic resistance $G = \rho_t C$, where ρ_t is the density of the target and C is the velocity of shock wave propagation in the target under the conditions encountered. If a compressive stress pulse σ_1 in a material with an acoustic resistance G_1, reaches an interface between this material and one with an acoustic resistance G_2, the pulse σ_r reflected from the interface will have the height of

$$\sigma_r = \frac{G_2 - G_1}{G_2 + G_1}\sigma_1 \qquad (4C.3)$$

and there will be a pulse σ_t transmitted through the second material with the height of

$$\sigma_t = \frac{2G_2}{G_2 + G_1}\sigma_1 \qquad (4C.4)$$

The above two equations contain several implications which aid in understanding why and how the pulse is modified at an interface. Taking the ratio of the stress transmitted to the stress reflected as,

$$\frac{\sigma_t}{\sigma_r} = \frac{2G_2}{G_2 - G_1} \qquad (4C.5)$$

the following points become evident: When G_2 is much less than G_1, nearly all the stress is reflected; when G_2 is approximately equal to G_1, nearly all the stress is transmitted; and when G_2 is much greater than G_1, about 2/3 of the stress is transmitted. Thus, the stress pulse may be divided and attenuated to a greater extent in a laminate than in an equal weight of a homogeneous material. It is necessary, however, that the joint efficiency be near unity to avoid spalling at the joint.

Another possible approach is to cover the front surface of the plate with fine granules (Ref. 2) with the idea of attenuating the pulse by reflecting it repeatedly at the particle boundaries. The granule layer must be thick enough so that most of the crater will occur in these granules and not in the underlying plate.

This approach leads to consideration of the effect of a thin shield or bumper (separated from the main structure by a void) to break up an incoming particle (see Section 4A). The main target then receives many small impacts over a large area, and many small compressive shock waves are generated. The tendency of the main target to spall will be reduced as these shock waves are spread over more area.

Also suggested to prevent spalling is the use of a ductile liner. This has been proposed for a space radiator (Ref. 4) where a perforation would cause a fluid leak, while spalling without perforation could cause damage or failure of the liquid-circulating pumps by injecting metal particles into the fluid. The beneficial effects of having an inner liner can be seen in Figs. 4A.11 and 4C.2. In Fig. 4A.11, one target was lined with Haynes Alloy No. 25 liner; the second target had no liner, but the aluminum armor was thicker, thus keeping the weight per unit length constant. Although severely dimpled, the inner HS-25 liner prevented spalling of metal into the coolant tube. Figure 4C.2 compares an all-columbium tube with an aluminum armor/HS-25 liner tube, again with equal weight per unit length. The columbium was not perforated but was badly spalled, while the HS-25 liner prevented spalling in the laminated tube.

There was no damage to the inner tube of the lined target, even though the depth of penetration exceeded the depth predicted to cause spalling.

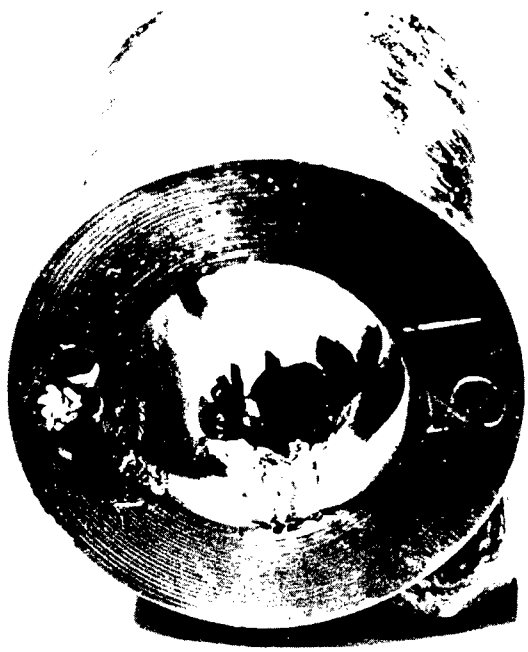

ALL COLUMBIUM WALL,
0.20-IN. THICK
NO PERFORATION
3/32-IN. GLASS SPHERE

0.40-IN. Al ARMOR, 0.02-IN. HS-25 LINER
NO PERFORATION
1/8-IN. GLASS SPHERE

$\bar{V} = 7.5$ km/sec

700^{O} F

(EQUAL WEIGHT PER UNIT LENGTH OF TUBE)

Fig. 4C.2 Protective Ability of Ductile Liner in Preventing Spall

This is attributed to the ability of the HS-25 liner to absorb the energy of the shock through deformation of the tube.

The phenomena of spalling and perforation are greater in a flat-plate target than in a section of cylindrical target (Fig. 4A. 10). The proximity to each other of the free surfaces in the cylindrical targets results in a more rapid attenuation of the pressure pulse; consequently, the cylindrical target offers more resistance to penetration than the flat plate. Referring again to Section 4A, Fig. 4A. 12 compares several laminated, flat structures, all of equal weight per unit area. Spall was observed in all cases. However, with the aluminum/polyethylene laminate, the spall was contained; with the aluminum/copper laminate, the spall was restricted to the copper.

Many references state that plate thickness (t) should be 1. 5 times the crater depth (p) in a semi-infinite target to prevent either perforation or spall. This value of 1. 5 does not have any theoretical basis and is probably a very optimistic (low) value for flat targets. Jaffe and Rittenhouse (Ref. 5) computed that spalling may occur at thicknesses up to 3. 0 times crater depth in a semi-infinite target. Loeffler, et al (Ref. 6) used 1. 75; Bjork (Ref. 7) used 1. 5; and Gehring and Lieblein (Ref. 4) found the ratio to vary from 1. 1 for a cylindrical tube with a liner, to 1. 6 for a cylindrical tube without a liner.

Recent data obtained at GM DRL concerning the onset of spall is illustrated in Fig. 4C. 3. Spall (the ejection of material from the back of the target) is seen to occur at a target thickness between 0. 50 inches and 0. 56 inches. This indicates that the ratio of plate thickness to crater depth (0. 26 inches) should be a minimum of about 2. 1:1 to prevent spall, at least for the conditions cited. Figure 4C. 3 also shows perforation to occur at a target thickness between 0. 40 inches and 0. 50 inches, indicating that the ratio of plate thickness to crater depth should be a minimum of about 1. 7:1 to prevent perforation. These conclusions are shown graphically in Fig. 4C. 4, which gives depth of penetration as a function of target thickness. Note the abrupt decrease in penetration as target thickness approaches four projectile diameters and the relatively narrow range over which spall without perforation occurs.

Summarizing, spall is a phenomena that is best investigated for actual targets on an experimental basis. The ratios of plate thickness to crater depth

TARGET MATERIAL: 2024-T3 ALUMINUM

PROJECTILE: 1/8-IN. DIAM ALUMINUM SPHERE,
0.047 gm.

VELOCITY = 7.4 km/sec

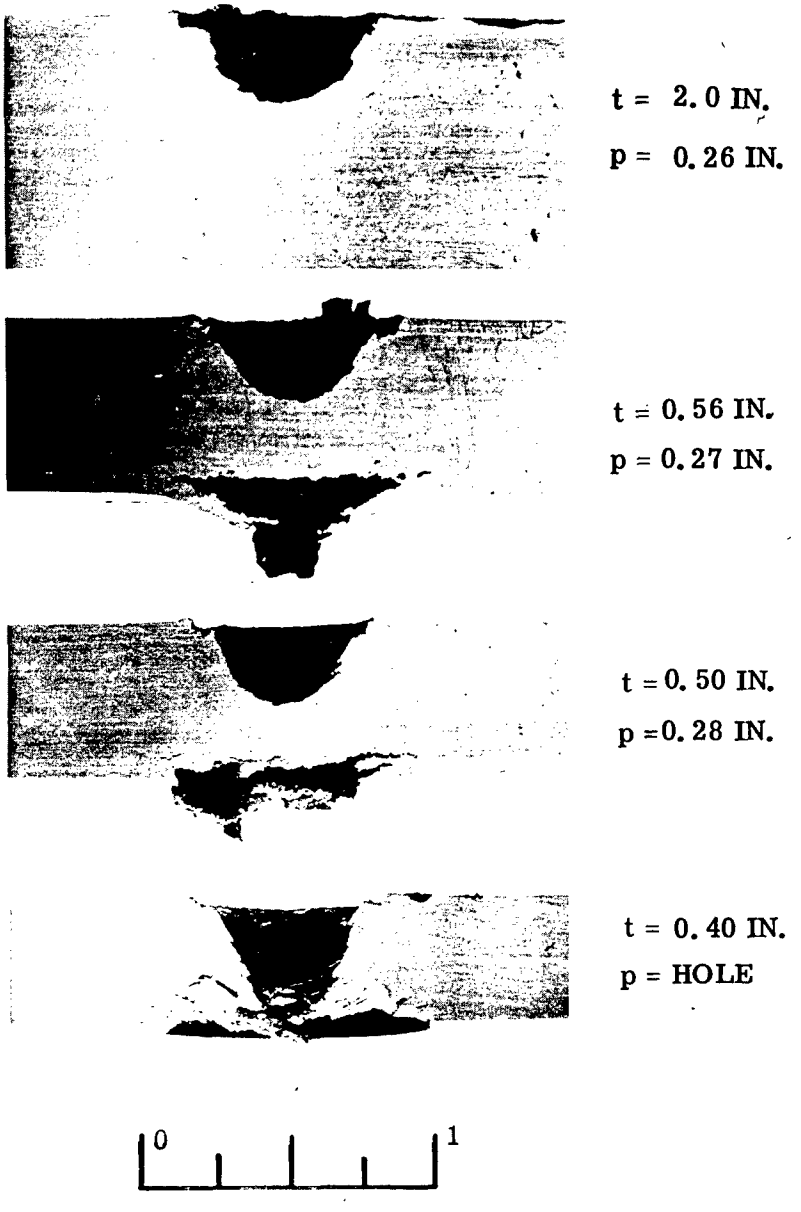

Fig. 4C.3 Depth of Penetration in Flat Targets of Various Thicknesses

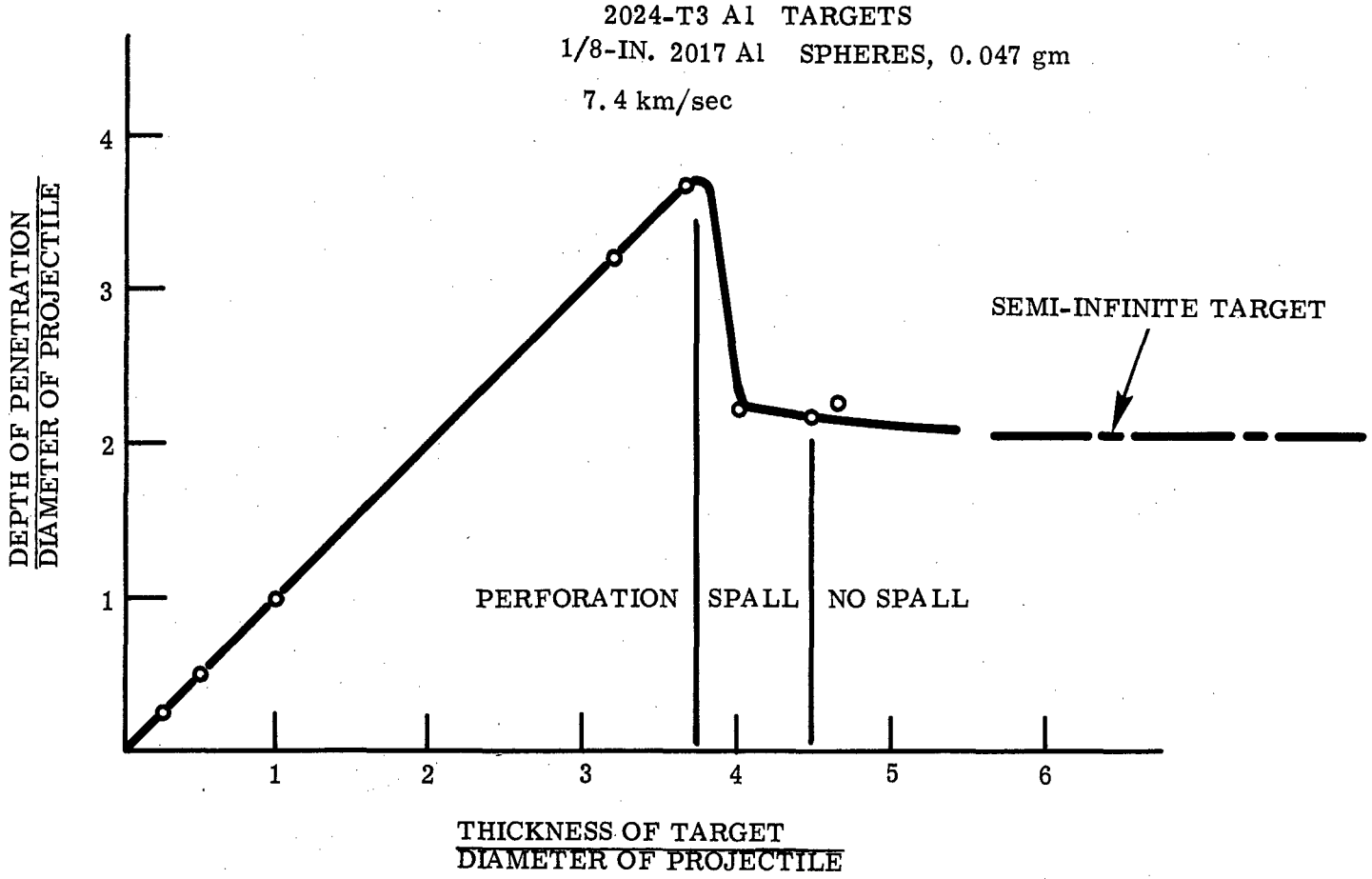

Fig. 4C.4 Depth of Penetration vs. Target Thickness – Flat Targets

necessary to prevent perforation or spall (in general, the ratio will be greater to prevent spall than to prevent perforation) are not firmly established and appear to be a function of velocity and target material.

REFERENCES FOR SECTION 4C - SPALLING

1. D. V. Keller and J. G. Trulis, "Mechanism of Spall in Lucite," J. Appl. Phys., Vol. 34, No. 1, Jan 1963

2. J. S. Rinehart, "Practical Countermeasures for the Prevention of Spallation," Colorado School of Mines Research Foundation, Report AF-SWC-TR-60-7 to Air Force Special Weapons Center, Albuquerque, N. M., 1960

3. J. S. Rinehart, "Some Quantitative Data Bearing on the Scabbing of Metals Under Explosive Attack," J. Appl. Phys., Vol. 22, No. 5, May 1951, pp. 555-560

4. J. W. Gehring and S. Lieblein, "Preliminary Results on Effects of Hypervelocity Impact on Space Radiator Tubes," ARS Paper No. 2544-62 (presented at the ARS Space Power Systems Conference, Santa Monica. Calif., Sep 1962)

5. L. D. Jaffe and J. B. Rittenhouse, "Behavior of Materials in Space Environments," ARS J., Vol. 32, No. 3, Mar 1962, pp. 320-346

6. I. J. Loeffler, S. Lieblein and N. Clough, "Meteoroid Protection for Space Radiators," ARS Paper No. 2543-62 (presented at the ARS Space Power Systems Conference, Santa Monica, Calif., Sep 1962)

7. R. L. Bjork, "Meteoroids vs. Space Vehicles," ARS J., Vol. 31, No. 6, Jun 1961, pp. 803-807

8. R. F. Rolsten, H. H. Hunt, and J. N. Wellnitz, "Study of Principles of Meteoroid Protection," General Dynamics/Astronautics Report No. AE 62-0413, San Diego, Calif., Apr 1962

9. R. W. Watson, K. R. Becker, and F.C. Gibson, "Hypervelocity Impact Phenomena," Bureau of Mines, Explosives Research Laboratory, Quarterly Report to the Ballistic Research Laboratory, Auth. No. 4086, Mar 1963

4D. OBLIQUE IMPACT

Of the phenomena related to the impact of a hypervelocity projectile, one that most evades theoretical description, derives from the case in which the projectile strikes the target at an oblique angle. Impacts which occur at a high angle of obliquity are of utmost concern to the vehicle designer, since it can be shown that in most cases the impact of natural meteoroids or the impact of antisatellite-produced fragments will probably strike the vehicle at some angle other than normal. Tests to evaluate the lethality of projectiles impacting at angles of obliquity have provided an approximation of the damage that might be expected; these tests, however, are far from conclusive.

Several investigators (Ref. 1) have noted that, for hypervelocity impact, the craters remain essentially hemispherical until a relatively narrow transition region is reached, when the component of projectile velocity normal to the target surface falls below some critical region – possibly related to the wave velocity in the target material. At this stage, the resulting crater becomes definitely asymmetrical as shown in Fig. 4D. 1. However, by increasing the projectile velocity until the normal component of velocity moves into the hypervelocity impact regime, the crater resumes a hemispherical shape.

Though it lacks a theoretical basis, this result serves as a criterion for all materials tested. Bryan (Ref. 2) carried out an approximation to a mathematical description of the shape of a crater formed under conditions of normal and oblique impact. His interpretation was in terms of the requirements of the conservation of energy and momentum of both the impacting projectile and the material ejected from the asymmetrical crater. This approach could provide enough information to estimate the fraction of energy that is carried away by the ejected material, provided the dynamic critical shear stress is known.

Bryan also relates crater depth and diameter to impact angle, describing the cratering mechanism as a process of hydrodynamic penetration followed by radial flow (afterflow) which continues until the dynamic pressure has decreased to the order of the strength of the target material. Considering the projectile to be a very short jet, and applying jet penetration theory where the primary phase is a function of projectile length and density but not velocity, the primary penetration becomes relatively small. The afterflow, however, will increase with increasing velocity and, since the afterflow has approximate

STEEL PROJECTILE
LEAD TARGET

30°
2.32 km/sec

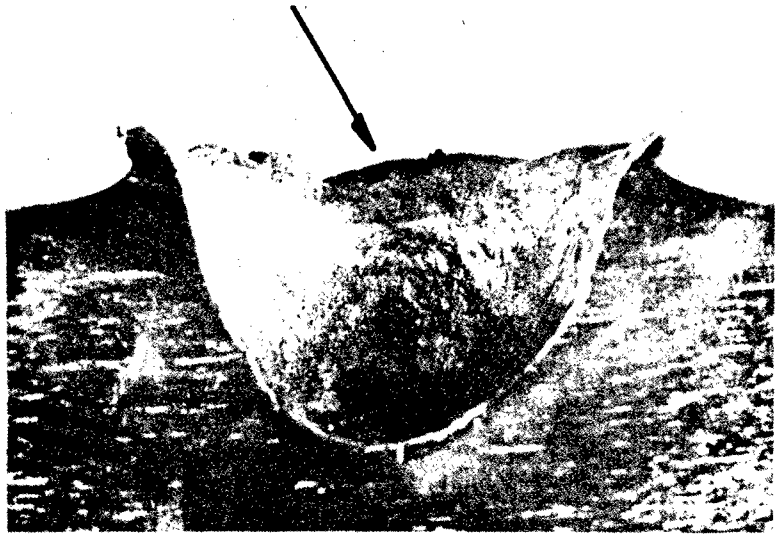

60°
2.32 km/sec

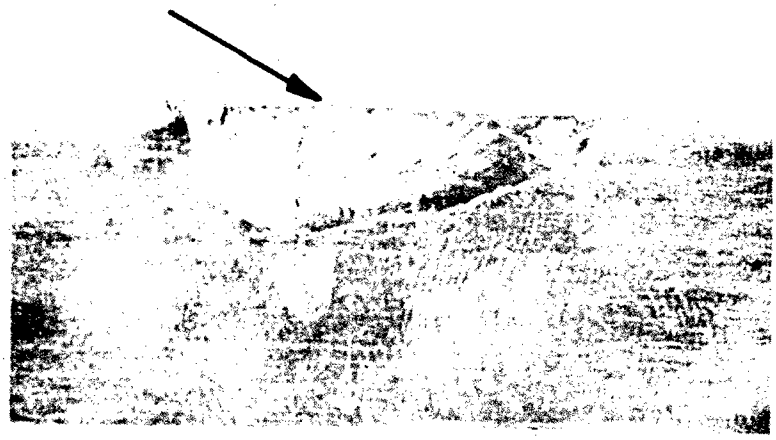

60°
3.22 km/sec

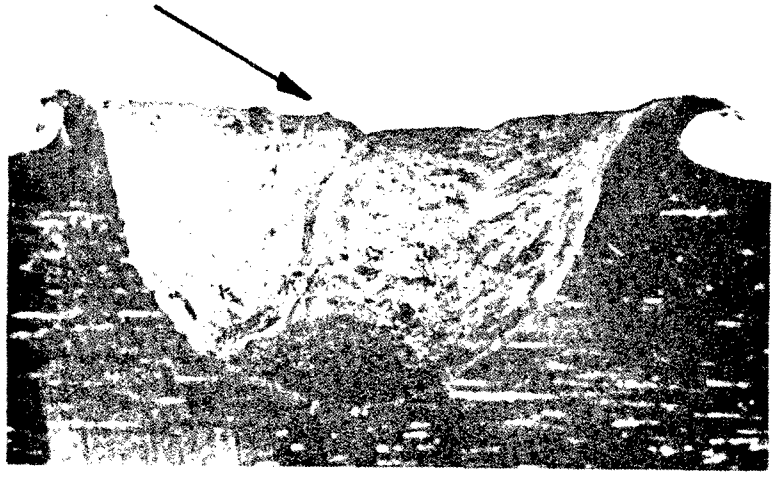

Fig. 4D.1 Crater Formation at Oblique Angles of Impact – Flat Targets (from Ref. 3)

spherical symmetry, the crater shape will tend to become hemispherical as velocity increases, regardless of the geometry of primary penetration.

Eichelberger and Gehring (Ref. 3) related crater depth and diameter to a process (produced by the initial high pressures) of hydrodynamic penetration followed by radial flow. This radial flow continues until the dynamic pressure falls below the strength of the target. Under conditions of oblique impact where the primary penetration of the causative projectile occurs at grazing angles, radial flow of the target material would be expected to be asymmetric also. A graphical illustration of the dependence of crater volume on impact angle is shown in Fig. 4D. 2 which is a plot of projectile energy per unit crater volume as a function of impact angle.

Beyond the critical region, the asymmetrical crater becomes deeper and steeper on the side of the crater from which the projectile approached. (See Fig. 4D. 1.) Figure 4D. 3 shows the results of oblique impact into thick-walled cylinders with liners. At grazing incidence and marginal impact velocities, the crater becomes very elongated, and the projectile has been seen to ricochet with little penetration of the target.

Experimental firings of a variety of projectiles into a variety of target materials have been conducted by Bryan (Ref. 2), Kineke (Ref. 4), Summers (Ref. 5), Anderson (Ref. 6), Gehring and Lieblein (Ref. 7), and Nysmith and Summers (Ref. 8). Several important conclusions can be drawn from the results of these investigations: For a given impact angle, the ratio of crater volume to projectile energy is approximately constant, being unaffected by changes in projectile energy; and this ratio is a linear function of the cosine of the angle of incidence.

These conclusions result from impacts on relatively thick targets. For oblique impact against thin targets which are more typical of vehicle structure, the results of the experiments of Kreyenhagen and Zernow (Ref. 9) and Becker, Watson, and Gibson (Ref. 10) are of interest. In their experiments, splashing from the target surface was seen to consist of tiny particles jetting out of the contact zone during the initial phase of impact. The projectile broke up as it penetrated the target plate, and a portion of the original projectile, together with fragments from the thin plate, emerged from the back of the target plate in a divergent pattern. These results are consistent with observations of the perforation of thin targets at normal angles of attack.

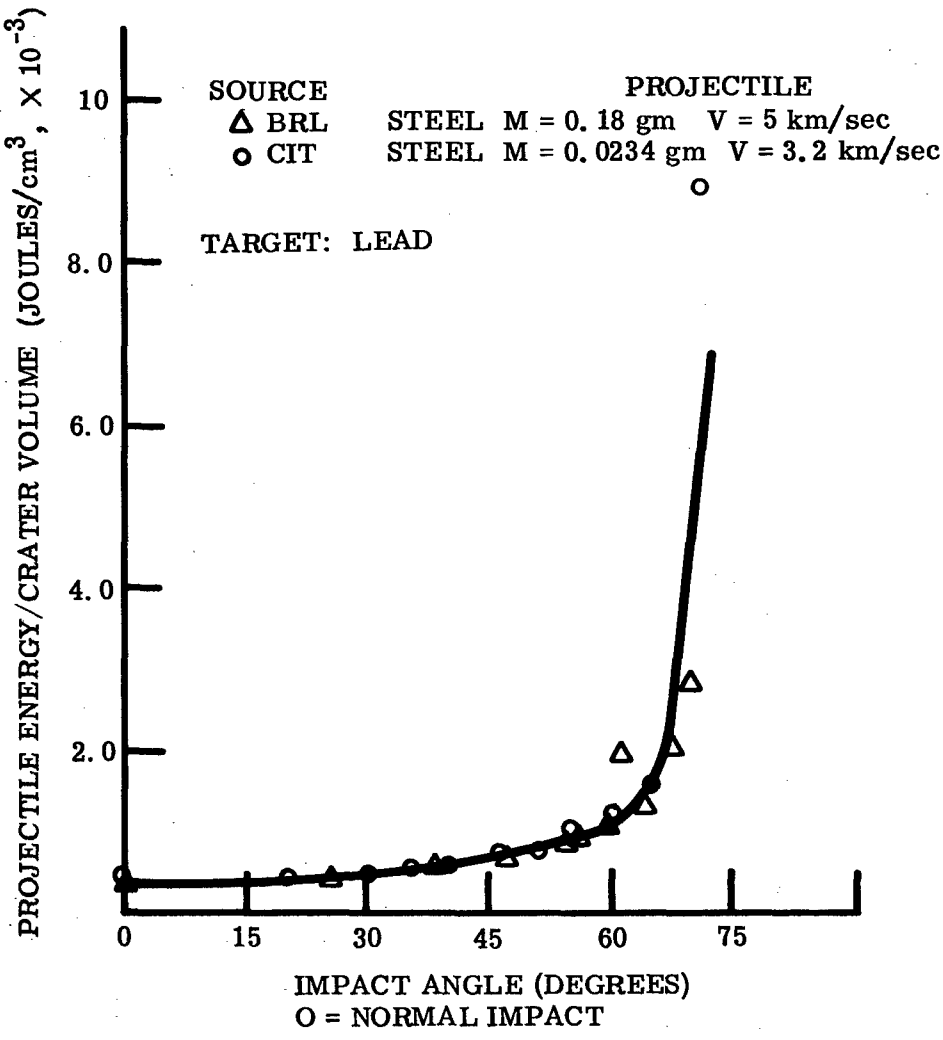

Fig. 4D.2 Cratering Efficiency vs. Angle of Impact

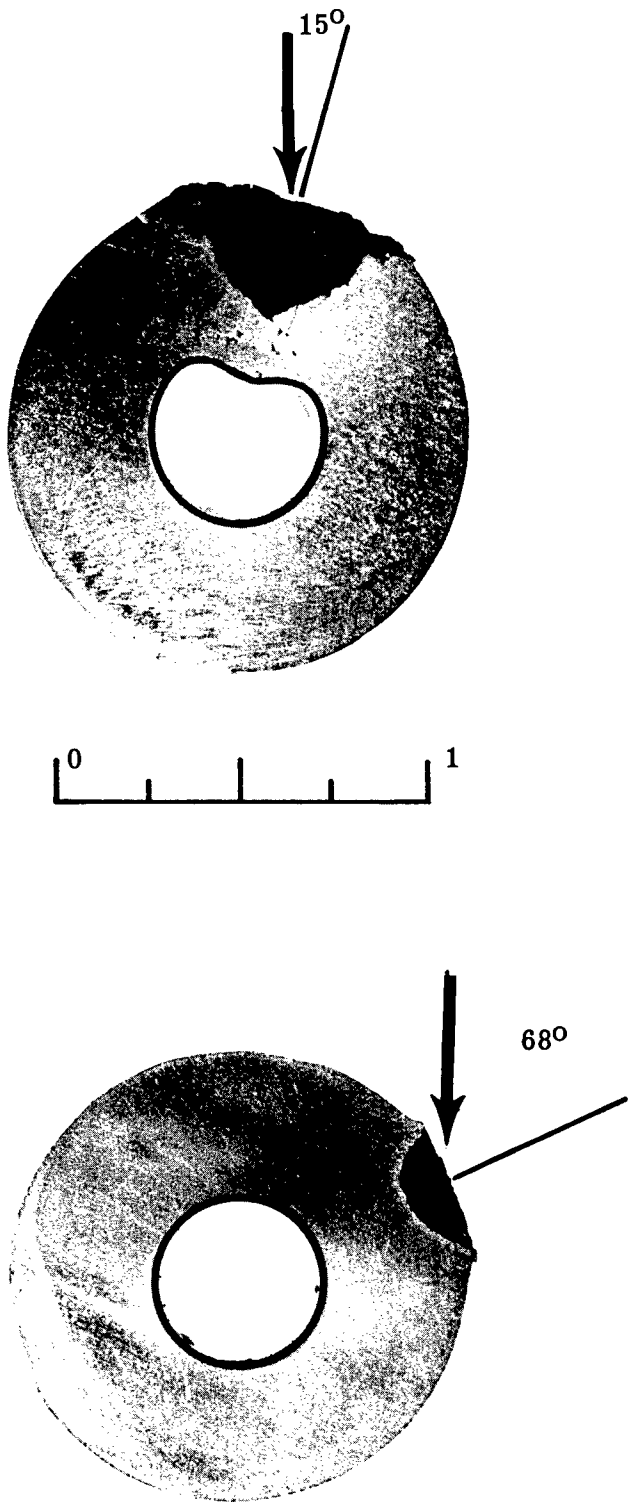

Fig. 4D.3 Crater Formation at Oblique Angles of Impact – Cylindrical Targets

0.10-IN. 2014-T6 ALUMINUM TARGET
1 gm TITANIUM PROJECTILE
4.6 km/sec

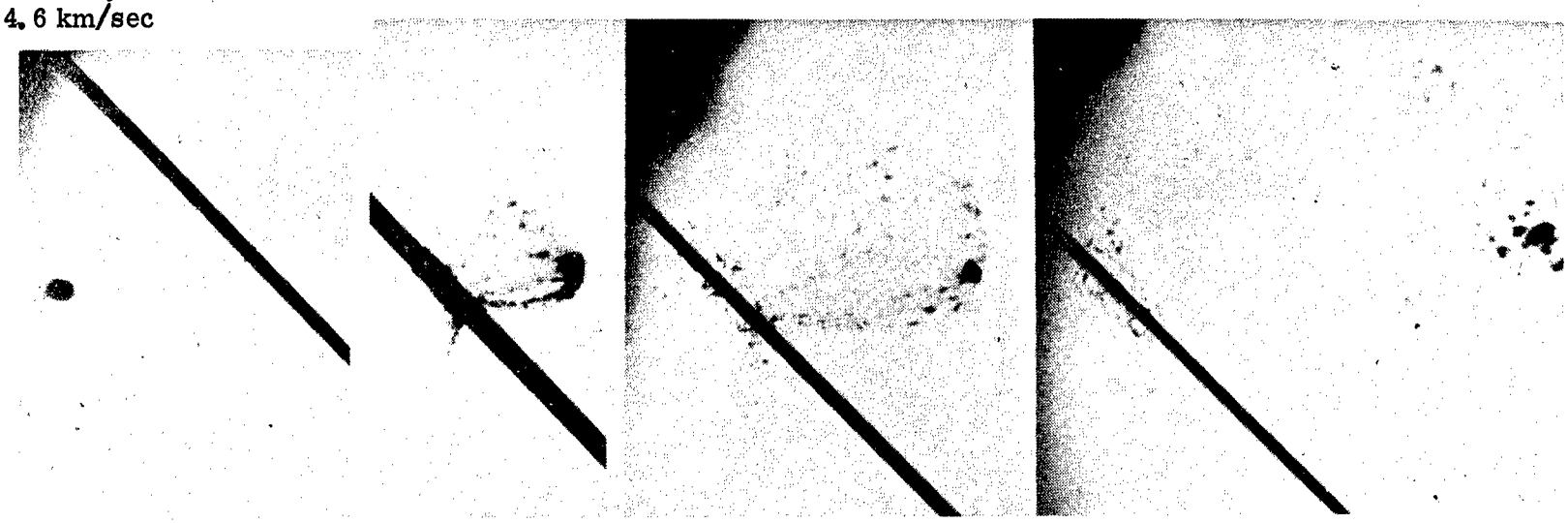

19.0 μsec BEFORE IMPACT | 16.0 μsec AFTER IMPACT | 29.0 μsec AFTER IMPACT | 51.5 μsec AFTER IMPACT

Fig. 4D.4 Spall Distribution from Oblique Impact (from Ref. 9)

However, a more important observation was made from these results: The direction of travel of the emerging pellet was seen to have remained unaltered by the deformation it suffered in perforating the thin plate; the fragments of the thin plate, however, were spewed from the back of the thin target in a direction normal to the target plate. This variance in the direction of travel of the ejecta behind the plate resulted in a displacement of the center of spall with respect to the point of impact of the remnants of the original projectile. The angle of displacement between the projectile remnants and the center of mass of the spall was observed to vary as much as 60 degrees (Fig. 4D. 4). A detailed analytical treatment of oblique impact into thin targets has been carried out by Zaid and Paul (Ref. 11); but because they were concerned primarily with conditions of low velocity (less than 2.0 km/sec), their results are inapplicable in cases of hypervelocity impact.

In conclusion then, it has been shown that the effects of oblique impact are important to protective design, as the damage caused by a given projectile against a specific target is markedly decreased as the impact angle increases.

REFERENCES FOR SECTION 4D

OBLIQUE IMPACT

1. W. H. Herrmann and A. H. Jones, "Survey of Hypervelocity Impact Information," Massachusetts Institute of Technology, Aeroelastic and Structures Research Laboratory, ASRL Report No. 99-1, Sep 1961

2. G. M. Bryan, "Oblique Impact of High Velocity Steel Pellets on Lead Targets," Proceedings of the Fifth Symposium on Hypervelocity Impact, Vol. 1, Part 2, Nonr-(G)-0020-62(X), Colorado School of Mines, Apr 1962

3. R. J. Eichelberger and J. W. Gehring, "Effects of Meteoroid Impacts on Space Vehicles," ARS J, Vol. 32, No. 10, Oct 1962, pp. 1583-1591

4. J. H. Kineke, Jr., "An Experimental Study of Crater Formation in Metallic Targets," Proceedings of the Fourth Symposium on Hypervelocity Impact, Vol. 1, APGC-TR-60-39, Eglin AFB, Florida, Sep 1960

5. J. L. Summers, "Investigation of High Speed Impact; Regions of Impact and Impact at Oblique Angles," NASA TN-D-94, Oct 1959

6. G. D. Anderson, "Studies in Hypervelocity Impact," Poulter Laboratory Tech. Report 018-59, Dec 1959

7. J. W. Gehring and S. Lieblein, "Preliminary Results on Effects of Hypervelocity Impact on Space Radiator Tubes" (ARS Paper No. 2544-62, presented at the ARS Space Power Systems Conference, Santa Monica, Calif., Sep 1962)

8. C. R. Nysmith and J. L. Summers," An Experimental Investigation of the Impact Resistance of Double-Sheet Structures at Velocities to 24,000 Feet/Second," NASA TN-D-1431, Oct 1962

9. K. N. Kreyenhagen and L. Zernow, "Penetration of Thin Targets," Proceedings of the Fifth Symposium on Hypervelocity Impact, Vol. 1, Part 2, Nonr-(G)-0020-62(X), Colorado School of Mines, Apr 1962

10. K. R. Becker, R. W. Watson, and F. C. Gibson, "Hypervelocity Impact Phenomena," Bureau of Mines, Explosives Research Laboratory, Quarterly Report to the Ballistic Research Laboratory, Auth. No. 4086, Aug 1962

11. M. Zaid and B. Paul, "Oblique Perforation of a Thin Plate by a Truncated Conical Projectile," Journal of The Franklin Institute, Vol. 268, No. 1, Jul 1959, pp. 24-45

4E. TARGET STRENGTH AND TEMPERATURE

The effects of variations in the strength of the target material upon the damage sustained as a result of high-speed impact is a matter of concern to a space vehicle designer. The expression, "strength of material," is an arbitrary term used to refer to the ability of the material to resist deformation. It is well known that the strength of a material is affected during its metallurgical history by such details as heat treatment, fabrication process, and the effect of the operating environment. The extent to which target strength and temperature are considered in some empirical approaches to hypervelocity cratering is discussed in Section 2.

The variations in mechanical properties of nominally identical target materials has called for a method of measuring resistance that can be used on individual targets. For this purpose, the Brinell hardness number (the ratio of the load to the area of indentation after the load is removed) has been found to provide a surprisingly good criterion (Refs. 1, 2). In Fig. 4E.1, the correlation (first reported by Feldman (Ref. 2)) between the energy per unit volume $dE/d\tau$ and the Brinell hardness number can be seen. These results were obtained with projectiles ranging in mass from 10^{-11} to 10 gm and in velocity to 15 km/sec; furthermore, pellets of a variety of shapes and of materials ranging from nylon to tungsten carbide have been used. It was reported that, without exception, the points lying farthest from the correlation line represent the cases in which the targets were least well known (handbook values have been used in some cases), and that experiments using targets of known hardness have invariably yielded closer agreement.

As the wealth of experimental data increases and attention is turned to the effects of alloys and their heat treatments, there seems to be little doubt that the plastic behavior of metals in compression will be the important consideration. This is brought into sharp focus by the data reported in Ref. 2 and in Fig. 4E.1 for three steels and five aluminum alloys.

Also important is the effect that an increase or decrease in temperature will have on the strength and/or the Brinell hardness number of a target material (Ref. 3). Because heated targets are of specific interest in applications such as solar-heated space vehicles, space radiators, and reentry nose cones, they have been studied by several investigators. Rockowitz, Carey, and

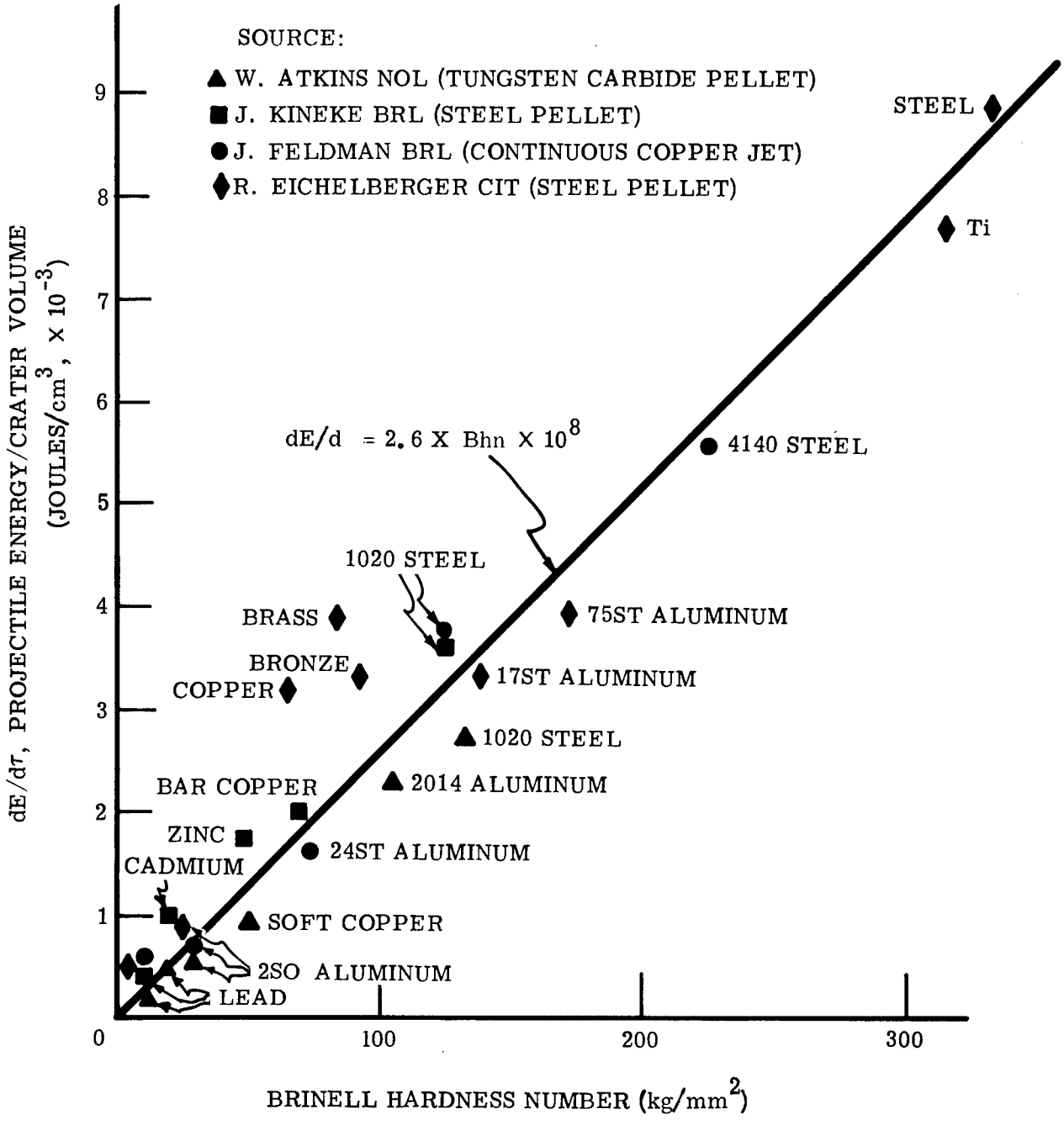

Fig. 4E.1 Cratering Efficiency vs. Target Hardness for Various Materials (from Ref. 2)

Dignam (Ref. 4) performed impact experiments on semi-infinite blocks of heated OFHC copper at temperatures ranging from 24°C to 870°C with projectiles of aluminum, steel, and tungsten carbide, all of 1/4-gm mass, at velocities up to 6.5 km/sec. Allison, Becker, and Vitali (Ref. 5) studied the impact behavior on lead (25°C to 287°C) and copper (148°C to 466°C) with a 0.18-gm steel projectile at velocities of 5 km/sec.

The results from these investigations are illustrated in Figs. 4E.2 and 4E.3. Figure 4E.2 shows the dependence of the crater volume on target temperature, and Fig. 4E.3 compares the dependence of energy per unit volume and tensile strength with temperature. From these it can be concluded that the dimensions of the crater increase with increasing target temperature. However, it has been found (Fig. 4E.3) that an increase in crater volume is not necessarily a linear function of the increasing temperature. The curves in Fig. 4E.3 are related to the changes in the solid-state phase taking place at the indicated temperatures.

Although no reference on the behavior of thin targets impacted at high temperatures has been found, some insight can be obtained from Ref. 6. Here the investigators studied the meteoroid hazard to space radiators by firing 0.016- and 0.04-gm glass spheres against aluminum and columbium targets at temperatures up to 370°C. Qualitatively, two effects were observed.

(1) The size of the hole made by the projectile was larger at higher temperatures.

(2) Less spall was observed at higher temperatures.

From this, it can be expected that at elevated temperatures the formation of a crater in a semi-infinite target will leave a better defined lip on the surface of the crater. Also, in the case of a thin target less back spall is expected because of increased ductility at higher temperatures.

From these studies, it can be seen that the cratering process is a complex phenomenon in which mechanical and metallurgical properties of the target play an important role. Referring to the model of crater formation described in Sections 3 and 4D, it is apparent that the bulk of the crater formation is caused by a process of energy dissipation and target deformation, during which the only restraining forces are the target properties. It was also

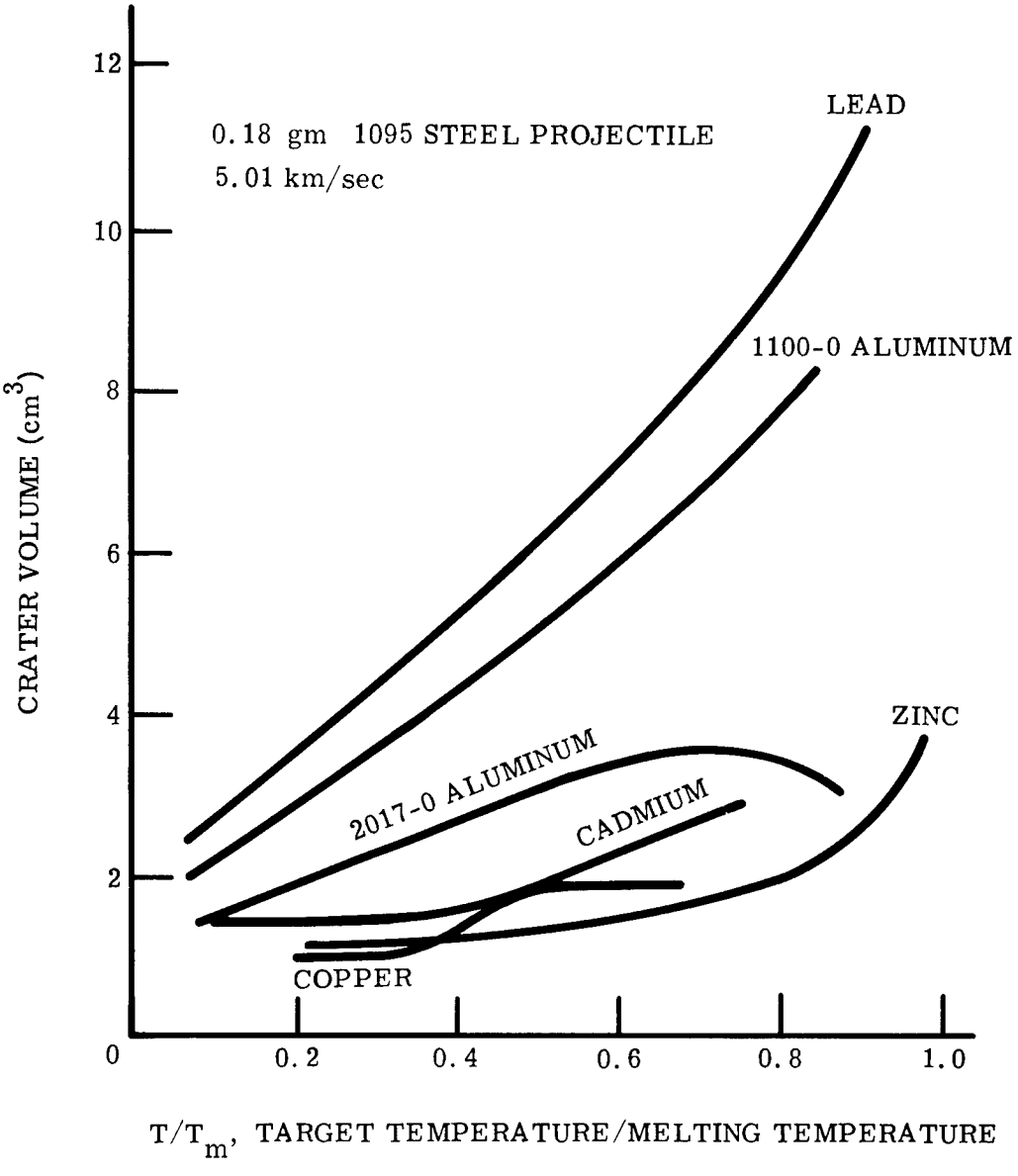

Fig. 4E.2 Crater Volume vs. Target Temperature
(from Refs. 1, 5)

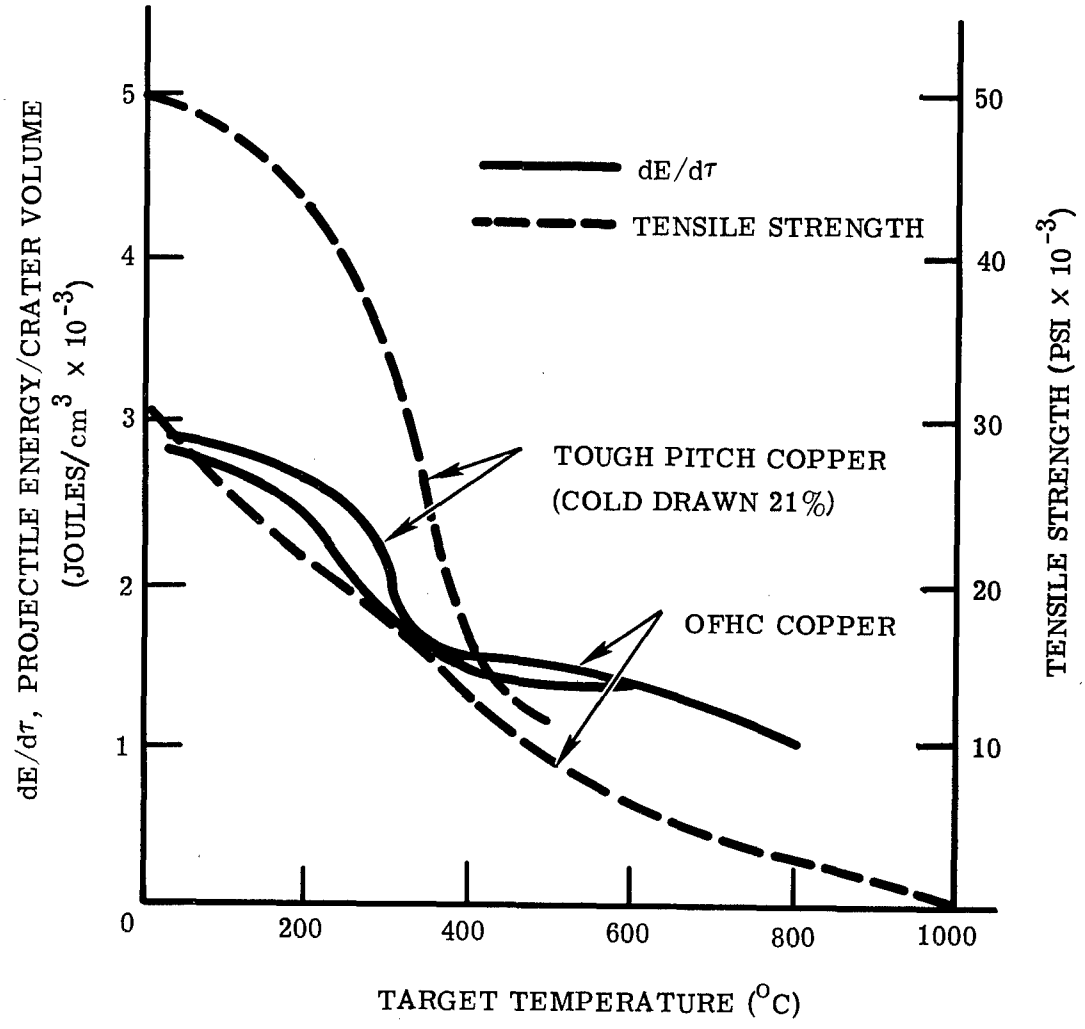

Fig. 4E.3 Cratering Efficiency and Target Strength vs. Target Temperature (from Ref. 4)

shown in Ref. 1 that the basic mechanisms of crater formation are the same for both ductile (aluminum) and brittle (lucite) materials; but that the brittle materials, through a process of latent fracturing, often evidence complete fracture and breakup. Therefore, it is logical to assume that soft, ductile targets, or heated targets, would yield a larger crater than would a high-strength target, or room-temperature target, and that brittle targets are more susceptible to spalling and crack failure.

REFERENCES FOR SECTION 4E

TARGET STRENGTH AND TEMPERATURE

1. R. J. Eichelberger and J. W. Gehring, "Effects of Meteoroid Impact on Space Vehicles," ARS J, Vol. 32, No. 10, Oct 1962, pp. 1583-1591

2. J. G. Feldman, "Volume-Energy Relations from Shape Charge Jet Penetrations," Proceedings of the Fourth Symposium on Hypervelocity Impact, Vol. 2, APGC TR-60-39, Eglin AFB, Florida, Sep 1960

3. J. H. Westbrook, "Temperature Dependence of the Hardness of Pure Metals," Trans. ASM 45, 1953, pp. 221

4. M. Rockowitz, C. Carey, and J. Dignam, "Hypervelocity Impact of Heated Copper," Proceedings of the Fifth Symposium on Hypervelocity Impact, Vol. 1, Part 2, Nonr-(G)-0020-62 (X), Colorado School of Mines, Apr 1962

5. F. E. Allison, K. R. Becker, and R. Vitali, "Effects of Target Temperature on Hypervelocity Cratering," Proceedings of the Fourth Symposium on Hypervelocity Impact, Vol. 1, APGC TR-60-39, Eglin AFB, Florida, Sep 1960

6. J. W. Gehring and S. Lieblein, "Preliminary Results on Effects of Hypervelocity Impact on Space Radiator Tubes" (ARS paper No. 2544-62, presented at the ARS Space Power Systems Conference, Santa Monica, Calif., Sep 1962)

7. W. W. Atkins, "Hypervelocity Penetration Studies," Proceedings of the Fourth Symposium on Hypervelocity Impact, Vol. 1, APGC TR-60-39, Eglin AFB, Florida, Sep 1960

8. W. J. Ferguson and K. R. McKinney, "The Influence of Temperature Elevation on the Penetration of Missiles into Copper Targets," NRL Report 5407, 1959

9. J. H. Kineke and L. G. Richards, "Effects of Target Strength on Hypervelocity Crater Formation" (paper presented at the Sixth Hypervelocity Impact Symposium, Cleveland, Ohio, Apr 30-May 2, 1963)

4F. PROJECTILE CONFIGURATIONS

The great majority of experimental research programs in the hypervelocity impact of fixed-shape projectiles have used solid spheres as the principal projectile (Ref. 1) Most theoretical treatments of hypervelocity impact have considered the impacting projectile to be a sphere, cube, or short cylinder (see, e.g., Ref. 2). There are, however, several other basic projectile configurations that could significantly affect the damage mechanisms that operate in hypervelocity impact, but there is little information available concerning these configurations. This lack can be attributed to the technical problems associated with performing experiments with unusual projectile configurations, and to the classified nature of most of the programs that are concerned with these odd shapes (Refs. 3-5). Actually, the unusual projectile shape is of most interest in the appraisal and enhancement of impact damage from antisatellite devices.

4F.1 Fixed-Shape Projectiles

Fixed-shape projectiles can be defined as those that have essentially the same size, shape, and mass at the instant of impact as they had before being accelerated. Some examples of fixed-shape projectiles can be seen in Fig. 4F.1. These projectiles are shown perforating a thin target, and a pictorial comparison can be made of the ejecta that comes out of the back of a thin target after impact by each of the projectiles. These illustrations are qualitative only, and the size and shape of any remaining projectile, or of "plugs" from the target, are a function of such parameters as material, thickness, and velocity.

Studies of rod impacts have been carried out by Atkins (Ref. 6), Summers and Niehaus (Ref. 7), Allan and Rogers (Ref. 8), Slattery and Clay (Ref. 9), and Nysmith, Summers, and Denardo (Ref. 10). Results have shown that for low-velocity (below the wave velocity in the projectile) end-on impacts, the craters tend to be cone shaped. This can be attributed to deceleration of the back end of the rod during impact of the front end. At high velocities (above the wave velocity of the projectile) the craters tend more toward a cylindrical shape; this is to be expected, since the cratering process involves the addition of energy at a constant rate for a time that is comparable to the total time of crater formation.

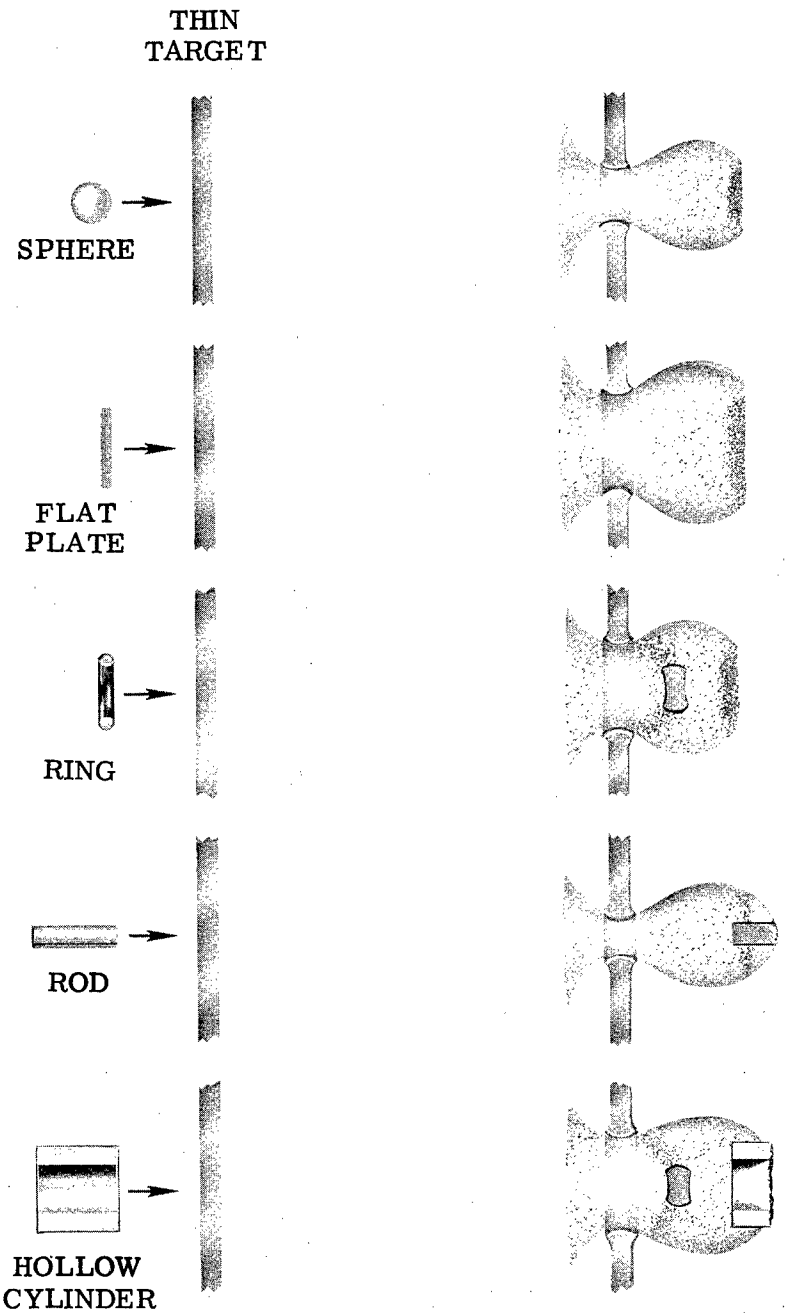

Fig. 4F.1 Thin Target Damage from Various Projectile Shapes

On the other hand, with a solid sphere the primary phase of cratering (or the phase during which the projectile is being used up) is short (compared to that of a long and slender rod) and leads to the creation of a hemispherical crater upon impact of an equiaxial projectile, since the projectile energy can be thought of as being deposited at the surface of the target almost instantaneously. Impact at intermediate angles (between "end-on" and "side-on" conditions) does not result in any new phenomena; it merely complicates the prediction and interpretation of results.

The results of a series of experiments conducted at GM DRL to assess the effects of projectile density and shape are given in Figs. 4F.2 and 4F.3 (Ref. 11). The targets in all cases were semi-infinite, 1100-F aluminum blocks, and impact velocity was 6.6 km/sec.

In Fig. 4F.2, the penetration depth and crater volume are given as functions of projectile density. The penetration is proportional to $\rho_p^{.19}$, and volume is proportional to $\rho_p^{.17}$. Results of a similar series of tests at 2.0 km/sec, reported by Charters and Summers in 1960 (Ref. 12), showed penetration to be proportional to $\rho_p^{.33}$ and volume to be proportional to $\rho_p^{.50}$. Note the significant decrease in exponents for an increase in velocity from 2.0 to 6.6 km/sec. Extrapolating these results to meteoroid velocities reveals that the influence of projectile density on penetration and volume may become negligible.

In Fig. 4F.3, the penetration depth and crater volume are given as functions of projectile shape. Note that the penetration and volume are strongly influenced by the length of the projectile along its flight axis (normalized with respect to sphere diameter). This result is significant in military applications where impact velocities are below 10 km/sec. However, for meteoroid impacts, it is reasonable to assume that the particles are approximately spherical and, consequently, that shape is not a governing factor in damage.

4F.2 Microparticles and Shaped-Charge Jets

Microparticles and shaped-charge jets can be differentiated from fixed-shape projectiles in that the projectile size, shape, and mass distribution may change significantly between launch and impact. However, these projectiles are of considerable importance in hypervelocity impact research, as illustrated in Fig. 1.5, Section 1.

TARGET: 1100-F ALUMINUM, SEMI-INFINITE

IMPACT VELOCITY: 6.6 km/sec

PROJECTILE:

	ZELUX (TYPE M)	ALUMINUM (2017)	STEEL (C1020)	
ρ_P =	1.20	2.70	7.80	gm/cm^3
Diam =	0.313	0.240	0.169	in.

(ALL PROJECTILES SAME MASS - 0.32 gm)

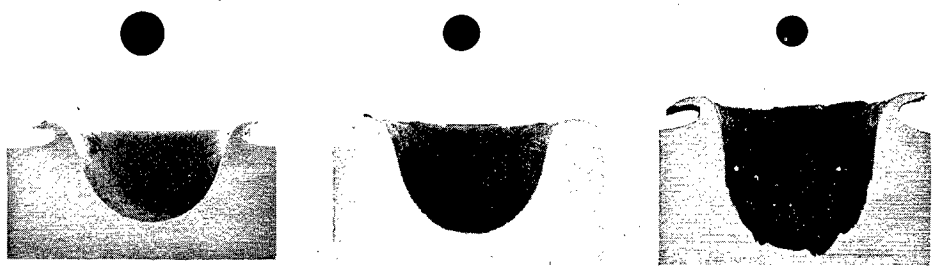

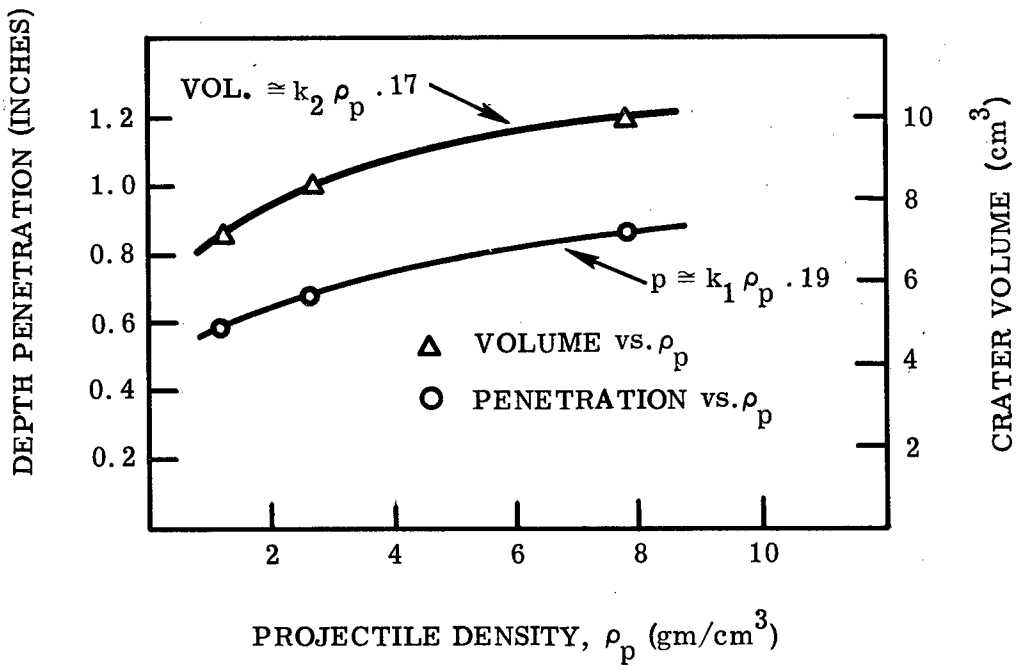

Fig. 4F.2 Crater Depth and Volume for Equal Mass Spheres of Various Densities

TARGET: 1100-F ALUMINUM, SEMI-INFINITE

IMPACT VELOCITY: 6.6 km/sec

PROJECTILE MATERIAL: 2017 ALUMINUM

SHAPE:	DISC	SPHERE	CYLINDER
LENGTH, ℓ =	0.062	0.240 (d_s)	0.500 in.

(ALL PROJECTILES SAME MASS - 0.32 gm)

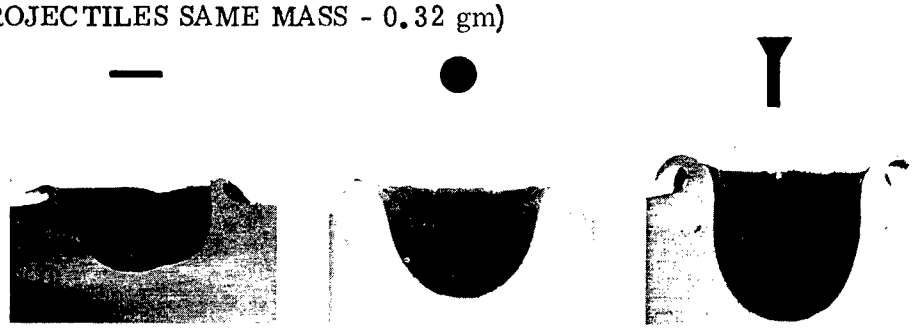

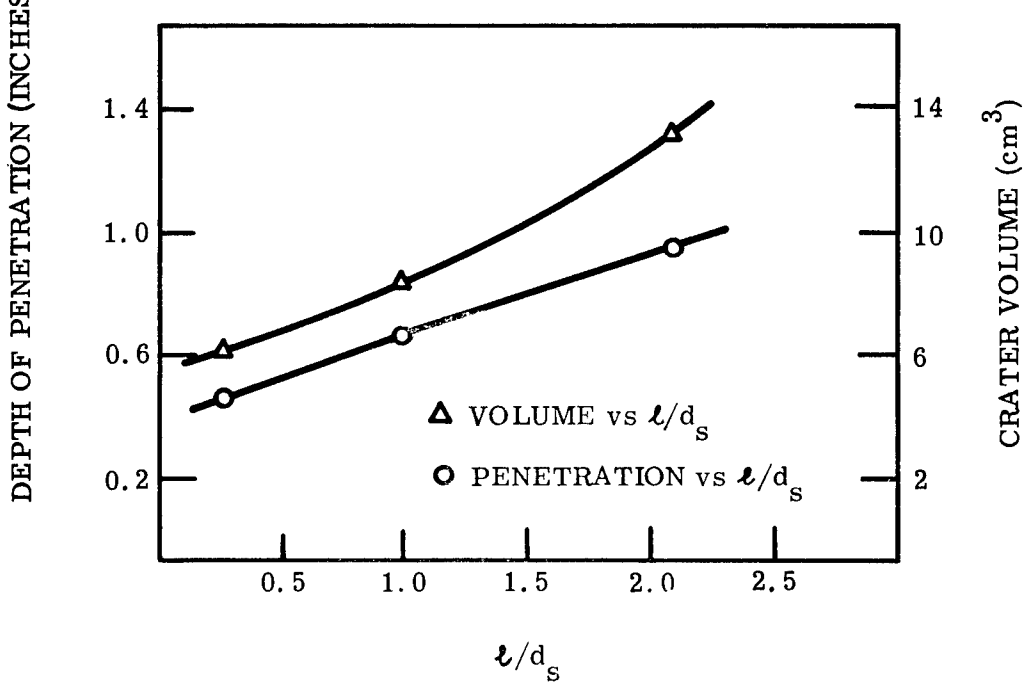

Fig. 4F.3 Crater Depth and Volume for Projectiles of Equal Mass and Various Densities

Microparticles are of interest because their potentially low mass (10^{-12}-10^{-4}gm) and high velocity (7-20 km/sec) permit simulation of a wide range of meteoroid impact conditions. This, in turn, has two applications: (1) evaluation of damage to spacecraft components (Ref. 13), and (2) calibration of meteoroid detectors for satellites and spacecraft (Ref. 14). The cratering process involved in microparticle impacts does not appear to be significantly different from that in macroparticle ($> 10^{-4}$gm) impacts, and appropriate scaling laws can be developed for the prediction of impact results.

There are three factors, however, that are of minor importance in macroparticle work but which become critical in microparticle work. These are (1) target grain size, (2) crystal structure, and (3) anistropy. Although microparticles are not usually spherical, their velocities are high enough so that projectile shape becomes less important than in the case of lower velocity, fixed-shape projectiles.

Shaped-charge jets, produced by explosive acceleration devices (Ref. 15), cover approximately the same mass range (10^{-2} 10.0 gms) as fixed-shape projectiles but are capable of much higher velocities (7-30 km/sec). The crater shape from shaped-charge jets may be significantly different from that of fixed-shape projectiles (Refs. 16, 17), but the crater volume per unit projectile kinetic energy seems to be essentially the same for the two types, at least under hypervelocity impact conditions (Ref. 18).

The experimental methods associated with microparticles and shaped-charge jets are more complicated than those with fixed-shape projectiles, particularly in the determination of projectile mass and velocity at the time of impact.

4F.3 Summary

Most hypervelocity impact research, both experimental and theoretical, has been concerned with fixed-shape projectiles – notably, spheres. This is justifiable, at least for meteoroid simulation, not only on the grounds that data of higher accuracy and reliability can be obtained, but because at very high velocities (up to 70 km/sec) the shape of the projectile should become of secondary importance. Therefore, spherical projectiles should cause essentially the same damage as meteoroids of comparable mass which are considered to be of irregular shape. This does not, of course, obviate the

need for research using other projectile shapes, especially in applications other than meteoroid simulation. In fact, a thorough understanding of the mechanisms of hypervelocity cratering and penetration will require detailed knowledge of the behavior of all projectile configurations, and not just those of simple shapes.

REFERENCES FOR SECTION 4F

PROJECTILE CONFIGURATIONS

1. W. Herrmann and A. H. Jones, "Survey of Hypervelocity Impact Information," Massachusetts Institute of Technology, Aeroelastic and Structures Research Laboratory, ASRL Report No. 99-1, Sep 1961

2. T. D. Riney, "A Visco-Plastic Model for Hypervelocity Impact," General Electric Company Space Systems Laboratory, SSL First Quarterly Report, Contract AF-08(635)-1713, Apr 1961

3. J. F. Cullinane, et al, "Hypervelocity Kill Mechanisms Program (U)," Aerojet-General Corporation Semiannual Progress Report (S), ARPA Order 149-60, 0404-04(12)FP, period ending 20 Mar 1962

4. D. R. Dudas, "On the Effects of Projectile Mass Distribution in Hypervelocity Impact (U)," Proceedings of the Fifth Symposium on Hypervelocity Impact, Vol. II (S), Nonr-(G)-0020-62(X), Colorado School of Mines, Apr 1962

5. D. R. Christman and J. W. Gehring, "Study of the Lethality of Hollow Spheres (U)," Summary Technical Report (S), Contract AF 08(635)-2833, ARPA Order No. 347-62, GM Defense Research Laboratories Report TR 63-207, Jun 1963 (work reported in this paper was presented at the Sixth Hypervelocity Impact Symposium, Cleveland, Ohio, Apr 30-May 2, 1963)

6. W. W. Atkins, "Hypervelocity Penetration Studies," Proceedings of the Third Symposium on Hypervelocity Impact, Armour Research Foundation, Chicago, Ill. Feb 1959

7. J. L. Summers and W. R. Niehaus, "A Preliminary Investigation of the Penetration of Slender Metal Rods in Thick Metal Targets," NASA TN-D-137, Dec 1959

8. W. Allen and J. W. Rogers, "Penetration of a Rod into a Thick Aluminum Target," Journal of The Franklin Institute, Oct 1961, pp. 275-284

9. R. E. Slattery and W. G. Clay, "The Penetration of Thin Rods into Aluminum," Proceedings of the Fourth Symposium on Hypervelocity Impact, Vol. 3, APGC-TR-60-39, Eglin AFB, Florida, Sep 1960

10. C. R. Nysmith, J. L. Summers, and B. P. Denardo, "Investigation of the Impact of Copper Filaments Into Aluminum Targets at Velocities to 16,000 Ft/Sec" (paper presented at Sixth Hypervelocity Impact Symposium, Cleveland, Ohio, Apr 30-May 2, 1963)

11. A. C. Charters, "A Critique of Accelerator Techniques for Hypervelocity Impact" (paper presented at the Sixth Hypervelocity Impact Symposium, Cleveland, Ohio, Apr 30-May 2, 1963)

12. A. C. Charters and J. L. Summers, "High-Speed Impact of Metal Projectiles in Targets of Various Materials," Proceedings of the Third Symposium on Hypervelocity Impact, Armour Research Foundation, Chicago, Ill., Feb 1959

13. J. W. Gehring and L. G. Richards, "Further Studies of Microparticle Cratering in a Variety of Target Materials," Proceedings of the Fourth Symposium on Hypervelocity Impact, Vol. 3, APGC-TR-60-39, Eglin AFB, Florida, Sep 1960

14. W. M. Alexander and O. E. Berg, "Microparticle Hypervelocity Impacts from Ranger I," Proceedings of the Fifth Symposium on Hypervelocity Impact, Vol. 1, Part 2, Nonr-(G)-0020-62(X), Colorado School of Mines, Apr 1962

15. G. Birkhoff, D. P. MacDougall, E. M. Pugh and G. Taylor, "Explosives with Lined Cavities," J. Appl. Phys., Vol. 19, No. 6, Jun 1948, pp. 563-582

16. R. J. Eichelberger, "Experimental Test of the Theory of Penetration by Metallic Jets," J. Appl. Phys., Vol. 27, No. 1, Jan 1956, pp. 63-68

17. G. R. Abrahamson and J. N. Goodier, "Penetration by Shaped Charge Jets of Nonuniform Velocity," J. Appl. Phys., Vol. 34, No. 1, Jan 1963, pp. 195-199

18. J. B. Feldman, "Volume Energy Relation from Shaped Charge Jet Penetrations," Proceedings of the Fourth Symposium on Hypervelocity Impact, Vol. 2, APGC-TR-60-39, Eglin AFB, Florida, Sep 1960

SECTION V

CONCLUSION AND RECOMMENDATIONS

5.1 CONCLUSIONS

This report has attempted to present a broad analysis of the phenomena of hypervelocity impact. The hypervelocity impact "hazard," especially as it concerns meteoroids, has been treated in enough detail to show that it warrants special attention by the vehicle designer. The lack of accurate, quantitative data on the mass and velocity distribution of meteoroids near Earth and in interplanetary space has been emphasized. In fact, very recent estimates of average meteoroid density (0.44 gm/cm^3) and mean velocity (22 km/sec) by Whipple* illustrate the continuous revisions that are being made of the meteoroid environment by the many investigators in the field. The trend in recent years has been to lower the mass frequency distribution curves, i.e., to reduce the meteoroid hazard, especially in interplanetary space.

The impact hazard is far from being eliminated, however, not only with respect to meteoroids but in military applications of hypervelocity projectiles. Accordingly, a method has been presented for determining how thick a vehicle skin must be in order to prevent perforation by a hypervelocity projectile under given impact conditions, even though estimates of the meteoroid hazard and of mission requirements may change. It should be emphasized, however, that the example considered in this report is for an elemental single-skin hull of homogenous material. Practical applications to structures more representative of actual spacecraft would require consideration of factors such as spall, multiple-sheet targets, laminates, pressure vessels, etc. This would require the use of different penetration laws, derived either experimentally or theoretically, to account for the behavior of complex targets under conditions of hypervelocity impact.

*American Astronautical Society Interplanetary Missions Conference, Jan 1963

The more basic problem of hypervelocity impact into semi-infinite targets has been treated in more detail, both empirically and theoretically. The reasonable accuracy with which some investigators have been able to predict impact damage has been illustrated. Extrapolation of the wealth of experimental data available for velocities below 10 km/sec into the meteoroid range (11–72 km/sec) is possible, and some estimates of damage can be made with reasonable assurance. However, experimental data in the velocity range of 10–40 km/sec would greatly improve the accuracy of these estimates.

The theoretical treatment of hypervelocity impact has described the basic mechanisms involved and has reviewed several of the models and methods used in describing and analyzing hypervelocity cratering. These include hydrodynamic theory, visco-plastic theory, explosion theory, and blast-wave analysis. The influence of such variables as strength, density, wave velocity, crystal structure, anisotropy, ductility, and, of course, impact velocity, has been considered. During the course of this work, however, it has become apparent that although there is a general understanding of the basics involved in hypervelocity impact (primary vs. secondary penetration, ductile vs. brittle materials, and normal vs. oblique impact), there is a decided lack of detailed knowledge concerning such specifics as impact radiation, target strength effects, projectile density effects, and high-strain-rate properties of materials.

Much information regarding multiple-sheet targets, most of it experimental, has been generated. The use of a thin bumper to protect a principal structure can, in most cases, lead to a saving in structural weight. The method of operation of the bumper has been described – it fragments and disperses the projectile – and there is some understanding of the effects of bumper material density and of spacing between sheets (in general, less penetration for denser materials and greater spacing); but experimental data in the velocity range of 10–40 km/sec and a more definitive theory of thin-target behavior is necessary before the effects of hypervelocity impact on multiple-sheet targets can be predicted accurately.

The behavior of laminates, composites, and stressed structures has been investigated only superficially on an experimental basis. There is good data available for specific cases, but the lack of general data for these structures

prevents the designer from making reasonable allowance for the impact hazard without resorting to experimental studies of the type of structure with which he is concerned.

Spalling is a problem of utmost concern to the designer since it can occur with almost any material and structure, regardless of size or shape. There are a number of equations for predicting spall size and for calculating the effectiveness of laminates in reducing spall, but these relationships apply only to cases where the stress wave is plane and its shape and magnitude are known, and they assume perfect bonding between laminates, which may not be a valid assumption in practice. Here again, an experimental study of the specific material or structure is the most reliable way of obtaining design data.

Oblique impact is of obvious interest to the designer, since most impacts of meteoroids or fragments on a structure will probably be at angles other than normal. The factor of primary importance here is the normal component of impact velocity (a function of projectile velocity and impact angle). In the hypervelocity range, the resulting damage to thick targets can be described as the damage that would have occurred at normal impact had the actual impact velocity been replaced by its normal component; this will be the case until the normal component of velocity becomes too low for impact at hypervelocity. At lower values of the normal component than this critical one (actually a transition region rather than a specific value), which correspond to higher angles of obliquity, the crater shape becomes asymmetrical, damage in terms of crater volume and depth of penetration decreases, and at very high angles of obliquity ricocheting may occur. On the other hand, damage to thin targets under conditions of oblique impact is not so well defined with regard either to hole area or to the distribution of spall behind the target or bumper.

One of the mechanical properties of materials that has been useful in analyzing impact damage to thick targets is hardness, and in particular, the Brinell hardness number. Cratering efficiency in terms of projectile energy/unit crater volume has been found to be directly proportional to target hardness in a wide range of materials and values of hardness. For a given target material, crater volume has been found to increase with target temperature in a manner related to decreases in target hardness and to material phase changes.

Although this report has concentrated on materials, properties, and shapes of targets, the projectile is also of interest. In the case of meteoroid impacts

where impact velocities can be expected to be in the range of 11–72 km/sec, the shape of the meteoroid may be unimportant since the shape will probably be approximately spherical. Meteoroid density may also be unimportant; however, because of the wide range of meteoroid density estimates (0.05 to 8.0 gm/cm^3), and the lack of quantitative data on projectile density effects at meteoroid velocities, an evaluation of the meteoroid hazard should make allowance for possible effects of density. From the military standpoint, where impact velocities could range from 1 to 12 km/sec, projectile shape and density are important enough to be the controlling factor in impact damage in some cases. Obviously, projectile mass is significant in all cases.

5.2 RECOMMENDATIONS

There are many aspects of the problem of hypervelocity impact that require detailed study on an experimental basis or a theoretical basis, or both. From the review of hypervelocity impact made in conjunction with this report, it has become apparent that many of these are being investigated. Several organizations are carrying out extensive research programs which cover such areas as multiple-sheet targets, impact radiation, theoretical models, and specific materials and structures (including space radiators, laminates, pressure vessels, simulated lunar materials, and filler materials). Studies directed at more specific areas, such as reentry materials, ablatives, thin targets, and cratering theory, are being made by many other organizations.

It has also become apparent, however, that these studies have not been sufficiently numerous or detailed to permit accurate predictions of the reaction of a complex missile or space vehicle structure to the impact of a hypervelocity projectile. The specific concern to the designer of a missile or space vehicle is to design a structure that will complete its mission in space without destructive damage from meteoroid impacts; this would include consideration of the case when the vehicle skin cannot prevent perforation, making it necessary to define the mass and velocity of the fragments that enter the vehicle and the conditions under which these fragments will cause damage to internal components.

Future studies, then, should include, first, basic investigations to provide a fundamental understanding of impact phenomena. Second, these basic studies should be followed by empirical investigations of simple targets in order to

relate the results to the actual demands of engineering structures. Last, the studies of simple targets can be expanded, as necessary, to cover the complex situations which are more representative of practical engineering structures.

5.2.1 Properties of Materials.

A basic research program should be undertaken to develop a more thorough understanding of the properties of materials under the exceedingly high strain rates associated with hypervelocity impact. This program should include determination of dynamic stress-strain curves for various materials, a study of the deformation mechanisms involved, and an analysis of the effects of grain size, orientation, anisotropy, etc., on such mechanisms. Also, the effect of material strength on the equations of state of various metals should be investigated, and the importance of material strength to the decay of shock waves studied.

It cannot be stated exactly what specific properties of materials are most important in defining impact damage; however, the research program outlined above should permit definition of the damage to a target as a function of material properties to allow a more intelligent and satisfactory selection of materials for use in future systems.

5.2.2 Cratering in Semi-Infinite Targets.

The analysis of impact cratering through theoretical approaches based on hydrodynamic theory has received considerable attention in the past and should be pursued; however, theoretical methods usually require complicated mathematical calculations and may be applicable only to the conditions existing early in the process of crater formation. Of real and immediate benefit to the spacecraft designer would be the development of a simple but comprehensive analytical theory which would permit both the prediction of the main features of the impact process and the assessment of the importance of the various parameters that are part of the process. Particularly relevant here would be the results of the study of the properties of materials that was outlined above.

5.2.3 Perforation of Thin Targets.

A study of perforation of thin targets is actually a refinement of the semi-infinite

target problem, with the added requirement that projectile behavior after penetration of the target must be considered (with a semi-infinite target, the projectile is used up and essentially eliminated from the problem during the first two stages of the cratering process). In particular, the fragmentation of the projectile must be examined, and the distribution of the fragments in terms of mass, velocity, and direction, should be established.

5.2.4 Impact Against Specific Structures.

The study of impact damage to specific structures is, of course, an extremely broad subject; however, an important source of experimental design data could be established through research programs in the following areas:

(1) Hypervelocity impact damage to materials and structures at subzero and elevated temperatures

(2) Behavior of stressed structures, pressure vessels, and load-bearing members under conditions of hypervelocity impact

(3) Hypervelocity impact damage to laminated structures, composite materials, and filler materials

(4) Calibration of meteoroid detection devices

(5) The influence of impact parameters such as materials, velocity, atmosphere, and pressure on impact radiation